CHAPTER 7

Thermoacoustic instability

7.1 Basic concepts of thermoacoustics

Thermoacoustic instability, also known as combustion instability, has been encountered in the development and operation of practical devices including rocket engines, gas turbines, boilers, and aeroengines, manifesting itself with large-amplitude pressure oscillations, which may cause detrimental consequences. The instabilities are excited by the feedback loop between the unsteady combustion and natural acoustic mode of combustors, as shown in Fig. 7.1. The heat transfer in the combustors is enhanced spontaneously when the instabilities occur. Therefore, the components in the combustors are more prone to be melted, and the systems then lose efficiency or become disabled.

The deadly catastrophic effect and imperative control of combustion instability have drawn more and more research interest. Many investigations have been carried out since it was noticed. However, research exploration began long before the birth of propulsion and power devices. In 1777, Higgins [1] found that the flame in a tube emitted a sound that was called "singing flame," and the Sondhauss tube and Rijke tube phenomena were discovered later.

Rayleigh criterion is widely known and frequently quoted for his physical elucidation about the necessary condition for the onset of self-sustained oscillations in a Rijke tube: "If heat is periodically communicated to, and abstracted from, a mass of air vibrating in a cylinder bounded by a piston, the effect produced will depend upon the phase of the vibration at which the transfer of heat takes place. If heat is given to the air at the moment of greatest condensation, or taken from it at the moment of greatest rarefaction, or abstracted at the moment of greatest condensation, the vibration is discouraged." [2] However, this does not necessarily imply the combustion is unstable, because the portion of the acoustic energy dissipated at the boundaries plays an important role as well. Only if the acoustic energy enhanced from the heat exceeds that dissipated at the

Fundamentals of Aeroacoustics with Applications to Aeropropulsion Systems
https://doi.org/10.1016/B978-0-12-408069-0.00007-5
© 2021 Shanghai Jiao Tong University Press. Published by Elsevier Inc.

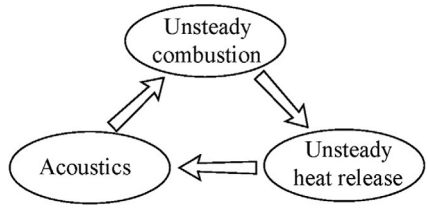

Fig. 7.1 Feedback loop between unsteady combustion and acoustics.

boundaries does the instability occur. This can be expressed by the following expression [3]:

$$\int_V \int_T p'(x,t)q'(x,t)dtdV \geq \int_V \int_T \sum_i L_i(x,t)dtdV, \tag{7.1}$$

where $p'(x,t)$, $q'(x,t)$, V, T, and L_i are the combustor pressure oscillations, heat addition oscillations, combustor volume, period of the oscillations, and the ith acoustic energy loss process (e.g., viscous dissipation, radiation of acoustic energy out of the combustor through its boundaries), respectively.

The research of combustion instability moved beyond purely academic interest with the arrival of large-amplitude oscillations in industrial equipment. Extensive efforts have been made on the characteristics of combustion instabilities in operational or laboratory systems and the methods for predicting and suppression in both theoretical and experimental approaches [4–8]. The mechanism is grouped into linear and nonlinear categories. A linearly unstable system is one that is unstable for infinitesimally small disturbances, thus the properties of the flow field can be decomposed into a time-mean and fluctuation quantity. The stability analysis is based on the decomposition. Linear stability analysis makes it convenient to solve the stability problem mathematically, although it is only an ideal assumption. In real unstable systems, there exists a process of evolution of the disturbance amplitude from small to the threshold valueA_T; this differs from the linear unstable system and is a nonlinearly unstable system. Zinn and Lieuwen [3] studied the characteristics of nonlinearities of thermoacoustic systems. However, the real system is always accompanied by many factors, and it is still very hard to analyze a thermoacoustic system using nonlinear methods, although it is mature and feasible to study the mechanisms and control methods of combustion instability through linear approaches. In this chapter, the second part will briefly introduce the one-dimensional thermoacoustic calculation methods, and the three-dimensional thermoacoustic derivation will be given in the third part. Some calculation results will be shown at the same time.

In the fourth part, some control methods of combustion instability will be presented, and conclusions will be summarized in the last section.

7.2 One-dimensional calculation method

The one-dimensional thermoacoustic calculation method is often easy to carry out and physically clear. Most investigations incorporate the Rijke tube. In this section, the method is briefly introduced based on the study of Dowling [9, 10] and Heckl [11].

Consider one-dimensional thermoacoustic oscillations in the geometry in Fig. 7.2; the heat source is located at $x = l$ within a length of Δ, which is small compared with the length of the tube. The density, pressure, and velocity can be decomposed into a time-mean property and a fluctuation property in the following forms:

$$\begin{aligned} p(x,t) &= \overline{p}(x) + p'(x,t), \\ u(x,t) &= \overline{u}(x) + u'(x,t), \\ \rho(x,t) &= \overline{\rho}(x) + \rho'(x,t). \end{aligned} \tag{7.2}$$

In a region added by heat, the density of the fluid is a function of two variables, i.e., the pressure and the specific entropy. Therefore,

$$\frac{D\rho}{Dt} = \frac{1}{c^2}\frac{Dp}{Dt} + \left.\frac{\partial\rho}{\partial s}\right|_p \frac{Ds}{Dt}, \tag{7.3}$$

where c is the speed of sound. The fluid is assumed to be inviscid, and the heat conduction effect is ignored, hence,

$$ds = \frac{\delta q_{rev}}{T}, \tag{7.4}$$

$$\rho ds = \frac{Q}{T}, \tag{7.5}$$

$$\rho T Ds/Dt = q(\mathbf{x}, t), \tag{7.6}$$

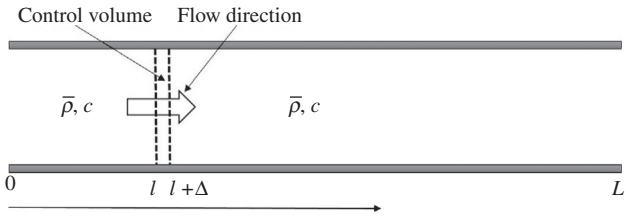

Fig. 7.2 Geometry of the Rijke tube.

where q is the heat addition per unit volume, and T is the absolute temperature. For perfect gas, $p=\rho RT$, $\left(\frac{\partial T}{\partial s}\right)_p=\frac{T}{c_p}$, $c_p=\frac{\gamma}{\gamma-1}R$, c_p is the specific heat at constant pressure and γ is the ratio of specific heats. Hence,

$$\left.\frac{\partial\rho}{\partial s}\right|_p=\frac{-\rho T(\gamma-1)}{c^2}. \tag{7.7}$$

Substituting Eqs. (7.4) and (7.5) into Eq. (7.3) yields:

$$\frac{D\rho}{Dt}=\frac{1}{c^2}\left(\frac{Dp}{Dt}-(\gamma-1)q\right). \tag{7.8}$$

For a linear perturbation region where there is no mean velocity and mean heat release, Eq. (7.8) can be linearized,

$$\frac{D\rho'}{Dt}=\frac{1}{\bar{c}^2}\left(\frac{\partial p'}{\partial t}-(\gamma-1)q'\right), \tag{7.9}$$

where the overbar denotes the mean property, and the prime denotes the fluctuation property.

The linearized mass equation and momentum equation are:

$$\frac{D\rho'}{Dt}+\bar{\rho}\frac{\partial u'}{\partial x}=0, \tag{7.10}$$

$$\bar{\rho}\frac{\partial u'}{\partial t}+\frac{\partial p'}{\partial x}=0, \tag{7.11}$$

respectively.

By differentiating Eq. (7.10) with respect to t, and Eq. (7.11) with respect to x, and subtracting, we obtain:

$$\frac{D^2\rho'}{Dt^2}-\frac{\partial^2 p'}{\partial x^2}=0. \tag{7.12}$$

Considering Eqs. (7.9) and (7.12), an inhomogeneous wave equation is obtained:

$$\frac{1}{\bar{c}^2}\frac{\partial^2 p'}{\partial t^2}-\frac{\partial^2 p'}{\partial x^2}=\frac{\gamma-1}{\bar{c}^2}\frac{\partial q'}{\partial t}. \tag{7.13}$$

According to the wave equation, the acoustic field is determined by definition:

$$p'(\mathbf{x},t)=\begin{cases}\left(Ae^{-i\omega(x-l)/\bar{c}_1}+Be^{i\omega(x-l)/\bar{c}_1}\right)e^{i\omega t}, & x<l\\ \left(Ce^{-i\omega(x-l)/\bar{c}_2}+De^{i\omega(x-l)/\bar{c}_2}\right)e^{i\omega t}, & x\geq l\end{cases}, \tag{7.14}$$

$$u'(x,t)=\begin{cases}\dfrac{1}{\overline{\rho}c}\left(Ae^{-i\omega(x-l)/\bar{c}_1}-Be^{i\omega(x-l)/\bar{c}_1}\right)e^{i\omega t}, & x<l\\ \dfrac{1}{\overline{\rho}c}\left(Ce^{-i\omega(x-l)/\bar{c}_2}-De^{i\omega(x-l)/\bar{c}_2}\right)e^{i\omega t}, & x\geq l\end{cases}, \tag{7.15}$$

where A, B and C, D are the complex amplitudes of the upstream and downstream traveling pressure waves in the tube. They are related by the conservation laws at the heat addition interface and the end boundary conditions.

Integration of Eq. (7.13) across the region $x=l$, we obtain:

$$p'_{x=l^+}=p'_{x=l^-}, \tag{7.16}$$

$$\frac{1}{\overline{\rho}}\frac{\partial p'}{\partial x}\bigg|_{x=l^-}^{x=l^+}=-\frac{(\gamma-1)}{\gamma\overline{p}}\frac{Q}{S}\quad i.e.\quad u'|_{x=l^-}^{x=l^+}=-\frac{(\gamma-1)}{\gamma\overline{p}}\frac{Q}{S}. \tag{7.17}$$

Eq. (7.16) is the continuous pressure condition, and Eq. (7.17) is velocity jump condition at the interface, where Q is the heat addition and S is the cross area. For simplicity, only the fundamental mode is considered. Reflection of the fundamental mode occurs at the two ends of the tube by the coefficients R_0, R_L, respectively. Therefore,

$$Ae^{-i\omega(x-l)/\bar{c}_1}=R_0Be^{i\omega(x-l)/\bar{c}_1}, \tag{7.18}$$

$$De^{i\omega(x-l)/\bar{c}_2}=R_lCe^{-i\omega(x-l)/\bar{c}_2}. \tag{7.19}$$

The heat release function is quoted from Heckl [11],

$$Q=\beta e^{-i\omega\tau}(A-B)/\overline{\rho}c. \tag{7.20}$$

By substituting Q from Eq. (7.20), p' from Eq. (7.14), and u' from Eq. (7.15), then Eqs. (7.16)–(7.19) can be written as a homogeneous set of four equations for the unknowns A, B, C, D,

$$X(\omega)\begin{pmatrix}A\\B\\C\\D\end{pmatrix}=\mathbf{0}. \tag{7.21}$$

The equations have non-trivial solutions if and only if the determinant of the matrix $X(\omega)$ equals zero, that is to say, the disturbances can propagate only if the determinant of $X(\omega)$ vanishes. As a consequence, an eigenvalue problem is established, and the resonance frequency and the growth rate of

the system can be calculated. The specific of the matrix can be easily obtained as:

$$X(\omega)=\begin{pmatrix} e^{i\omega l/c} & -R_0 e^{-i\omega l/c} & 0 & 0 \\ 0 & 0 & R_L e^{-i\omega(L-l)/c} & -e^{-i\omega(L-l)/c} \\ 1 & 1 & -1 & -1 \\ -1-\dfrac{(\gamma-1)\beta e^{-i\omega\tau}}{\overline{\rho}c^2 S} & 1+\dfrac{(\gamma-1)\beta e^{-i\omega\tau}}{\overline{\rho}c^2 S} & 1 & -1 \end{pmatrix}. \tag{7.22}$$

The eigenvalues are the solutions of $\det X(\omega)=0$. With the specific time dependence $e^{i\omega t}$ of the fluctuation component, the stability of the Rijke tube can be determined by examining the imaginary part of the complex eigenfrequency.

Dowling [9] gave a systematic investigation of the various factors that have an influence on the one-dimensional thermoacoustic frequency oscillations. It is found that the form of coupling between the heat input and unsteady flow has a crucial effect on the frequency of oscillation. Actually, by a mean temperature ratio of six, there is about a 60% difference between the lowest frequency predicted for Case II (when the instantaneous rate of heat input is proportional to the instantaneous mass flow rate) and for Case I (when there is no unsteady rate of heat input). The mean flow effects can become significant even at modest inlet Mach numbers, and Dowling indicated a distributed heat input treated as a concentrated one requires not only $\omega d/\overline{c}\ll 1$ but also $\omega d/\overline{u}\ll 1$. It means the entropy wave will be affected by modest spatial distributed heat input. Then, the frequency of the thermoacoustic resonance is significantly altered when the entropy wave is coupled with the acoustic wave.

The one-dimensional calculation method is a prevalent choice to investigate the "reheat buzz," which is an instability phenomenon of the reheat system of a jet engine. The low-frequency instability is caused by the coupling of longitudinal acoustic waves and unsteady combustion [12]. In addition, the model combustor or real aeroengine is often modeled by some individual straight ducts that can be described by one-dimensional disturbances [13–15], as shown in Fig. 7.3. By relating the disturbances in two adjacent ducts through appropriate conservation laws, a closed set of equations is established. Thus, the thermoacoustic dynamics of the system can be analyzed in the preliminary design stage.

The one-dimensional linear calculation is able to analyze the mechanism and characteristic of combustion instability with the advantage of

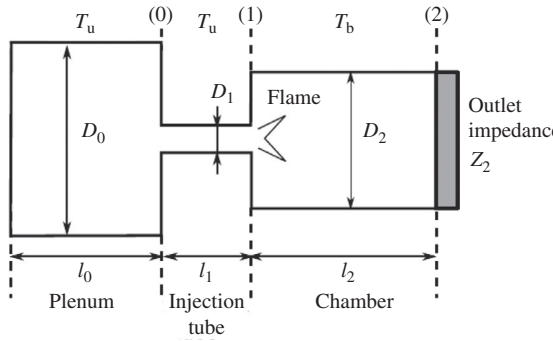

Fig. 7.3 Schematic view of a combustor modeled by three coupled cavities with an arbitrary outlet impedance [13].

convenience and fastness. However, it is deficient for treating more complex situations, for example, it is unable to solve the problem with non-uniform mean velocity or heat distribution, and it cannot solve the eigenvalue problems that involve complex geometries and soft wall boundary conditions. Also, the vorticity plays an important role in the issue of combustion instability, whereas the one-dimensional approach fails to do that. Therefore, researchers have devoted a lot of time and resources toward developing three-dimensional methods of combustion instability.

7.3 Three-dimensional linear combustion instability analysis method

7.3.1 Analytical approach

Although the numerical approach can solve the problem caused by oversimplification, it creates other problems. Actually, whether it is chosen or not depends on the tended object and available resources. For industrial applications, however, fast and reliable calculations for prediction are widely used, which have the following benefits: (1) less cost of both cost and time; (2) more direct physical understanding; and (3) promoting the development of numerical methods. Thus, aiming at the issue of combustion instability, it is necessary to develop a three-dimensional analytical method (AM) for prediction and prevention. This section is based on the work of You et al. [16, 17]. The formulation is created on the premise of uniform mean flow and uniform heat release.

7.3.1.1 Formulation

In the previous section, the basic equations that encompass the circumferential non-uniformities were established. For simplicity, the mean flow is assumed to be one-dimensional homogeneous. The three-dimensional linear equations in cylindrical coordinates of x, r, θ are:

$$\frac{\partial \rho'}{\partial t} + U\frac{\partial \rho'}{\partial x} + \rho_0\left(\frac{\partial u'}{\partial x} + \frac{\partial v'}{r\partial \theta} + \frac{\partial (rw')}{r\partial r}\right) = 0, \tag{7.23}$$

$$\frac{\partial u'}{\partial t} + U\frac{\partial u'}{\partial x} = -\frac{1}{\rho_0}\frac{\partial p'}{\partial x}, \tag{7.24}$$

$$\frac{\partial v'}{\partial t} + U\frac{\partial v'}{\partial x} = -\frac{1}{\rho_0}\frac{\partial p'}{r\partial \theta}, \tag{7.25}$$

$$\frac{\partial w'}{\partial t} + U\frac{\partial w'}{\partial x} = -\frac{1}{\rho_0}\frac{\partial p'}{\partial r}, \tag{7.26}$$

$$\frac{1}{P_0}\left(\frac{\partial p'}{\partial t} + U\frac{\partial p'}{\partial x}\right) - \frac{\gamma}{\rho_0}\left(\frac{\partial \rho'}{\partial t} + U\frac{\partial \rho'}{\partial x}\right) = 0, \tag{7.27}$$

where U is the mean flow velocity, and P_0, ρ_0 are the mean pressure and density, respectively. ρ', u', v', w', p' are the fluctuation quantity of the density, axial velocity, circumferential velocity, radial velocity, and pressure, respectively.

According to Eqs. (7.23) and (7.27), we have:

$$\frac{1}{P_0}\left(\frac{\partial p'}{\partial t} + U\frac{\partial p'}{\partial x}\right) + \gamma\left(\frac{\partial u'}{\partial x} + \frac{\partial v'}{r\partial \theta} + \frac{\partial (rw')}{r\partial r}\right) = 0. \tag{7.28}$$

By differentiating Eq. (7.28) with respect to t and x, we obtain:

$$\frac{1}{P_0}\left(\frac{\partial^2 p'}{\partial t^2} + U\frac{\partial^2 p'}{\partial x \partial t}\right) + \gamma\left(\frac{\partial^2 u'}{\partial x \partial t} + \frac{\partial^2 v'}{r\partial \theta \partial t} + \frac{\partial^2 (rw')}{r\partial r \partial t}\right) = 0, \tag{7.29}$$

$$\frac{1}{P_0}\left(\frac{\partial^2 p'}{\partial t \partial x} + U\frac{\partial^2 p'}{\partial x^2}\right) + \gamma\left(\frac{\partial^2 u'}{\partial x^2} + \frac{\partial^2 v'}{r\partial \theta \partial x} + \frac{\partial^2 (rw')}{r\partial r \partial x}\right) = 0. \tag{7.30}$$

Differentiate Eqs. (7.24), (7.25), and (7.26) with respect to x, r, θ, and add them to Eq. (7.26), then the following partial differential equation is achieved:

$$\begin{aligned}\frac{U}{P_0\gamma}\left(\frac{\partial^2 p'}{\partial x \partial t} + U\frac{\partial^2 p'}{\partial x^2}\right) - \frac{1}{\rho_0}\left(\frac{\partial^2 p'}{\partial x^2} + \frac{\partial^2 p'}{r^2 \partial \theta^2} + \frac{\partial^2 p'}{\partial r^2} + \frac{\partial p'}{r\partial r}\right) \\ - \left(\frac{\partial^2 u'}{\partial t \partial x} + \frac{\partial^2 v'}{r\partial \theta \partial t} + \frac{\partial (rw')}{r\partial t \partial r}\right) = 0.\end{aligned} \tag{7.31}$$

Then, considered together with Eqs. (7.29) and (7.30), we have the final wave equation:

$$\left(M_a^2-1\right)\frac{\partial^2 p'}{\partial x^2}-\frac{\partial^2 p'}{r^2\partial\theta^2}-\frac{\partial^2 p'}{\partial r^2}-\frac{\partial p'}{r\partial r}+\frac{1}{C_0^2}\frac{\partial^2 p'}{\partial t^2}+\frac{2M_a}{C_0}\frac{\partial^2 p'}{\partial x\partial t}=0, \tag{7.32}$$

where M_a is the Mach number of the mean flow, and C_0 is the mean sound speed of the flow field.

According to the theory of mathematical physics, the general solutions of the wave equation can be written as:

$$p'(x,r,\theta,t)=P(x)\psi(r)H(\theta)e^{i\omega t}. \tag{7.33}$$

By substituting Eq. (7.33) into Eq. (7.32), and separating the variables, we have:

$$r^2\left(M_a^2-1\right)\frac{1}{P}\frac{\partial^2 P}{\partial x^2}-r^2\frac{1}{\psi}\frac{\partial^2\psi}{\partial r^2}-\frac{r}{\psi}\frac{\partial\psi}{\partial r}+\frac{2i\omega M_a r^2}{C_0}\frac{1}{P}\frac{\partial P}{\partial x}-\frac{r^2\omega^2}{C_0^2}=\frac{1}{H}\frac{\partial^2 H}{\partial\theta^2}, \tag{7.34}$$

which satisfies:

$$\frac{1}{H}\frac{\partial^2 H}{\partial\theta^2}=\zeta, \tag{7.35}$$

$$r^2\left(M_a^2-1\right)\frac{1}{P}\frac{\partial^2 P}{\partial x^2}-r^2\frac{1}{\psi}\frac{\partial^2\psi}{\partial r^2}-\frac{r}{\psi}\frac{\partial\psi}{\partial r}+\frac{2i\omega M_a r^2}{C_0}\frac{1}{P}\frac{\partial P}{\partial x}-\frac{r^2\omega^2}{C_0^2}=\zeta, \tag{7.36}$$

where ζ denotes a constant. The general solution of Eq. (7.35) is:

$$H=e^{im\theta}, m=\ldots,-2,-1,0,1,2,3,\ldots \tag{7.37}$$

The periodic boundary condition requires that m should be an integer. Therefore,

$$\zeta=-m^2. \tag{7.38}$$

Eq. (7.34) is then equivalent to:

$$\left(M_a^2-1\right)\frac{1}{P}\frac{\partial^2 P}{\partial x^2}-\frac{1}{\psi}\frac{\partial^2\psi}{\partial r^2}-\frac{1}{r\psi}\frac{\partial\psi}{\partial r}+\frac{2i\omega M_a}{C_0}\frac{1}{P}\frac{\partial P}{\partial x}-\frac{\omega^2}{C_0^2}+\frac{m^2}{r^2}=0. \tag{7.39}$$

Separating the variables again gives:

$$\left(M_a^2-1\right)\frac{1}{P}\frac{\partial^2 P}{\partial x^2}+\frac{2i\omega M_a}{a_0}\frac{1}{P}\frac{\partial P}{\partial x}-\frac{\omega^2}{C_0^2}=\frac{1}{\psi}\frac{\partial^2\psi}{\partial r^2}+\frac{1}{r\psi}\frac{\partial\psi}{\partial r}-\frac{m^2}{r^2}. \tag{7.40}$$

It is reasonable only if the following relation is satisfied:

$$\frac{1}{\psi}\frac{\partial^2\psi}{\partial r^2}+\frac{1}{r\psi}\frac{\partial\psi}{\partial r}-\frac{m^2}{r^2}=-\mu. \tag{7.41}$$

If $\mu<0$, the general solutions of Eq. (7.41) are the virtual Bessel equations. However, these kinds of solutions are not significant because the homogenous boundary conditions are not satisfied in this situation. Hence, the situation of $\mu\geq 0$ is what we are going to consider.

If $\mu=0$, to satisfy the natural boundary condition at the center of the cylinder, the general solutions of Eq. (7.41) are:

$$\psi(r)=\begin{cases}E,(m=0)\\ Er^m,(m=1,2,..)\end{cases}. \tag{7.42}$$

The solutions Er^m, $(m=1,2,..)$ should be abandoned because of the homogeneous boundary condition. Therefore, $\psi(r)=E$, $(m=0)$, as this is the solution of a plane wave. Then, it comes to the situation of $\mu>0$. In this situation, the general solutions of Eq. (7.41) are:

$$\psi(r)=AJ_m(k_{mn}r)+BY_m(k_{mn}r), \tag{7.43}$$

where $\mu=k_{mn}^2$, $J_m(k_{mn}r)$, $Y_m(k_{mn}r)$ are m order Bessel function and $-m$ order Bessel function, respectively, and m, n represent the circumferential wave number and the radial wave number, respectively. For the natural boundary condition consideration, the general solutions are reduced to:

$$\psi(r)=AJ_m(k_{mn}r). \tag{7.44}$$

If the wall boundary condition is $\psi'(R)=0$, then:

$$\frac{d}{dr}J_m(k_{mn}R)=0. \tag{7.45}$$

The previous equation determines the eigenvaluek_{mn}. When $m=0$, zero order Bessel function has only one zero eigenvalue, which corresponds to the plane wave. In addition, the primary wave equation has only one unknown function $P(x)$ as follows:

$$\left({M_a}^2-1\right)\frac{1}{P}\frac{\partial^2 P}{\partial x^2}+\frac{2i\omega M_a}{C_0}\frac{1}{P}\frac{\partial P}{\partial x}-\frac{\omega^2}{C_0^2}+k_{mn}^2=0. \tag{7.46}$$

As stated before, the disturbance is assumed to be harmonic for simplicity consideration, thus, $P(x)$ can be written as:

$$P(x)=P_{mn}e^{i\alpha x}, \tag{7.47}$$

where P_{mn} is the complex amplitude. Substituting Eq. (7.47) into Eq. (7.46) leads to:

$$-\left(M_a^2-1\right)\alpha^2-\frac{2\omega M_a}{C_0}\alpha-\left(\frac{\omega^2}{C_0^2}-k_{mn}^2\right)=0. \tag{7.48}$$

Therefore,

$$\alpha_{mn}^{+,-}=\frac{M_a^2\left(\frac{\omega}{C_0}\right)\pm\sqrt{\left(\frac{\omega}{C_0}\right)^2-\left(1-M_a^2\right)k_{mn}^2}}{1-M_a^2}, \tag{7.49}$$

where "+" denotes the downstream direction, and "−" denotes the upstream direction. Hence, the general solution is:

$$P(x)=P_{mn}^{+}e^{i\alpha_{mn}^{+}x}+P_{mn}^{-}e^{i\alpha_{mn}^{-}x}. \tag{7.50}$$

If the waves propagate at the position of x^j, hence,

$$P(x)=P_{mn}^{+}e^{i\alpha_{mn}^{+}(x-x^j)}+P_{mn}^{-}e^{i\alpha_{mn}^{-}(x-x^j)}. \tag{7.51}$$

Consequently, we get the general solution of Eq. (7.32),

$$p^j(x,\theta,r,t)=\sum_{m=-\infty}^{+\infty}\sum_{n=1}^{\infty}\left(P_{mn}^{+\,j}\psi_{mn}^{+\,j}(r)e^{i\alpha_{mn}^{+\,j}(x-x^j)}+P_{mn}^{-\,j}\psi_{mn}^{-\,j}(r)e^{i\alpha_{mn}^{-\,j}(x-x^j)}\right)e^{i(m\theta+\omega t)}. \tag{7.52}$$

The fluctuating velocity solution can be found by solving Eqs. (7.24), (7.25), and (7.26). Also, the velocity can be decomposed into two parts, the velocity induced by pressure fluctuation and the velocity induced by vorticity. Thus,

$$\begin{cases} u'=u_p+u_v \\ v'=v_p+v_v \\ w'=w_p+w_v \end{cases}. \tag{7.53}$$

As the fluctuating pressure is already obtained, according to Eq. (7.24), the first part of the axial velocity fluctuation component is:

$$u_p^j(x,\theta,r,t)=-\sum_{m=-\infty}^{+\infty}\sum_{n=1}^{\infty}\frac{1}{\rho_0^j}\left(\frac{\alpha_{mn}^{+\,j}P_{mn}^{+\,j}\psi_{mn}^{+\,j}(r)e^{i\alpha_{mn}^{+\,j}(x-x^j)}}{\omega+\alpha_{mn}^{+\,j}U^j}+\frac{\alpha_{mn}^{-\,j}P_{mn}^{-\,j}\psi_{mn}^{-\,j}(r)e^{i\alpha_{mn}^{-\,j}(x-x^j)}}{\omega+\alpha_{mn}^{-\,j}U^j}\right)e^{i(m\theta+\omega t)}, \tag{7.54}$$

which is the same as the other two components,

$$v_p^j(x,\theta,r,t) = -\sum_{m=-\infty}^{+\infty}\sum_{n=1}^{\infty}\frac{1}{\rho_0^j}\left(\frac{mP_{mn}^{+\,j}\psi_{mn}^{+\,j}(r)e^{i\alpha_{mn}^{+\,j}(x-x^j)}}{r\left(\omega+\alpha_{mn}^{+\,j}U^j\right)} + \frac{mP_{mn}^{-\,j}\psi_{mn}^{-\,j}(r)e^{i\alpha_{mn}^{-\,j}(x-x^j)}}{r\left(\omega+\alpha_{mn}^{-\,j}U^j\right)}\right)e^{i(m\theta+\omega t)}, \quad (7.55)$$

$$w_p^j(x,\theta,r,t) = \sum_{m=-\infty}^{+\infty}\sum_{n=1}^{\infty}\frac{1}{\rho_0^j}\left(\frac{ik_{mn}P_{mn}^{+\,j}\phi_{mn}^{+\,j}(z)e^{i\alpha_{mn}^{+\,j}(x-x^j)}}{\omega+\alpha_{mn}^{+\,j}U^j} + \frac{ik_{mn}P_{mn}^{-\,j}\phi_{mn}^{-\,j}(z)e^{i\alpha_{mn}^{-\,j}(x-x^j)}}{\omega+\alpha_{mn}^{-\,j}U^j}\right)e^{i(m\theta+\omega t)}, \quad (7.56)$$

where $z = k_{mn}r$, $\phi_{mn}^{+\,j}(z) = \frac{d\psi_{mn}^{+\,j}(r)}{dz}$, $\phi_{mn}^{-\,j}(z) = \frac{d\psi_{mn}^{-\,j}(r)}{dz}$.

On the other hand, we know $Tds = C_p dT + \frac{1}{\rho}dp$, which is equivalent to $d\rho = \frac{1}{c^2}dp - \frac{\rho}{C_p}ds$. From this relation, it can be concluded that the density fluctuation is induced by two factors, the pressure oscillation and the entropy oscillation. Obviously, the density fluctuation induced by pressure oscillation is $\rho_p = \frac{1}{C_0^2}p$, thereby,

$$\rho_p^j(x,\theta,r,t) = \frac{1}{C_0^2}\sum_{m=-\infty}^{+\infty}\sum_{n=1}^{\infty}\left(P_{mn}^{+\,j}\psi_{mn}^{+\,j}(r)e^{i\alpha_{mn}^{+\,j}(x-x^j)} + P_{mn}^{-\,j}\psi_{mn}^{-\,j}(r)e^{i\alpha_{mn}^{-\,j}(x-x^j)}\right)e^{i(m\theta+\omega t)}. \quad (7.57)$$

If the pressure oscillation is zero, Eqs. (7.24), (7.25), and (7.26) have different forms,

$$\frac{\partial u'}{\partial t} + U\frac{\partial u'}{\partial x} = 0, \quad (7.58)$$

$$\frac{\partial v'}{\partial t} + U\frac{\partial v'}{\partial x} = 0, \quad (7.59)$$

$$\frac{\partial w'}{\partial t} + U\frac{\partial w'}{\partial x} = 0. \quad (7.60)$$

The solution of these equations is the vorticity wave that is independent of the pressure wave. The general solution can be written as:

$$u_v^j = \sum_{m=-\infty}^{+\infty}\sum_{n=1}^{+\infty}\overline{u}_{vmn}^j\psi_{vmn}^j(z)e^{-i\frac{\omega}{U^j}(x-x^j)}e^{i(m\theta+\omega t)}, \quad (7.61)$$

$$v_v^j = \sum_{m=-\infty}^{+\infty}\sum_{n=1}^{+\infty}\overline{v}_{vmn}^j\psi_{vmn}^j(z)e^{-i\frac{\omega}{U^j}(x-x^j)}e^{i(m\theta+\omega t)}, \quad (7.62)$$

$$w_v^j = \sum_{m=-\infty}^{+\infty} \sum_{n=1}^{+\infty} \overline{w}_{vmn}^j \phi_{vmn}^j(z) e^{-i\frac{\omega}{U^j}(x-x^j)} e^{i(m\theta+\omega t)}, \tag{7.63}$$

where $\psi_{vmn}^j(z)$ and $\phi_{vmn}^j(z)$ are the corresponding eigenfunctions, respectively.

To obtain the entropy wave, we look back to Eq. (7.27), thus,

$$\frac{\partial s^j}{\partial t} + U\frac{\partial s^j}{\partial x} = 0. \tag{7.64}$$

Because of the adiabatic condition of the wall boundary, we have:

$$\left.\frac{\partial T}{\partial r}\right|_{r=R} = 0. \tag{7.65}$$

Therefore, the general solution of Eq. (7.64) can be written as:

$$s^j = \sum_{m=-\infty}^{+\infty} \sum_{n=1}^{\infty} S_{vmn}^j \psi_{vmn}^j(z) e^{-i\frac{\omega}{U^j}(x-x^j)} e^{i(m\theta+\omega t)}. \tag{7.66}$$

Thereby, we obtain the fluctuating density induced by the entropy oscillation $\rho_s = -\frac{\rho}{C_p} ds$,

$$\rho_s^j = -\frac{\rho_0}{C_p} \sum_{m=-\infty}^{+\infty} \sum_{n=1}^{\infty} S_{vmn}^j \psi_{vmn}^j(z) e^{-i\frac{\omega}{U^j}(x-x^j)} e^{i(m\theta+\omega t)}. \tag{7.67}$$

Finally, we have the fluctuating density in the form of,

$$\begin{aligned}\rho^j(x,\theta,r,t) = \frac{1}{C_0^2} \sum_{m=-\infty}^{+\infty} \sum_{n=1}^{\infty} &\left(P_{mn}^{+\,j} \psi_{mn}^{+\,j}(r) e^{i\alpha_{mn}^{+\,j}(x-x^j)} \right. \\ &\left. + P_{mn}^{-\,j} \psi_{mn}^{-\,j}(r) e^{i\alpha_{mn}^{-\,j}(x-x^j)}\right) e^{i(m\theta+\omega t)} \\ -\frac{\rho_0}{C_p} \sum_{m=-\infty}^{+\infty} \sum_{n=1}^{\infty} &S_{vmn}^j \psi_{vmn}^j(z) e^{-i\frac{\omega}{U^j}(x-x^j)} e^{i(m\theta+\omega t)}.\end{aligned} \tag{7.68}$$

As the pressure, velocity, and density fluctuation quantities are obtained, the discontinuities of temperature or geometry in the flow field can be treated by matching relations. That is to say, the geometry can be divided into as many cells as needed, and the mean flow field can be regarded as approximately even in each cell, which is a good simplification. The different properties in adjacent cells are related by matching conditions, the conservation of mass, momentum, and energy.

As shown in Fig. 7.4, two adjacent cells are separated by a control volume where the discontinuity is located. The matching equations are established at the control volume.

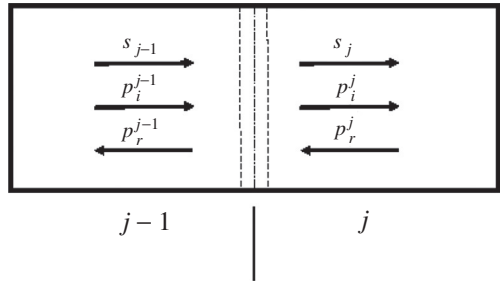

Fig. 7.4 Two adjacent cells.

According to the conservation of mass, for the control volume, it should satisfy,

$$\oint_s \rho \boldsymbol{v} \cdot d\boldsymbol{S} = -\frac{\partial}{\partial t}\int_V \rho d\tau. \tag{7.69}$$

The left-hand side of the equation is the surface integral of the control volume with the infinitesimal $d\boldsymbol{S}$, and the right-hand side of the equation is the volume integral, with the infinitesimal $d\tau$. By linearizing the integral equation, and if the sectional area is assumed to be constant, we obtain:

$$\left(\rho_0^j u^j + \rho^j U^j\right) - \left(\rho_0^{j+1} u^{j+1} + \rho^{j+1} U^{j+1}\right) = 0. \tag{7.70}$$

Substituting Eqs. (7.54) and (7.68) into Eq. (7.70) gives:

$$\begin{aligned}
\rho_0^j u^j + \rho^j U^j = &\sum_{m=-\infty}^{+\infty}\sum_{n=1}^{\infty} -\left(\frac{\alpha_{mn}^{+\,j} P_{mn}^{+\,j} \psi_{mn}^{+\,j}(r) e^{i\alpha_{mn}^{+\,j}(x-x^j)}}{\omega + \alpha_{mn}^{+\,j} U^j} + \frac{\alpha_{mn}^{-\,j} P_{mn}^{-\,j} \psi_{mn}^{-\,j}(r) e^{i\alpha_{mn}^{-\,j}(x-x^j)}}{\omega + \alpha_{mn}^{-\,j} U^j}\right) \\
&+ \frac{1}{C_0^2}\sum_{m=-\infty}^{+\infty}\sum_{n=1}^{\infty}\Big[\Big(P_{mn}^{+\,j}\psi_{mn}^{+\,j}(r)e^{i\alpha_{mn}^{+\,j}(x-x^j)} \\
&\qquad + P_{mn}^{-\,j}\psi_{mn}^{-\,j}(r)e^{i\alpha_{mn}^{-\,j}(x-x^j)}\Big) - \frac{\rho_0}{C_p} S_{\nu mn}^j \psi_{\nu mn}^j(z) e^{-i\frac{\omega}{U^j}(x-x^j)}\Big] U^j \\
= &\sum_{m=-\infty}^{+\infty}\sum_{n=1}^{\infty}\left(\frac{U_j}{C_0^2} - \frac{\alpha_{mn}^{+\,j}}{\omega + \alpha_{mn}^{+\,j} U^j}\right) P_{mn}^{+\,j}\psi_{mn}^{+\,j}(r) e^{i\alpha_{mn}^{+\,j}(x-x^j)} \\
&+ \left(\frac{U_j}{C_0^2} - \frac{\alpha_{mn}^{-\,j}}{\omega + \alpha_{mn}^{-\,j} U^j}\right) P_{mn}^{-\,j}\psi_{mn}^{-\,j}(r) e^{i\alpha_{mn}^{-\,j}(x-x^j)} \\
&+ U^j \rho_{\nu mn}^j \psi_{\nu mn}^j(z) e^{-i\frac{\omega}{U^j}(x-x^j)},
\end{aligned} \tag{7.71}$$

$$\rho_0^j u^j + \rho^j U^j = \sum_{m=-\infty}^{+\infty}\sum_{n=1}^{\infty} -\left(\frac{\alpha_{mn}^{+\,j} P_{mn}^{+\,j}\psi_{mn}^{+\,j}(r)e^{i\alpha_{mn}^{+\,j}(x-x^j)}}{\omega+\alpha_{mn}^{+\,j}U^j} + \frac{\alpha_{mn}^{-\,j} P_{mn}^{-\,j}\psi_{mn}^{-\,j}(r)e^{i\alpha_{mn}^{-\,j}(x-x^j)}}{\omega+\alpha_{mn}^{-\,j}U^j}\right)$$

$$+\sum_{m=-\infty}^{+\infty}\sum_{n=1}^{\infty}\left[\frac{1}{C_0^2}\left(P_{mn}^{+\,j}\psi_{mn}^{+\,j}(r)e^{i\alpha_{mn}^{+\,j}(x-x^j)} + P_{mn}^{-\,j}\psi_{mn}^{-\,j}(r)e^{i\alpha_{mn}^{-\,j}(x-x^j)}\right) - \frac{\rho_0}{C_p}S_{vmn}^j\psi_{vmn}^j(z)e^{-i\frac{\omega}{U^j}(x-x^j)}\right]U^j$$

$$=\sum_{m=-\infty}^{+\infty}\sum_{n=1}^{\infty}\left(\frac{U_j}{C_0^2}-\frac{\alpha_{mn}^{+\,j}}{\omega+\alpha_{mn}^{+\,j}U^j}\right)P_{mn}^{+\,j}\psi_{mn}^{+\,j}(r)e^{i\alpha_{mn}^{+\,j}(x-x^j)} + \left(\frac{U_j}{C_0^2}-\frac{\alpha_{mn}^{-\,j}}{\omega+\alpha_{mn}^{-\,j}U^j}\right)P_{mn}^{-\,j}\psi_{mn}^{-\,j}(r)e^{i\alpha_{mn}^{-\,j}(x-x^j)} + U^j\rho_{vmn}^j\psi_{vmn}^j(z)e^{-i\frac{\omega}{U^j}(x-x^j)},$$

where $\rho_{vmn}{}^j = -\frac{\rho_0}{C_p}S_{vmn}^j$, which is the fluctuating density induced by the entropy fluctuation. Let $L^j = x - x^j$. Because every term contains the dependent $e^{i(m\theta+\omega t)}$, Eq. (7.71) is then reduced to:

$$\rho_0^j u^j + \rho^j U^j = \sum_{m=-\infty}^{+\infty}\sum_{n=1}^{\infty}\left(\frac{U^j}{C_0^2}-\frac{\alpha_{mn}^{+\,j}}{\omega+\alpha_{mn}^{+\,j}U^j}\right)P_{mn}^{+\,j}\psi_{mn}^{+\,j}(r)e^{i\alpha_{mn}^{+\,j}L^j} + \left(\frac{U_j}{C_0^2}-\frac{\alpha_{mn}^{-\,j}}{\omega+\alpha_{mn}^{-\,j}U^j}\right)P_{mn}^{-\,j}\psi_{mn}^{-\,j}(r)e^{i\alpha_{mn}^{-\,j}L^j} + U^j\rho_{vmn}^j\psi_{vmn}^j(z)e^{-i\frac{\omega}{U^j}L^j}. \tag{7.72}$$

Similarly,

$$\rho_0^{j+1}u^{j+1} + \rho^{j+1}U^{j+1} = \sum_{m=-\infty}^{+\infty}\sum_{n=1}^{\infty}\left(\frac{U^{j+1}}{C_0^2}-\frac{\alpha_{mn}^{+\,j+1}}{\omega+\alpha_{mn}^{+\,j+1}U^{j+1}}\right)P_{mn}^{+\,j+1}\psi_{mn}^{+\,j+1}(r) + \left(\frac{U^{j+1}}{C_0^2}-\frac{\alpha_{mn}^{-\,j+1}}{\omega+\alpha_{mn}^{-\,j+1}U^{j+1}}\right)P_{mn}^{-\,j+1}\psi_{mn}^{-\,j+1}(r) + U^{j+1}\rho_{vmn}^{j+1}\psi_{vmn}^{j+1}(z). \tag{7.73}$$

In fact, for every circumferential mode, according to Eq. (7.70), we obtain,

$$\begin{aligned}&\sum_{n=1}^{\infty}[A_{mn}^{+\,j}\psi_{mn}^{+\,j}(r)P_{mn}^{+\,j} + A_{mn}^{-\,j}\psi_{mn}^{-\,j}(r)P_{mn}^{-\,j} + A_{vmn}^{+\,j}\psi_{vmn}^{+\,j}(r)\rho_{vmn}^{+\,j}\\ &+A_{mn}^{+\,j+1}\psi_{mn}^{+\,j+1}(r)P_{mn}^{+\,j+1} + A_{mn}^{-\,j+1}\psi_{mn}^{-\,j+1}(r)P_{mn}^{-\,j+1}\\ &+A_{vmn}^{+\,j+1}\psi_{vmn}^{+\,j+1}(r)\rho_{vmn}^{+\,j+1}] = 0.\end{aligned} \tag{7.74}$$

The coefficients are listed in Appendix A.

According to the momentum conservation of the control volume,

$$\int_v \frac{\partial \rho \boldsymbol{v}}{\partial t} d\tau + \oint_s \rho u_n \boldsymbol{v} d\boldsymbol{s} + \oint_s n_u \cdot p d\boldsymbol{s} = 0. \tag{7.75}$$

Similarly, by taking the linearization and expansion, we obtain:

$$\left(2U^j \rho_0^j u^j + U^{j^2} \rho^j\right) - \left(2U^{j+1} \rho_0^{j+1} u^{j+1} + U^{(j+1)^2} \rho^{j+1}\right) = p^{j+1} - p^j. \tag{7.76}$$

Substituting Eqs. (7.54) and (7.68) into Eq. (7.76) leads to:

$$\begin{aligned} &\sum_{n=1}^{\infty} [B_{mn}^{+\,j} \psi_{mn}^{+\,j}(r) P_{mn}^{+\,j} + B_{mn}^{-\,j} \psi_{mn}^{-\,j}(r) P_{mn}^{-\,j} + B_{vmn}^{+\,j} \psi_{vmn}^{+\,j}(r) \rho_{vmn}^{+\,j} \\ &+ B_{mn}^{+\,j+1} \psi_{mn}^{+\,j+1}(r) P_{mn}^{+\,j+1} + B_{mn}^{-\,j+1} \psi_{mn}^{-\,j+1}(r) P_{mn}^{-\,j+1} \\ &+ B_{vmn}^{+\,j+1} \psi_{vmn}^{+\,j+1}(r) \rho_{vmn}^{+\,j+1}] = 0. \end{aligned} \tag{7.77}$$

The coefficients are presented in Appendix A.

For the conservation of energy, the following relation is to be satisfied,

$$\int_v \frac{\partial}{\partial t} \rho \left(e + \frac{u^2}{2}\right) d\tau + \oint_s \left(e + \frac{p}{\rho} + \frac{u^2}{2}\right) \rho u ds = 0. \tag{7.78}$$

Similarly, we can have the following form equation,

$$\begin{aligned} &U^j \left(\frac{\gamma}{\gamma - 1} + \frac{\left(M_a^j\right)^2}{2}\right) p^j + \left(\frac{\gamma P_0^j}{\gamma - 1} + \frac{3}{2} \rho_0^j \left(U^j\right)^2\right) u^j \\ &- \frac{\rho_0^j \left(U^j\right)^3}{2C_p} s^j = U^{j+1} \left(\frac{\gamma}{\gamma - 1} + \frac{\left(M_a^{j+1}\right)^2}{2}\right) p^{j+1} \\ &+ \left(\frac{\gamma P_0^{j+1}}{\gamma - 1} + \frac{3}{2} \rho_0^{j+1} \left(U^{j+1}\right)^2\right) u^{j+1} - \frac{\rho_0^{j+1} \left(U^{j+1}\right)^3}{2C_p} s^{j+1} - Q_h^j, \end{aligned} \tag{7.79}$$

where Q_h^j is the heat release at the interface, and $s^j = \frac{C_p}{\rho_0} \frac{1}{c_0^2} p^j - \frac{C_p}{\rho_0} \rho^j$. Substituting the fluctuation quantities into this equation results in:

$$\begin{aligned} &\sum_{n=1}^{\infty} [C_{mn}^{+\,j} \psi_{mn}^{+\,j}(r) P_{mn}^{+\,j} + C_{mn}^{-\,j} \psi_{mn}^{-\,j}(r) P_{mn}^{-\,j} + C_{vmn}^{+\,j} \psi_{vmn}^{+\,j}(r) \rho_{vmn}^{+\,j} \\ &+ C_{mn}^{+\,j+1} \psi_{mn}^{+\,j+1}(r) P_{mn}^{+\,j+1} + C_{mn}^{-\,j+1} \psi_{mn}^{-\,j+1}(r) P_{mn}^{-\,j+1} \\ &+ C_{vmn}^{+\,j+1} \psi_{vmn}^{+\,j+1}(r) \rho_{vmn}^{+\,j+1}] = Q_h^j. \end{aligned} \tag{7.80}$$

The coefficients are also listed in Appendix A. To close the equations, the boundary conditions and heat release functions should be given. Here, the inlet and the outlet boundary conditions are given as impedance forms:

$$\frac{p^j}{u^j} = z_0, \frac{p^{j+1}}{u^{j+1}} = z_{end}, \tag{7.81}$$

where z_0 and z_{end} are the impedance of the inlet and outlet of the combustor, respectively. The two boundary conditions can also be expanded as:

$$\begin{aligned}&\sum_{n=1}^{\infty}[D_{mn}^{+\,j}\psi_{mn}^{+\,j}(r)P_{mn}^{+\,j} + D_{mn}^{-\,j}\psi_{mn}^{-\,j}(r)P_{mn}^{-\,j} + D_{vmn}^{+\,j}\psi_{vmn}^{+\,j}(r)\rho_{vmn}^{+\,j}\\&+D_{mn}^{+\,j+1}\psi_{mn}^{+\,j+1}(r)P_{mn}^{+\,j+1} + D_{mn}^{-\,j+1}\psi_{mn}^{-\,j+1}(r)P_{mn}^{-\,j+1}\\&+D_{vmn}^{+\,j+1}\psi_{vmn}^{+\,j+1}(r)\rho_{vmn}^{+\,j+1}] = 0,\end{aligned} \tag{7.82}$$

$$\begin{aligned}&\sum_{n=1}^{\infty}[E_{mn}^{+\,j}\psi_{mn}^{+\,j}(r)P_{mn}^{+\,j} + E_{mn}^{-\,j}\psi_{mn}^{-\,j}(r)P_{mn}^{-\,j} + E_{vmn}^{+\,j}\psi_{vmn}^{+\,j}(r)\rho_{vmn}^{+\,j}\\&+E_{mn}^{+\,j+1}\psi_{mn}^{+\,j+1}(r)P_{mn}^{+\,j+1} + E_{mn}^{-\,j+1}\psi_{mn}^{-\,j+1}(r)P_{mn}^{-\,j+1}\\&+E_{vmn}^{+\,j+1}\psi_{vmn}^{+\,j+1}(r)\rho_{vmn}^{+\,j+1}] = 0.\end{aligned} \tag{7.83}$$

The unsteady heat release is written as a function of pressure oscillation and velocity oscillation,

$$Q_h^j = R_p p^j + R_v u^j, \tag{7.84}$$

which is similarly expanded as:

$$\begin{aligned}&\sum_{n=1}^{\infty}[F_{mn}^{+\,j}\psi_{mn}^{+\,j}(r)P_{mn}^{+\,j} + F_{mn}^{-\,j}\psi_{mn}^{-\,j}(r)P_{mn}^{-\,j} + F_{vmn}^{+\,j}\psi_{vmn}^{+\,j}(r)\rho_{vmn}^{+\,j}\\&+F_{mn}^{+\,j+1}\psi_{mn}^{+\,j+1}(r)P_{mn}^{+\,j+1} + F_{mn}^{-\,j+1}\psi_{mn}^{-\,j+1}(r)P_{mn}^{-\,j+1}\\&+F_{vmn}^{+\,j+1}\psi_{vmn}^{+\,j+1}(r)\rho_{vmn}^{+\,j+1}] = Q_h^j.\end{aligned} \tag{7.85}$$

The coefficients D_{mn}, E_{mn}, F_{mn} are listed in Appendix A.

In summary, three conservation equations are established on every interface without heat release when the cooling air and dissipation of the wall are ignored. The two boundary conditions need to be satisfied at the inlet and outlet of the combustor. Therefore, when one more interface is added for consideration, three new unknowns are produced, and three more conservation equations of the new unknowns of P^+, P^-, ρ^+ are established. For the interface added with heat release, apart from the three conservation equations, the heat release function equation is formed. Hence, four more equations with four more unknowns can be established. This also implies that, no matter how many interfaces are concerned, the equations are closed.

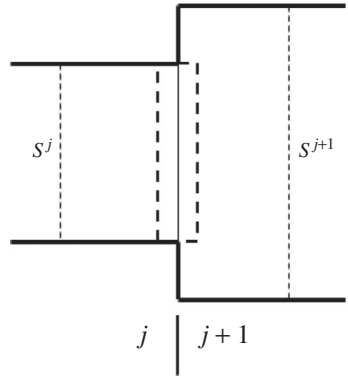

Fig. 7.5 Break section.

7.3.1.2 Solution to variable cross-section cases

In the previous model, the variation of cross-section of the tube is ignored, thus, it is only valid for the straight tube. However, in practical use, few combustors are designed without cross-section variation. To update the model, we use the method developed by Alfredson [18], which is initially applied to study the characteristic of acoustics propagation in a variable cross-section.

As shown in Fig. 7.5, the cross-section of the right side is larger than that of the left side. By applying the conservation of mass and linearizing it, we obtain:

$$\left(\rho_0^j u^j + \rho^j U^j\right) S^j - \left(\rho_0^{j+1} u^{j+1} + \rho^{j+1} U^{j+1}\right) S^{j+1} = 0, \tag{7.86}$$

where S^j is the area of cross-section of the left straight tube, and S^{j+1} is the area of that of the right straight tube. Because of the different areas, the radial eigenfunction $\psi_{mn}^j(r)$ in Eq. (7.72) and $\psi_{mn}^{j+1}(r)$ in Eq. (7.73) are not the same. Substitute the fluctuation quantities into Eq. (7.86), we get,

$$\begin{aligned}
&\sum_{n=1}^{\infty}[A_{mn}^{+\,j}\psi_{mn}^{+\,j}(r)P_{mn}^{+\,j} + A_{mn}^{-\,j}\psi_{mn}^{-\,j}(r)P_{mn}^{-\,j} + A_{vmn}^{+\,j}\psi_{vmn}^{+\,j}(r)\rho_{vmn}^{+\,j} \\
&+A_{mn}^{+\,j+1}\psi_{mn}^{+\,j+1}(r)P_{mn}^{+\,j+1} + A_{mn}^{-\,j+1}\psi_{mn}^{-\,j+1}(r)P_{mn}^{-\,j+1} \\
&+A_{vmn}^{+\,j+1}\psi_{vmn}^{+\,j+1}(r)\rho_{vmn}^{+\,j+1}] = 0.
\end{aligned} \tag{7.87}$$

Although Eq. (7.87) is similar to Eq. (7.74), the difference between $\psi_{mn}^j(r)$ and $\psi_{mn}^{j+1}(r)$ makes them different. As a result, we cannot separate the radial mode from each other as before. They are tangled with each other. Without consideration of the circumferential modes, Alfredson presented an

approach to figure it out. For example, if $m = 0$, multiply Eq. (7.87) by r, and integrate it from 0 to r_j that is the radius of the left tube, then we have:

$$\begin{aligned}
&A_{01}^{+\,j}P_{01}^{+\,j}\int_0^{r_j} rdr + A_{01}^{-\,j}P_{01}^{-\,j}\int_0^{r_j} rdr + A_{\nu 01}^{+\,j}\rho_{\nu 01}^{+\,j}\int_0^{r_j} rdr \\
&+\sum_{n=2}^{N}\left[A_{mn}^{+\,j}P_{mn}^{+\,j}\int_0^{r_j} r\psi_{mn}^{j}(r)dr + A_{mn}^{-\,j}P_{mn}^{-\,j}\int_0^{r_j} r\psi_{mn}^{j}(r)dr + A_{\nu mn}^{+\,j}\rho_{\nu mn}^{+\,j}\int_0^{r_j} r\psi_{mn}^{j}(r)dr\right] \\
&+A_{01}^{+\,j+1}P_{01}^{+\,j+1}\int_0^{r_j} rdr + A_{01}^{-\,j+1}P_{01}^{-\,j+1}\int_0^{r_j} rdr + A_{\nu 01}^{+\,j+1}\rho_{\nu 01}^{+\,j+1}\int_0^{r_j} rdr \\
&+\sum_{n=2}^{N}[A_{mn}^{+\,j+1}P_{mn}^{+\,j+1}\int_0^{r_j} r\psi_{mn}^{j+1}(r)dr + A_{mn}^{-\,j+1}P_{mn}^{-\,j+1}\int_0^{r_j} r\psi_{mn}^{j+1}(r)dr \\
&+A_{\nu mn}^{+\,j+1}\rho_{\nu mn}^{+\,j+1}\int_0^{r_j} r\psi_{mn}^{j+1}(r)dr] = 0.
\end{aligned} \tag{7.88}$$

Because in the range of (r_j, r_{j+1}) in the control volume, $u = 0$. Therefore, $\rho_0^{j+1}u^{j+1} = 0$. Multiplying it by r and then integrating it from r_j to r_{j+1} gives:

$$\begin{aligned}
&\frac{\alpha_{01}^{+\,j+1}P_{01}^{+\,j+1}}{\omega + \alpha_{mn}^{+\,j+1}U^{j+1}}\int_{r_j}^{r_{j+1}} rdr + \frac{\alpha_{01}^{-\,j+1}P_{01}^{-\,j+1}}{\omega + \alpha_{mn}^{-\,j+1}U^{j+1}}\int_{r_j}^{r_{j+1}} rdr \\
&+\sum_{n=2}^{\infty}\left(\frac{\alpha_{mn}^{+\,j+1}P_{mn}^{+\,j+1}\int_{r_j}^{r_{j+1}} r\psi_{mn}^{j+1}(r)dr}{\omega + \alpha_{mn}^{+\,j+1}U^{j+1}} + \frac{\alpha_{mn}^{-\,j+1}P_{mn}^{-\,j+1}\int_{r_j}^{r_{j+1}} r\psi_{mn}^{j+1}(r)dr}{\omega + \alpha_{mn}^{-\,j+1}U^{j+1}}\right) = 0,
\end{aligned} \tag{7.89}$$

Add Eqs. (7.88) and (7.89) together, and we get:

$$\begin{aligned}
&Ab_{101}^{+\,j}P_{01}^{+\,j} + Ab_{101}^{-\,j}P_{01}^{-\,j} + Ab_{\nu 101}^{+\,j}\rho_{\nu 01}^{+\,j} \\
&+\sum_{n=2}^{N}\left[Ab_{1mn}^{+\,j}P_{0n}^{+\,j} + Ab_{1mn}^{-\,j}P_{0n}^{-\,j} + Ab_{\nu 1mn}^{+\,j}\rho_{\nu 0n}^{+\,j}\right] \\
&+Ab_{101}^{+\,j+1}P_{01}^{+\,j+1} + Ab_{101}^{-\,j+1}P_{01}^{-\,j+1} + Ab_{\nu 101}^{+\,j+1}\rho_{\nu 01}^{+\,j+1} \\
&+\sum_{n=2}^{N}\left[Ab_{1mn}^{+\,j+1}P_{0n}^{+\,j+1} + Ab_{1mn}^{-\,j+1}P_{0n}^{-\,j+1} + Ab_{\nu 1mn}^{+\,j+1}\rho_{\nu mn}^{+\,j+1}\right] = 0.
\end{aligned} \tag{7.90}$$

where Ab_{10n} is an expression including A and integration of ψ. "1" in the subscript represents the first kind of integration, distinguishing it from the other kind to be presented next. "n" means the radial mode number.

The circumferential mode number is zero. The specific coefficients are shown in Appendix B.

Similarly, for the momentum integral,

$$\left(2U^j\rho_0^j u^j + U^{j^2}\rho^j\right)S^j - \left(2U^{j+1}\rho_0^{j+1}u^{j+1} + U^{(j+1)^2}\rho^{j+1}\right)S^j = p^{j+1}S^j - p^jS^j. \tag{7.91}$$

It can be written as the same form with Eq. (7.90) as:

$$\begin{aligned}&\sum_{n=1}^{\infty}[B_{mn}^{+\,j}\psi_{mn}^{+\,j}(r)P_{mn}^{+\,j} + B_{mn}^{-\,j}\psi_{mn}^{-\,j}(r)P_{mn}^{-\,j} + B_{vmn}^{+\,j}\psi_{vmn}^{+\,j}(r)\rho_{vmn}^{+\,j}\\&+B_{mn}^{+\,j+1}\psi_{mn}^{+\,j+1}(r)P_{mn}^{+\,j+1} + B_{mn}^{-\,j+1}\psi_{mn}^{-\,j+1}(r)P_{mn}^{-\,j+1}\\&+B_{vmn}^{+\,j+1}\psi_{vmn}^{+\,j+1}(r)\rho_{vmn}^{+\,j+1}] = 0.\end{aligned} \tag{7.92}$$

By the same token, the circumferential mode number $m = 0$, when $n = 1$, $K_{mn} = 0$, then $\psi_{01}^{+j}(r) = 1$. Thus, if Eq. (7.92) is multiplied by r, and integrated from 0 to r_j, we obtain,

$$\begin{aligned}&B_{01}^{+\,j}P_{01}^{+\,j}\int_0^{r_j} r dr + B_{01}^{-\,j}P_{01}^{-\,j}\int_0^{r_j} r dr + B_{v01}^{+\,j}\rho_{v01}^{+\,j}\int_0^{r_j} r dr\\&+\sum_{n=2}^{N}\left[\begin{array}{c}B_{mn}^{+\,j}P_{mn}^{+\,j}\int_0^{r_j} r\psi_{mn}^{j}(r)dr + B_{mn}^{-\,j}P_{mn}^{-\,j}\int_0^{r_j} r\psi_{mn}^{j}(r)dr\\+B_{vmn}^{+\,j}\rho_{vmn}^{+\,j}\int_0^{r_j} r\psi_{mn}^{j}(r)dr\end{array}\right]\\&+B_{01}^{+\,j+1}P_{01}^{+\,j+1}\int_0^{r_j} r dr + B_{01}^{-\,j+1}P_{01}^{-\,j+1}\int_0^{r_j} r dr + B_{v01}^{+\,j+1}\rho_{v01}^{+\,j+1}\int_0^{r_j} r dr\\&+\sum_{n=2}^{N}\left[\begin{array}{c}B_{mn}^{+\,j+1}P_{mn}^{+\,j+1}\int_0^{r_j} r\psi_{mn}^{j+1}(r)dr + B_{mn}^{-\,j+1}P_{mn}^{-\,j+1}\int_0^{r_j} r\psi_{mn}^{j+1}(r)dr\\+B_{vmn}^{+\,j+1}\rho_{vmn}^{+\,j+1}\int_0^{r_j} r\psi_{mn}^{j+1}(r)dr\end{array}\right]\\&= 0.\end{aligned} \tag{7.93}$$

Because the axial velocity in the range of (r_j, r_{j+1}) is zero, therefore, $2U^{j+1}\rho_0^{j+1}u^{j+1} = 0$. Multiplying it by r and integrating it from r_j to r_{j+1} results in:

$$2U^{j+1}\sum_{n=1}^{\infty}\left[\begin{array}{c}\dfrac{\alpha_{mn}^{+\,j+1}P_{mn}^{+\,j+1}\int_{r^j}^{r^{j+1}} r\psi_{mn}^{j+1}(r)dr}{\omega + \alpha_{mn}^{+\,j+1}U^{j+1}}\\+\dfrac{\alpha_{mn}^{-\,j+1}P_{mn}^{-\,j+1}\int_{r^j}^{r^{j+1}} r\psi_{mn}^{j+1}(r)dr}{\omega + \alpha_{mn}^{-\,j+1}U^{j+1}}\end{array}\right] = 0. \tag{7.94}$$

Adding Eq. (7.93) to Eq. (7.94), we obtain,

$$\begin{aligned}
&Bb_{101}^{+\,j}P_{01}^{+\,j}+Bb_{101}^{-\,j}P_{01}^{-\,j}+Bb_{\nu101}^{+\,j}\rho_{\nu01}^{+\,j}\\
&+\sum_{n=2}^{N}\left[Bb_{1mn}^{+\,j}P_{mn}^{+\,j}+Bb_{1mn}^{-\,j}P_{mn}^{-\,j}+Bb_{\nu1mn}^{+\,j}\rho_{\nu mn}^{+\,j}\right]\\
&+Bb_{101}^{+\,j+1}P_{01}^{+\,j+1}+Bb_{101}^{-\,j+1}P_{01}^{-\,j+1}+Bb_{\nu101}^{+\,j+1}\rho_{\nu01}^{+\,j+1}\\
&+\sum_{n=2}^{N}\left[Bb_{1mn}^{+\,j+1}P_{mn}^{+\,j+1}+Bb_{1mn}^{-\,j+1}P_{mn}^{-\,j+1}+Bb_{\nu1mn}^{+\,j+1}\rho_{\nu mn}^{+\,j+1}\right]=0,
\end{aligned}\tag{7.95}$$

The explanation about the subscripts in Bb_{101}^{j} is the same with that in Ab_{10n}. When Eq. (7.92) is multiplied by $r\psi_{0\nu}^{+\,j}(r)(\nu\neq 1)$ and integrated from 0 to r_j, we have:

$$\begin{aligned}
&B_{01}^{+\,j}P_{01}^{+\,j}\int_0^{r_j}r\psi_{m\nu}^{j}(r)dr+B_{01}^{-\,j}P_{01}^{-\,j}\int_0^{r_j}r\psi_{m\nu}^{j}(r)dr\\
&+B_{\nu01}^{+\,j}\rho_{\nu01}^{+\,j}\int_0^{r_j}r\psi_{m\nu}^{j}(r)dr\\
&+\sum_{n=2}^{N}\begin{bmatrix}B_{mn}^{+\,j}P_{mn}^{+\,j}\int_0^{r_j}r\psi_{mn}^{j}(r)\psi_{m\nu}^{j}(r)dr\\+B_{mn}^{-\,j}P_{mn}^{-\,j}\int_0^{r_j}r\psi_{mn}^{j}(r)\psi_{m\nu}^{j}(r)dr\\+B_{\nu mn}^{+\,j}\rho_{\nu mn}^{+\,j}\int_0^{r_j}r\psi_{mn}^{j}\psi_{m\nu}^{j}(r)(r)dr\end{bmatrix}\\
&+B_{01}^{+\,j+1}P_{01}^{+\,j+1}\int_0^{r_j}r\psi_{m\nu}^{j}(r)dr+B_{01}^{-\,j+1}P_{01}^{-\,j+1}\int_0^{r_j}r\psi_{m\nu}^{j}(r)dr\\
&+B_{\nu01}^{+\,j+1}\rho_{\nu01}^{+\,j+1}\int_0^{r_j}r\psi_{m\nu}^{j}(r)dr\\
&+\sum_{n=2}^{N}\begin{bmatrix}B_{mn}^{+\,j+1}P_{mn}^{+\,j+1}\int_0^{r_j}r\psi_{mn}^{j+1}(r)\psi_{m\nu}^{j}(r)dr\\+B_{mn}^{-\,j+1}P_{mn}^{-\,j+1}\int_0^{r_j}r\psi_{mn}^{j+1}(r)\psi_{m\nu}^{j}(r)dr\\+B_{\nu mn}^{+\,j+1}\rho_{\nu mn}^{+\,j+1}\int_0^{r_j}r\psi_{mn}^{j+1}(r)\psi_{m\nu}^{j}(r)dr\end{bmatrix}=0,
\end{aligned}\tag{7.96}$$

In the range of (r_j, r_{j+1}) in the control volume, $u = 0$. Therefore, $2U^{j+1}\rho_0^{j+1}u^{j+1} = 0$. Multiplying it by $n\psi_{0\nu}^{+j}(r)$ and then integrating it from r_j to r_{j+1}, and then combined with Eq. (7.93), we obtain:

$$\begin{aligned}
&Bb_{201}^{+j}P_{01}^{+j} + Bb_{201}^{-j}P_{01}^{-j} + Bb_{\nu 201}^{+j}\rho_{\nu 01}^{+j} \\
&+\sum_{n=2}^{N}\left[Bb_{2mn}^{+j}P_{mn}^{+j} + Bb_{2mn}^{-j}P_{mn}^{-j} + Bb_{\nu 2mn}^{+j}\rho_{vmn}^{+j}\right] \\
&+Bb_{201}^{+j+1}P_{01}^{+j+1} + Bb_{201}^{-j+1}P_{01}^{-j+1} + Bb_{\nu 201}^{+j+1}\rho_{\nu 01}^{+j+1} \\
&+\sum_{n=2}^{N}\left[Bb_{2mn}^{+j+1}P_{mn}^{+j+1} + Bb_{2mn}^{-j+1}P_{mn}^{-j+1} + Bb_{\nu 2mn}^{+j+1}\rho_{vmn}^{+j+1}\right] = 0
\end{aligned} \tag{7.97}$$

The coefficients are presented in Appendix B.

For energy conservation, we have,

$$\begin{aligned}
&U^j\left(\frac{\gamma}{\gamma-1} + \frac{\left(M_a^j\right)^2}{2}\right)p^j + \left(\frac{\gamma P_0^j}{\gamma-1} + \frac{3}{2}\rho_0^j\left(U^j\right)^2\right)u^j - \frac{\rho_0^j\left(U^j\right)^3}{2C_p}s^j \\
&= U^{j+1}\left(\frac{\gamma}{\gamma-1} + \frac{\left(M_a^{j+1}\right)^2}{2}\right)p^{j+1} + \left(\frac{\gamma P_0^{j+1}}{\gamma-1} + \frac{3}{2}\rho_0^{j+1}\left(U^{j+1}\right)^2\right)u^{j+1} \\
&\quad - \frac{\rho_0^{j+1}\left(U^{j+1}\right)^3}{2C_p}s^{j+1}.
\end{aligned} \tag{7.98}$$

Substituting the fluctuation quantities into Eq. (7.98) leads to:

$$\sum_{n=1}^{\infty}\begin{bmatrix}
C_{mn}^{+j}\psi_{mn}^{+j}(r)P_{mn}^{+j} + C_{mn}^{-j}\psi_{mn}^{-j}(r)P_{mn}^{-j} \\
+C_{vmn}^{+j}\psi_{vmn}^{+j}(r)\rho_{vmn}^{+j} \\
+C_{mn}^{+j+1}\psi_{mn}^{+j+1}(r)P_{mn}^{+j+1} + C_{mn}^{-j+1}\psi_{mn}^{-j+1}(r)P_{mn}^{-j+1} \\
+C_{vmn}^{+j+1}\psi_{vmn}^{+j+1}(r)\rho_{vmn}^{+j+1}
\end{bmatrix} = Q_h^j. \tag{7.99}$$

By the same token, the circumferential mode number $m = 0$, when $n = 1$, $K_{mn} = 0$, then $\psi_{01}^{+j}(r) = 1$. Thus, if Eq. (7.99) is multiplied by r, and integrated from 0 to r_j, we obtain:

$$
\begin{aligned}
&C_{01}^{+\,j}P_{01}^{+\,j}\int_0^{r_j} rdr + C_{01}^{-\,j}P_{01}^{-\,j}\int_0^{r_j} rdr + C_{\nu 01}^{+\,j}\rho_{\nu 01}^{+\,j}\int_0^{r_j} rdr \\
&+\sum_{n=2}^{N}\left[C_{mn}^{+\,j}P_{mn}^{+\,j}\int_0^{r_j} r\psi_{mn}^{j}(r)dr + C_{mn}^{-\,j}P_{mn}^{-\,j}\int_0^{r_j} r\psi_{mn}^{j}(r)dr + C_{\nu mn}^{+\,j}\rho_{\nu mn}^{+\,j}\int_0^{r_j} r\psi_{mn}^{j}(r)dr\right] \\
&+C_{01}^{+\,j+1}P_{01}^{+\,j+1}\int_0^{r_j} rdr + C_{01}^{-\,j+1}P_{01}^{-\,j+1}\int_0^{r_j} rdr \\
&+C_{\nu 01}^{+\,j+1}\rho_{\nu 01}^{+\,j+1}\int_0^{r_j} rdr \\
&+\sum_{n=2}^{N}[C_{mn}^{+\,j+1}P_{mn}^{+\,j+1}\int_0^{r_j} r\psi_{mn}^{j+1}(r)dr + C_{mn}^{-\,j+1}P_{mn}^{-\,j+1}\int_0^{r_j} r\psi_{mn}^{j+1}(r)dr \\
&+C_{\nu mn}^{+\,j+1}\rho_{\nu mn}^{+\,j+1}\int_0^{r_j} r\psi_{mn}^{j+1}(r)dr] = 0.
\end{aligned}
\tag{7.100}
$$

Because the axial velocity in the range of (r_j, r_{j+1}) is zero, therefore, $\left(\frac{\gamma P_0^{j+1}}{\gamma-1} + \frac{3}{2}\rho_0^{j+1}U^{j+1^2}\right)\rho_0^{j+1}u^{j+1} = 0$, multiplying it by r, and integrating it from r_j to r_{j+1}gives:

$$
\left(\frac{\gamma P_0^{j+1}}{\gamma-1} + \frac{3}{2}\rho_0^{j+1}U^{j+1^2}\right)\sum_{n=1}^{\infty}\left[\begin{aligned}
&\frac{\alpha_{mn}^{+\,j+1}P_{mn}^{+\,j+1}\int_{r^j}^{r^{j+1}} r\psi_{mn}^{j+1}(r)dr}{\omega + \alpha_{mn}^{+\,j+1}U^{j+1}} \\
&+\frac{\alpha_{mn}^{-\,j+1}P_{mn}^{-\,j+1}\int_{r^j}^{r^{j+1}} r\psi_{mn}^{j+1}(r)dr}{\omega + \alpha_{mn}^{-\,j+1}U^{j+1}}
\end{aligned}\right] = 0.
\tag{7.101}
$$

Adding Eqs. (7.100) and (7.101) up, we have:

$$
\begin{aligned}
&Cb_{101}^{+\,j}P_{01}^{+\,j} + Cb_{101}^{-\,j}P_{01}^{-\,j} + Cb_{\nu 101}^{+\,j}\rho_{\nu 01}^{+\,j} \\
&+\sum_{n=2}^{N}\left[Cb_{1mn}^{+\,j}P_{mn}^{+\,j} + Cb_{1mn}^{-\,j}P_{mn}^{-\,j} + Cb_{\nu 1mn}^{+\,j}\rho_{\nu mn}^{+\,j}\right] \\
&+Cb_{101}^{+\,j+1}P_{01}^{+\,j+1} + Cb_{101}^{-\,j+1}P_{01}^{-\,j+1} + Cb_{\nu 101}^{+\,j+1}\rho_{\nu 01}^{+\,j+1} \\
&+\sum_{n=2}^{N}\left[Cb_{1mn}^{+\,j+1}P_{mn}^{+\,j+1} + Cb_{1mn}^{-\,j+1}P_{mn}^{-\,j+1} + Cb_{\nu 1mn}^{+\,j+1}\rho_{\nu mn}^{+\,j+1}\right] = 0,
\end{aligned}
\tag{7.102}
$$

Therefore, we have obtained three conservation equations of mass, momentum, and energy. If n radial modes are considered, then the number of conservation equations is $3n$. Thus, one interface corresponds to $3n$ conservation equations and $3n$ unknowns. For example, if $n = 2$, then, for an individual interface,

$$\begin{pmatrix} Ab^j & Ab^{j+1} \\ Bb^j & Bb^{j+1} \\ Cb^j & Cb^{j+1} \end{pmatrix} \begin{pmatrix} P^j \\ P^{j+1} \end{pmatrix}, \tag{7.103}$$

where Ab, Bb, and Cb are the coefficients of mass equation, momentum equation, and energy equation, respectively, in the form of:

$$Ab^j = \begin{pmatrix} Ab_{101}^{+j} & Ab_{101}^{-j} & Ab_{\nu 101}^{+j} & Ab_{102}^{+j} & Ab_{102}^{-j} & Ab_{\nu 102}^{+j} \\ Ab_{201}^{+j} & Ab_{201}^{-j} & Ab_{\nu 201}^{+j} & Ab_{202}^{+j} & Ab_{202}^{-j} & Ab_{\nu 202}^{+j} \end{pmatrix} \tag{7.104}$$

$$Bb^j = \begin{pmatrix} Bb_{101}^{+j} & Bb_{101}^{-j} & Bb_{\nu 101}^{+j} & Bb_{102}^{+j} & Bb_{102}^{-j} & Bb_{\nu 102}^{+j} \\ Bb_{201}^{+j} & Bb_{201}^{-j} & Bb_{\nu 201}^{+j} & Bb_{202}^{+j} & Bb_{202}^{-j} & Bb_{\nu 202}^{+j} \end{pmatrix} \tag{7.105}$$

$$Cb^j = \begin{pmatrix} Cb_{101}^{+j} & Cb_{101}^{-j} & Cb_{\nu 101}^{+j} & Cb_{102}^{+j} & Cb_{102}^{-j} & Cb_{\nu 102}^{+j} \\ Cb_{201}^{+j} & Cb_{201}^{-j} & Cb_{\nu 201}^{+j} & Cb_{202}^{+j} & Cb_{202}^{-j} & Cb_{\nu 202}^{+j} \end{pmatrix} \tag{7.106}$$

$$P^j = \left(P_{01}^{+j} \; P_{01}^{-j} \; \rho_{\nu 01}^{+j} \; P_{02}^{+j} \; P_{02}^{-j} \; \rho_{\nu 02}^{+j} \right) \tag{7.107}$$

The coefficients Ab^{j+1}, Bb^{j+1}, Bb^{j+1}, P^{j+1} have the same form. Actually, the previous discussion is only valid for the situation of Fig. 7.5, which describes the cross-section becoming larger. For the other situation, in which, the cross-section becomes smaller, the equations can be derived similarly.

It should be pointed out that the previous formulation only considers that the circumferential mode number equals zero, that is to say, the circumferential instability is ignored. However, if there exists the circumferential instability, the method for a variable cross-section problem can't be directly applied. In contrast, all matching relations must be re-deduced with a different circumferential mode number to set up a new eigenvalue equation.

7.3.2 Numerical calculation method

7.3.2.1 Formulation

When the viscosity and the sources apart from the heat source are ignored, the equations of mass, momentum, and energy are written as:

$$\frac{\partial \rho}{\partial t} + \nabla \cdot (\rho \boldsymbol{v}) = q_m(\mathbf{x}, t), \tag{7.108}$$

$$\rho\frac{d\boldsymbol{v}}{dt}+\nabla p=\mathbf{0}, \tag{7.109}$$

$$\rho T\frac{ds}{dt}=q_h(\mathbf{x},t), \tag{7.110}$$

where ρ, $\boldsymbol{v}$, s, T are the density, velocity, entropy, and absolute temperature, respectively. The bold fonts mean they are vectors. q_m denotes the mass input per unit volume, whereas q_h is the heat input per unit volume. As the density varies through two variables, the pressure and the entropy,

$$\rho=\rho(p,s). \tag{7.111}$$

Hence, the complete differential of the density is,

$$d\rho=\left.\frac{\partial\rho}{\partial p}\right|_s dp+\left.\frac{\partial\rho}{\partial s}\right|_p ds. \tag{7.112}$$

For perfect gas,

$$p=R_g\rho T, \tag{7.113}$$

where R_g is the constant of ideal gas. According to Eq. (7.113), we obtain:

$$dp=R_gTd\rho+R_g\rho dT, \tag{7.114}$$

thus,

$$dT=\frac{dp}{R_g\rho}-\frac{Td\rho}{\rho}, \tag{7.115}$$

according to the definition of entropy s,

$$dQ=Tds, \tag{7.116}$$

and the first law of thermodynamics,

$$dQ=C_pdT-\frac{1}{\rho}dp, \tag{7.117}$$

where Q is the quantity of heat, and C_p is the specific heat capacity at constant pressure. The differential of s, T, and p are related by Eqs. (7.116) and (7.117),

$$Tds=C_pdT-\frac{1}{\rho}dp, \tag{7.118}$$

Substituting Eq. (7.114) into Eq. (7.118), we have,

$$Tds=\frac{C_v}{R_g\rho}dp-\frac{C_pT}{\rho}d\rho, \tag{7.119}$$

where C_v is specific heat capacity at constant volume. Therefore,

$$\left.\frac{\partial\widetilde{\rho}}{\partial\widetilde{s}}\right|_p = -\frac{\widetilde{\rho}}{C_p}, \tag{7.120}$$

The definition of the sound speed is,

$$\left.\frac{\partial\rho}{\partial p}\right|_s = \frac{1}{c^2}, \tag{7.121}$$

where c is the sound speed. Substitute Eqs. (7.120) and (7.121) into Eq. (7.112), we obtain,

$$d\rho = \frac{1}{c^2}dp - \frac{\rho}{C_p}ds \tag{7.122}$$

The previous equation can also be written as:

$$ds = \frac{C_p}{\rho c^2}dp - \frac{C_p}{\rho}d\rho \tag{7.123}$$

Substituting Eq. (7.123) into Eq. (7.110), we have,

$$\frac{C_p T}{c^2}\frac{dp}{dt} - C_p T\frac{d\rho}{dt} = q_h(\mathbf{x}, t) \tag{7.124}$$

because, for perfect gas, $C_p\widetilde{T} = \frac{\gamma R g\widetilde{T}}{\gamma-1} = \frac{\widetilde{c^2}}{\gamma-1}$, where γ is the specific heat ratio. Thus, Eq. (7.124) is equivalent to,

$$\frac{dp}{dt} - c^2\frac{d\rho}{dt} = (\gamma-1)q_h(\mathbf{x}, t) \tag{7.125}$$

Therefore, the basic equations involving the unknowns of the density, velocity, pressure, and sound speed are obtained.

As shown by the one-dimensional part, the unknowns can be decomposed into two quantities, the mean quantity and the fluctuation quantity.

$$\begin{aligned} \rho &= \overline{\rho} + \rho' \\ \boldsymbol{v} &= \overline{\boldsymbol{v}} + \boldsymbol{v}' \\ p &= \overline{p} + p' \end{aligned} \tag{7.126}$$

It is the same for the source terms of mass and heat,

$$\begin{aligned} q_m &= \overline{q}_m + q'_m \\ q_h &= \overline{q}_h + q'_h \end{aligned} \tag{7.127}$$

The overbar means the mean quantity, whereas the prime means the fluctuation quantity. Substitute Eqs. (7.126) and (7.127) into Eq. (7.108), we obtain:

$$\frac{\partial \overline{\rho}}{\partial t}+\frac{\partial \rho'}{\partial t}+\nabla\cdot(\overline{\rho}\overline{\boldsymbol{v}})+\nabla\cdot(\overline{\rho}\boldsymbol{v}')+\nabla\cdot(\rho'\overline{\boldsymbol{v}})+\nabla\cdot(\rho'\boldsymbol{v}')=\overline{q}_m+q'_m. \quad (7.128)$$

The mean values satisfy Eq. (7.108),

$$\frac{\partial \overline{\rho}}{\partial t}+\nabla\cdot(\overline{\rho}\overline{\boldsymbol{v}})=\overline{q}_m(\mathbf{x},t). \quad (7.129)$$

Subtracting Eqs. (7.128) and (7.129), and ignoring the high-order small quantities yield:

$$\frac{\partial \rho'}{\partial t}+\nabla\cdot(\overline{\rho}\boldsymbol{v}')+\nabla\cdot(\rho'\overline{\boldsymbol{v}})=q'_m. \quad (7.130)$$

When the same treatment is applied to Eqs. (7.109) and (7.125), the following two equations are obtained:

$$\overline{\rho}\frac{\partial \boldsymbol{v}'}{\partial t}+\rho'\frac{\partial \overline{\boldsymbol{v}}}{\partial t}+\overline{\rho}\overline{\boldsymbol{v}}\cdot\nabla\boldsymbol{v}'+\overline{\rho}\boldsymbol{v}'\cdot\nabla\overline{\boldsymbol{v}}+\rho'\overline{\boldsymbol{v}}\cdot\nabla\overline{\boldsymbol{v}}+\nabla p'=\mathbf{0}, \quad (7.131)$$

$$\begin{aligned}&\frac{\partial p'}{\partial t}+\overline{\boldsymbol{v}}\cdot\nabla p'+\boldsymbol{v}'\cdot\nabla\overline{p}-\overline{c}^2\frac{\partial \rho'}{\partial t}-c'^2\frac{\partial \overline{\rho}}{\partial t}\\&-\overline{c}^2\overline{\boldsymbol{v}}\cdot\nabla\rho'-\overline{c}^2\boldsymbol{v}'\cdot\nabla\overline{\rho}-c'^2\overline{\boldsymbol{v}}\cdot\nabla\overline{\rho}=(\gamma-1)q'_h.\end{aligned} \quad (7.132)$$

Because the perfect gas equation requires:

$$\overline{\rho}c'^2+\rho'\overline{c}^2=\gamma p'. \quad (7.133)$$

Substituting Eq. (7.133) into Eq. (7.132) leads to:

$$\begin{aligned}&\frac{\partial p'}{\partial t}+\overline{\boldsymbol{v}}\cdot\nabla p'+\boldsymbol{v}'\cdot\nabla\overline{p}-\overline{c}^2\frac{\partial \rho'}{\partial t}-\frac{\gamma}{\overline{\rho}}p'\frac{\partial \overline{\rho}}{\partial t}+\frac{\overline{c}^2}{\overline{\rho}}\rho'\frac{\partial \overline{\rho}}{\partial t}-\overline{c}^2\overline{\boldsymbol{v}}\cdot\nabla\rho'\\&-\overline{c}^2\boldsymbol{v}'\cdot\nabla\overline{\rho}-\frac{\gamma}{\overline{\rho}}p'\overline{\boldsymbol{v}}\cdot\nabla\overline{\rho}+\frac{\overline{c}^2}{\overline{\rho}}\rho'\overline{\boldsymbol{v}}\cdot\nabla\overline{\rho}=(\gamma-1)q'_h.\end{aligned} \quad (7.134)$$

Now we obtain the linearized equations of mass, momentum, and energy as:

$$\begin{aligned}&\frac{\partial \rho'}{\partial t}+\nabla\cdot(\overline{\rho}\boldsymbol{v}')+\nabla\cdot(\rho'\overline{\boldsymbol{v}})=q'_m,\\&\overline{\rho}\frac{\partial \boldsymbol{v}'}{\partial t}+\rho'\frac{\partial \overline{\boldsymbol{v}}}{\partial t}+\overline{\rho}\overline{\boldsymbol{v}}\cdot\nabla\boldsymbol{v}'+\overline{\rho}\boldsymbol{v}'\cdot\nabla\overline{\boldsymbol{v}}+\rho'\overline{\boldsymbol{v}}\cdot\nabla\overline{\boldsymbol{v}}+\nabla p'=\mathbf{0},\\&\frac{\partial p'}{\partial t}+\overline{\boldsymbol{v}}\cdot\nabla p'+\boldsymbol{v}'\cdot\nabla\overline{p}-\overline{c}^2\frac{\partial \rho'}{\partial t}-\frac{\gamma}{\overline{\rho}}p'\frac{\partial \overline{\rho}}{\partial t}+\frac{\overline{c}^2}{\overline{\rho}}\rho'\frac{\partial \overline{\rho}}{\partial t}-\overline{c}^2\overline{\boldsymbol{v}}\cdot\nabla\rho'\\&-\overline{c}^2\boldsymbol{v}'\cdot\nabla\overline{\rho}-\frac{\gamma}{\overline{\rho}}p'\overline{\boldsymbol{v}}\cdot\nabla\overline{\rho}+\frac{\overline{c}^2}{\overline{\rho}}\rho'\overline{\boldsymbol{v}}\cdot\nabla\overline{\rho}=(\gamma-1)q'_h.\end{aligned} \quad (7.135)$$

The linearized equations have the unknowns of ρ', $\boldsymbol{v}'$, and p'. If the mean quantities, mass input, and heat input are given, it is viable to investigate the issue of combustion instability, which is induced by the thermoacoustic coupling.

For simplicity, the fluctuation quantity is expanded in the harmonic forms:

$$\begin{aligned} \rho' &= \widetilde{\rho} e^{i\omega t} \\ p' &= \widetilde{p} e^{i\omega t} \\ \boldsymbol{v}' &= \widetilde{\boldsymbol{v}} e^{i\omega t} \end{aligned} \tag{7.136}$$

Then, Eq. (7.135) can be written as:

$$\begin{aligned} & i\omega\widetilde{\rho} + \nabla\cdot(\widetilde{\rho}\overline{\boldsymbol{v}}) + \nabla\cdot(\overline{\rho}\widetilde{\boldsymbol{v}}) = \widetilde{q}_m, \\ & \widetilde{\rho}\left(\frac{\partial\overline{\boldsymbol{v}}}{\partial t} + \overline{\boldsymbol{v}}\cdot\nabla\overline{\boldsymbol{v}}\right) + i\omega\overline{\rho}\widetilde{\boldsymbol{v}} + \overline{\rho}\overline{\boldsymbol{v}}\cdot\nabla\widetilde{\boldsymbol{v}} + \overline{\rho}\widetilde{\boldsymbol{v}}\cdot\nabla\overline{\boldsymbol{v}} + \nabla\widetilde{p} = \boldsymbol{0}, \\ & \left(-i\omega\overline{c}^2 + \frac{\overline{c}^2}{\overline{\rho}}\frac{\partial\overline{\rho}}{\partial t} + \frac{\overline{c}^2}{\overline{\rho}}\overline{\boldsymbol{v}}\cdot\nabla\overline{\rho}\right)\widetilde{\rho} - \overline{c}^2\overline{\boldsymbol{v}}\cdot\nabla\widetilde{\rho} + \widetilde{\boldsymbol{v}}\cdot\nabla\overline{p} - \overline{c}^2\widetilde{\boldsymbol{v}}\cdot\nabla\overline{\rho} \\ & + \left(i\omega - \frac{\gamma}{\overline{\rho}}\frac{\partial\overline{\rho}}{\partial t} - \frac{\gamma}{\overline{\rho}}\overline{\boldsymbol{v}}\cdot\nabla\overline{\rho}\right)\widetilde{p} + \overline{\boldsymbol{v}}\cdot\nabla\widetilde{p} = (\gamma-1)\widetilde{q}_h. \end{aligned} \tag{7.137}$$

If the unsteady effects of the mean flow are ignored, then we obtain,

$$\begin{aligned} & i\omega\widetilde{\rho} + \nabla\cdot(\widetilde{\rho}\overline{\boldsymbol{v}}) + \nabla\cdot(\overline{\rho}\widetilde{\boldsymbol{v}}) = \widetilde{q}_m, \\ & \widetilde{\rho}\overline{\boldsymbol{v}}\cdot\nabla\overline{\boldsymbol{v}} + i\omega\overline{\rho}\widetilde{\boldsymbol{v}} + \overline{\rho}\overline{\boldsymbol{v}}\cdot\nabla\widetilde{\boldsymbol{v}} + \overline{\rho}\widetilde{\boldsymbol{v}}\cdot\nabla\overline{\boldsymbol{v}} + \nabla\widetilde{p} = \boldsymbol{0}, \\ & \left(-i\omega\overline{c}^2 + \frac{\overline{c}^2}{\overline{\rho}}\overline{\boldsymbol{v}}\cdot\nabla\overline{\rho}\right)\widetilde{\rho} - \overline{c}^2\overline{\boldsymbol{v}}\cdot\nabla\widetilde{\rho} + \widetilde{\boldsymbol{v}}\cdot\nabla\overline{p} - \overline{c}^2\widetilde{\boldsymbol{v}}\cdot\nabla\overline{\rho} \\ & + \left(i\omega - \frac{\gamma}{\overline{\rho}}\overline{\boldsymbol{v}}\cdot\nabla\overline{\rho}\right)\widetilde{p} + \overline{\boldsymbol{v}}\cdot\nabla\widetilde{p} = (\gamma-1)\widetilde{q}_h. \end{aligned} \tag{7.138}$$

Because most combustion instabilities take place in cylindrical or annular combustors, therefore, we expand Eq. (7.138) in cylindrical coordinates of x, r, θ, thus:

$$\begin{aligned} & \left(i\omega + \frac{\partial\overline{v}_r}{\partial r} + \frac{\overline{v}_r}{r} + \frac{1}{r}\frac{\partial\overline{v}_\theta}{\partial\theta} + \frac{\partial\overline{v}_x}{\partial x}\right)\widetilde{\rho} \\ & + \overline{v}_r\frac{\partial\widetilde{\rho}}{\partial r} + \frac{\overline{v}_\theta}{r}\frac{\partial\widetilde{\rho}}{\partial\theta} + \overline{v}_x\frac{\partial\widetilde{\rho}}{\partial x} \\ & + \overline{\rho}\frac{\partial\widetilde{v}_r}{\partial r} + \frac{\overline{\rho}}{r}\frac{\partial\widetilde{v}_\theta}{\partial\theta} + \overline{\rho}\frac{\partial\widetilde{v}_x}{\partial x} + \left(\frac{\overline{\rho}}{r} + \frac{\partial\overline{\rho}}{\partial r}\right)\widetilde{v}_r + \frac{1}{r}\frac{\partial\overline{\rho}}{\partial\theta}\widetilde{v}_\theta + \frac{\partial\overline{\rho}}{\partial x}\widetilde{v}_x = \widetilde{q}_m, \end{aligned} \tag{7.139}$$

$$\left(\overline{v}_r\frac{\partial\overline{v}_r}{\partial r}+\frac{\overline{v}_\theta}{r}\frac{\partial\overline{v}_r}{\partial\theta}+\overline{v}_x\frac{\partial\overline{v}_r}{\partial x}\right)\widetilde{\rho}+i\omega\overline{\rho}\widetilde{v}_r+\overline{\rho}\overline{v}_r\frac{\partial\widetilde{v}_r}{\partial r}+\frac{\overline{\rho}\overline{v}_\theta}{r}\frac{\partial\widetilde{v}_r}{\partial\theta}$$
$$+\overline{\rho}\overline{v}_x\frac{\partial\widetilde{v}_r}{\partial x}+\overline{\rho}\frac{\partial\overline{v}_r}{\partial r}\widetilde{v}_r+\frac{\overline{\rho}}{r}\frac{\partial\overline{v}_r}{\partial\theta}\widetilde{v}_\theta+\overline{\rho}\frac{\partial\overline{v}_r}{\partial x}\widetilde{v}_x+\frac{\partial\widetilde{p}}{\partial r}=0, \tag{7.140}$$

$$\left(\overline{v}_r\frac{\partial\overline{v}_\theta}{\partial r}+\frac{\overline{v}_\theta}{r}\frac{\partial\overline{v}_\theta}{\partial\theta}+\overline{v}_x\frac{\partial\overline{v}_\theta}{\partial x}\right)\widetilde{\rho}+i\omega\overline{\rho}\widetilde{v}_\theta+\overline{\rho}\overline{v}_r\frac{\partial\widetilde{v}_\theta}{\partial r}+\frac{\overline{\rho}\overline{v}_\theta}{r}\frac{\partial\widetilde{v}_\theta}{\partial\theta}$$
$$+\overline{\rho}\overline{v}_x\frac{\partial\widetilde{v}_\theta}{\partial x}+\overline{\rho}\frac{\partial\overline{v}_\theta}{\partial r}\widetilde{v}_r+\frac{\overline{\rho}}{r}\frac{\partial\overline{v}_\theta}{\partial\theta}\widetilde{v}_\theta+\overline{\rho}\frac{\partial\overline{v}_\theta}{\partial x}\widetilde{v}_x+\frac{1}{r}\frac{\partial\widetilde{p}}{\partial\theta}=0, \tag{7.141}$$

$$\left(\overline{v}_r\frac{\partial\overline{v}_x}{\partial r}+\frac{\overline{v}_\theta}{r}\frac{\partial\overline{v}_x}{\partial\theta}+\overline{v}_x\frac{\partial\overline{v}_x}{\partial x}\right)\widetilde{\rho}+i\omega\overline{\rho}\widetilde{v}_x+\overline{\rho}\overline{v}_r\frac{\partial\widetilde{v}_x}{\partial r}+\frac{\overline{\rho}\overline{v}_\theta}{r}\frac{\partial\widetilde{v}_x}{\partial\theta}$$
$$+\overline{\rho}\overline{v}_x\frac{\partial\widetilde{v}_x}{\partial x}+\overline{\rho}\frac{\partial\overline{v}_x}{\partial r}\widetilde{v}_r+\frac{\overline{\rho}}{r}\frac{\partial\overline{v}_x}{\partial\theta}\widetilde{v}_\theta+\overline{\rho}\frac{\partial\overline{v}_x}{\partial x}\widetilde{v}_x+\frac{\partial\widetilde{p}}{\partial x}=0, \tag{7.142}$$

$$\left[-i\omega\overline{c}^2+\frac{\overline{c}^2}{\overline{\rho}}\left(\overline{v}_r\frac{\partial\overline{\rho}}{\partial r}+\frac{\overline{v}_\theta}{r}\frac{\partial\overline{\rho}}{\partial\theta}+\overline{v}_x\frac{\partial\overline{\rho}}{\partial x}\right)\right]\widetilde{\rho}-\overline{c}^2\overline{v}_r\frac{\partial\widetilde{\rho}}{\partial r}-\overline{c}^2\frac{\overline{v}_\theta}{r}\frac{\partial\widetilde{\rho}}{\partial\theta}$$
$$-\overline{c}^2\overline{v}_x\frac{\partial\widetilde{\rho}}{\partial x}+\left(\frac{\partial\overline{p}}{\partial r}-\overline{c}^2\frac{\partial\overline{\rho}}{\partial r}\right)\widetilde{v}_r+\frac{1}{r}\left(\frac{\partial\overline{p}}{\partial\theta}-\overline{c}^2\frac{\partial\overline{\rho}}{\partial\theta}\right)\widetilde{v}_\theta+\left(\frac{\partial\overline{p}}{\partial x}-\overline{c}^2\frac{\partial\overline{\rho}}{\partial x}\right)\widetilde{v}_x$$
$$+\left[i\omega-\frac{\gamma}{\overline{\rho}}\left(\overline{v}_r\frac{\partial\overline{\rho}}{\partial r}+\frac{\overline{v}_\theta}{r}\frac{\partial\overline{\rho}}{\partial\theta}+\overline{v}_x\frac{\partial\overline{\rho}}{\partial x}\right)\right]\widetilde{p}$$
$$+\overline{v}_r\frac{\partial p}{\partial r}+\frac{\overline{v}_\theta}{r}\frac{\partial\widetilde{p}}{\partial\theta}+\overline{v}_x\frac{\partial\widetilde{p}}{\partial x}=(\gamma-1)\widetilde{q}_h, \tag{7.143}$$

where v_x, v_r, and v_θ are the axial, radial, and circumferential velocity components, respectively. Because the primary issue we care about is the effect of the circumferential non-uniformities, thus, the radial and the tangential components are ignored, which is reasonable. Therefore, Eqs. (7.139)–(7.143) are simplified as the following equations:

$$r\left(i\omega+\frac{\partial\widetilde{v}_x}{\partial x}\right)\widetilde{\rho}+r\overline{v}_x\frac{\partial\widetilde{\rho}}{\partial x}+r\overline{\rho}\frac{\partial\widetilde{v}_r}{\partial r}+\overline{\rho}\frac{\partial\widetilde{v}_\theta}{\partial\theta}+r\overline{\rho}\frac{\partial\widetilde{v}_x}{\partial x}$$
$$+\left(\overline{\rho}+r\frac{\partial\overline{\rho}}{\partial r}\right)\widetilde{v}_r+\frac{\partial\overline{\rho}}{\partial\theta}\widetilde{v}_\theta+r\frac{\partial\overline{\rho}}{\partial x}\widetilde{v}_x=r\widetilde{q}_m, \tag{7.144}$$

$$i\omega\overline{\rho}\widetilde{v}_r+\overline{\rho}\overline{v}_x\frac{\partial\widetilde{v}_r}{\partial x}+\frac{\partial\widetilde{p}}{\partial r}=0, \tag{7.145}$$

$$i\omega r\overline{\rho}\widetilde{v}_\theta+r\overline{\rho}\overline{v}_x\frac{\partial\widetilde{v}_\theta}{\partial x}+\frac{\partial\widetilde{p}}{\partial\theta}=0, \tag{7.146}$$

$$
\begin{aligned}
&r\overline{v}_x\frac{\partial\widetilde{v}_x}{\partial x}\widetilde{\rho}+r\left(i\omega\overline{\rho}+\overline{\rho}\frac{\partial\widetilde{v}_x}{\partial x}\right)\widetilde{v}_x+r\overline{\rho}\overline{v}_x\frac{\partial\widetilde{v}_x}{\partial x}\\
&+r\overline{\rho}\frac{\partial\overline{v}_x}{\partial r}\widetilde{v}_r+\overline{\rho}\frac{\partial\overline{v}_x}{\partial\theta}\widetilde{v}_\theta+r\frac{\partial\widetilde{p}}{\partial x}=0,
\end{aligned}
\tag{7.147}
$$

$$
\begin{aligned}
&\left(-ir\omega+\frac{r\overline{v}_x}{\overline{\rho}}\frac{\partial\overline{\rho}}{\partial x}\right)\widetilde{\rho}-r\overline{v}_x\frac{\partial\widetilde{\rho}}{\partial x}+r\left(\frac{1}{\overline{c}^2}\frac{\partial\overline{p}}{\partial r}-\frac{\partial\overline{\rho}}{\partial r}\right)\widetilde{v}_r\\
&+\left(\frac{1}{\overline{c}^2}\frac{\partial\overline{p}}{\partial\theta}-\frac{\partial\overline{\rho}}{\partial\theta}\right)\widetilde{v}_\theta+r\left(\frac{1}{\overline{c}^2}\frac{\partial\overline{p}}{\partial x}-\frac{\partial\overline{\rho}}{\partial x}\right)\widetilde{v}_x\\
&+\frac{r}{\overline{c}^2}\left(i\omega-\frac{\gamma\overline{v}_x}{\overline{\rho}}\frac{\partial\overline{\rho}}{\partial x}\right)\widetilde{p}+r\overline{v}_x\frac{1}{\overline{c}^2}\frac{\partial\widetilde{p}}{\partial x}=\frac{r}{\overline{c}^2}(\gamma-1)\widetilde{q}_h.
\end{aligned}
\tag{7.148}
$$

The constants that are only related to the mean values can be written in reduced form. Then the renewed equations are:

$$
\begin{aligned}
&A_1\widetilde{\rho}+A_2\frac{\partial\widetilde{\rho}}{\partial x}+A_3\frac{\partial\widetilde{v}_r}{\partial r}+A_4\frac{\partial\widetilde{v}_\theta}{\partial\theta}+A_5\frac{\partial\widetilde{v}_x}{\partial x}+A_6\widetilde{v}_r+A_7\widetilde{v}_\theta+A_8\widetilde{v}_x=\widetilde{q}_m,\\
&B_1\widetilde{v}_r+B_2\frac{\partial\widetilde{v}_r}{\partial x}+B_3\frac{\partial\widetilde{p}}{\partial r}=0,\\
&C_1\widetilde{v}_\theta+C_2\frac{\partial\widetilde{v}_\theta}{\partial x}+C_3\frac{\partial\widetilde{p}}{\partial\theta}=0,\\
&D_1\widetilde{\rho}+D_2\widetilde{v}_x+D_3\frac{\partial\widetilde{v}_x}{\partial x}+D_4\widetilde{v}_r+D_5\widetilde{v}_\theta+D_6\frac{\partial\widetilde{p}}{\partial x}=0,\\
&E_1\widetilde{\rho}+E_2\frac{\partial\widetilde{\rho}}{\partial x}+E_3\widetilde{v}_r+E_4\widetilde{v}_\theta+E_5\widetilde{v}_x+E_6\widetilde{p}+E_7\frac{\partial\widetilde{p}}{\partial x}=(\gamma-1)\widetilde{q}_h.
\end{aligned}
\tag{7.149}
$$

And the renewed constants are presented in Appendix C. Thus far, the first-order differential equations have been presented as the basic equations for investigating the combustion instability, which is able to account for the circumferential non-uniform effects. In the formulation, the radial and circumferential mean flow are ignored for simplicity. Actually, if we can also account for the effects of these two velocity components, it only makes the equations more complex without enlarging the computation cost.

7.3.2.2 Discretization method

The spectral method is adopted here for solving the eigenvalue problem, which is superior to the finite difference method for higher accuracy and faster convergence. This method has been widely used in solving the eigenvalue problems of flow instability and other mechanics. The method is briefly introduced here, and more detail can be found in Peyret [19].

In Eq. (7.149), the unknowns are discretized by Fourier methods in the circumferential direction and Chebyshev methods in the axial direction,

$$\chi(x, r, \theta) = \sum_{i=0}^{N_x} \sum_{j=0}^{N_r} \sum_{k=1}^{N_\theta} F_{ijk} T_i(x) T_j(r) e^{ik\theta}, \tag{7.150}$$

where χ represents unknowns; F_{ijk} denotes the unknown coefficients; N_x, N_r, and N_θ are numbers of collocation points in axial, radial, and circumferential directions, respectively; and $T_i(x)$ is the Chebyshev polynomial of degree i defined for x in the range of $[-1, 1]$. Thus, the derivatives of the variables at the collocation points can be obtained,

$$\left.\frac{\partial \chi}{\partial x}\right|_{i,j,k} = \chi_x^1(x_i, r_j, \theta_k) = \sum_{m=0}^{N_x} d_{i,m}^1 \chi(x_m, r_j, \theta_k), \tag{7.151}$$

$$\left.\frac{\partial \chi}{\partial r}\right|_{i,j,k} = \chi_r^1(x_i, r_j, \theta_k) = \sum_{n=0}^{N_r} d_{j,n}^1 \chi(x_i, r_n, \theta_k), \tag{7.152}$$

$$\left.\frac{\partial \chi}{\partial \theta}\right|_{i,j,k} = \chi_\theta^1(x_i, r_j, \theta_k) = \sum_{p=1}^{N_\theta} e_{k,p}^1 \chi(x_i, r_j, \theta_p), \tag{7.153}$$

where $i = 0, \ldots, N_x$, $j = 0, \ldots, N_r$ and $k = 0, \ldots, N_\theta$. $e_{k,\,p}^1$, $d_{i,\,m}^1$ and $d_{j,\,n}^1$ are the first-order Fourier and Chebyshev derivative matrix given by Peyret [19].

7.3.2.3 Treatment of heat source

In our model, the mass source is not included, i.e., $q_m = 0$. For the heat source, the combustion takes place in a region,

$$q_h = q_h(x, r, \theta). \tag{7.154}$$

The heat source will be treated in two ways. First and usually, the flame is assumed to be compacted in a plate, then,

$$q_h = \delta(x - x_0)(\lambda_p p + \lambda_v v_x). \tag{7.155}$$

It is convenient to make such assumptions, especially for an analytical approach. Eq. (7.155) means that the unsteady heat release is related to the axial velocity fluctuation and the pressure fluctuation. δ is the delta function. This kind of heat release function means in the two regions upstream, the heat release plate, and downstream of the plate, the heat source q_h is zero. Most heat release function can be written in this form. Thus, the energy equation in Eq. (7.149) becomes:

$$E_1\widetilde{\rho}+E_2\frac{\partial\widetilde{\rho}}{\partial x}+E_3\widetilde{v}_r+E_4\widetilde{v}_\theta+E_5\widetilde{v}_x+E_6\widetilde{p}+E_7\frac{\partial\widetilde{p}}{\partial x}=0, \tag{7.156}$$

where E_1 E_2 E_3 E_4 E_7 remain unchanged, whereas E_5 and E_6 become:

$$E_5=\frac{1}{\overline{c}^2}\frac{\partial\overline{p}}{\partial x}-\frac{\partial\overline{\rho}}{\partial x}-\frac{1}{\overline{c}^2}\delta(x-x_0)\lambda_p, \tag{7.157}$$

and

$$E_6=i\omega\frac{1}{\overline{c}^2}-\frac{\gamma\overline{v}_x}{\overline{c}^2\overline{\rho}}\frac{\partial\overline{\rho}}{\partial x}-\overline{c}^2\delta(x-x_0)\lambda_p, \tag{7.158}$$

respectively.

This reveals a problem. Because of the heat input, Eq. (7.156) is different across the heat release plate, and the flow parameters change after the heat release plate. The discretization method is unable to conquer it directly. Thus, we need to discretize the equations for different zones separately as shown in Fig. 7.6, and relate the flow parameters with the conservation laws.

The subscripts 1 and 2 in Fig. 7.6 denote the variables of up- and downstream regions of the heat release region. For the control volume, applying conservation of mass, momentum, and energy, the following relations are obtained,

Mass equation is:

$$\oint_s\widetilde{\rho}\widetilde{\boldsymbol{v}}\cdot d\boldsymbol{s}=0. \tag{7.159}$$

By linearizing the equation, we obtain,

$$\overline{\rho}_1v_{xA}+\overline{v}_{x1}\rho_A=\overline{\rho}_2v_{xB}+\overline{v}_{x2}\rho_B, \tag{7.160}$$

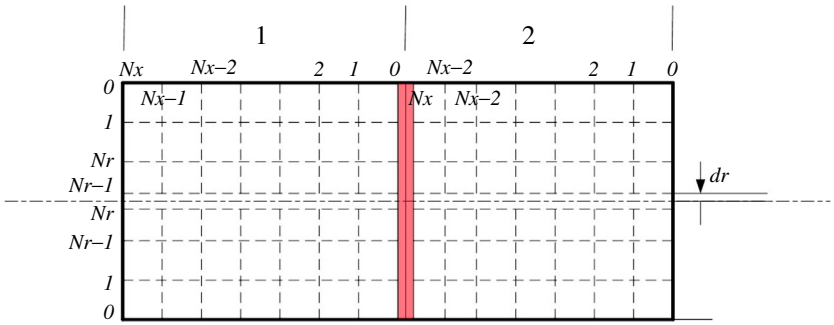

Fig. 7.6 Schematic of spectral discretization method.

where the subscripts 1 and 2 represent the region, and A and B denote the right boundary of region 1 and the left boundary of region 2, respectively.

Momentum equation is:

$$\oint_s \widetilde{\rho}\widetilde{v}_n\widetilde{\boldsymbol{v}}d\boldsymbol{s} + \oint_s n_v \cdot \widetilde{p}d\boldsymbol{s} = 0. \tag{7.161}$$

The linearized equations are:

$$p_A + \rho_A\overline{v}_{x1}^2 + 2\overline{\rho}_1\overline{v}_{x1}v_{xA} = p_B + \rho_B\overline{v}_{x2}^2 + 2\overline{\rho}_2\overline{v}_{x2}v_{xB}, \tag{7.162}$$

$$\overline{\rho}_1\overline{v}_{x1}v_{rA} = \overline{\rho}_2\overline{v}_{x2}v_{rB}, \tag{7.163}$$

$$\overline{\rho}_1\overline{v}_{x1}v_{\theta A} = \overline{\rho}_2\overline{v}_{x2}v_{\theta B}. \tag{7.164}$$

Energy is:

$$\delta\widetilde{Q} + \oint_s \left(e + \frac{\widetilde{p}}{\widetilde{\rho}} + \frac{\widetilde{u}^2}{2}\right)\rho\widetilde{v}_n ds = 0. \tag{7.165}$$

By linearizing the equation, we have:

$$\begin{aligned} &Q' + \left(c_p\overline{T}_{01}\overline{\rho}_1 + \overline{\rho}_1\overline{v}_{x1}^2\right)v_{xA} + \left(c_p\overline{T}_{01}\overline{v}_{x1} - c_pT_1\overline{v}_{x1}\right)\rho_A + \frac{c_p\overline{v}_{x1}}{Rg}p_A \\ &= \left(c_p\overline{T}_{02}\overline{\rho}_2 + \overline{\rho}_2\overline{v}_{x2}^2\right)v_{xB} + \left(c_p\overline{T}_{02}\overline{v}_{x2} - c_pT_2v_{x2}\right)\rho_B + \frac{c_pv_{x2}}{Rg}p_B, \end{aligned} \tag{7.166}$$

where Q' is the unsteady heat release per unit area, $\overline{T}_{01}$ and $\overline{T}_{02}$ are the total temperature of region 1 and region 2, respectively, $\overline{T}_0 = \overline{T} + \frac{\overline{u}^2}{2C_p}$.

If the unsteady heat release can be expressed as:

$$Q' = \lambda_p p + \lambda_v v_x. \tag{7.167}$$

Then, it is obtained:

$$\begin{aligned} &\left(\lambda_v + c_p\overline{T}_{01}\overline{\rho}_1 + \overline{\rho}_1\overline{v}_{x1}^2\right)v_{xA} + \left(c_p\overline{T}_{01}\overline{v}_{x1} - c_pT_1\overline{v}_{x1}\right)\rho_A + \left(\lambda_p + \frac{c_p\overline{v}_{x1}}{Rg}\right)p_A \\ &= \left(c_p\overline{T}_{02}\overline{\rho}_2 + \overline{\rho}_2\overline{v}_{x2}^2\right)v_{xB} + \left(c_p\overline{T}_{02}\overline{v}_{x2} - c_pT_2v_{x2}\right)\rho_B + \frac{c_pv_{x2}}{Rg}p_B. \end{aligned} \tag{7.168}$$

The five linearized conservation equations can be written as:

$$\begin{aligned} &K_{a1}\rho_{x1} + K_{a2}v_{x1} + K_{a3}\rho_{x2} + K_{a4}v_{x2} = 0, \\ &K_{b1}\rho_1 + K_{b2}v_{x1} + K_{b3}p_1 + K_{b4}\rho_2 + K_{b5}v_{x2} + K_{b6}p_2 = 0, \\ &K_{c1}v_{r1} + K_{c2}v_{r2} = 0, \\ &K_{d1}v_{\theta 1} + K_{d1}v_{\theta 2} = 0, \\ &K_{e1}\rho_1 + K_{e2}v_{x1} + K_{e3}p_1 + K_{e4}\rho_2 + K_{e5}v_{x2} + K_{e6}p_2 = 0, \end{aligned} \tag{7.169}$$

where the coefficients K can be found in Appendix D.

For a specific problem, it should satisfy some kind of boundary conditions, for example, for a hard-wall condition, the following equation should be met,

$$\left.\frac{\partial p}{\partial r}\right|_{r=R_o} = 0, \tag{7.170}$$

where R_o is the radius of the tube. If the wall has a damping effect, we need to know the impedance of the wall, with the impedance boundary condition as:

$$\frac{p}{v_r} = Z_n, \tag{7.171}$$

where Z_n is the impedance of the wall. With all of the conditions taken into account, Eq. (7.149) can be discretized as:

$$\begin{pmatrix} \zeta_1 & \zeta_3 \\ \zeta_4 & \zeta_2 \end{pmatrix} \begin{pmatrix} \xi_1 \\ \xi_2 \end{pmatrix} = 0, \tag{7.172}$$

Where ζ_1, ζ_2, ζ_3, and ζ_4 are submatrices of size $[5(N+1)]^2$ with only the complex frequency ω as the unknown, where $N = (N_x + 1)(N_r + 1)$ $N_t - 1$. The column vectors ξ_1 and ξ_2 of length $5(N+1)$ contain the discrete unknowns in regions 1 and 2, respectively. If Eq. (7.149) has non-zero solutions, the determinant of the matrix must be zero, and the complex frequency ω can be obtained by solving the equation:

$$\begin{vmatrix} \zeta_1 & \zeta_3 \\ \zeta_4 & \zeta_2 \end{vmatrix} = 0. \tag{7.173}$$

7.3.3 Effect of vorticity waves on azimuthal instabilities in annular chambers

In this section, the effect of vorticity disturbance on azimuthal instabilities in an annular geometry is investigated analytically. The investigated problem is depicted in Fig. 7.7. In an annular chamber, a compacted flame is located at $x = L_f$. The flame separates uniform regions of cold reactants (region 1) and hot products (region 2). For simplicity, the following assumptions are made about the problem: (1) the flame is thin enough that the thickness is considered to be zero; (2) the effect of the flame is embodied in unsteady heat release, but the mechanisms are not discussed here, e.g., the flame speed and flame area disturbances; (3) because the geometry is axisymmetric, no circumferential modal coupling occurs, so the azimuthal modes of two directions are considered separately; (4) only axial mean velocity is

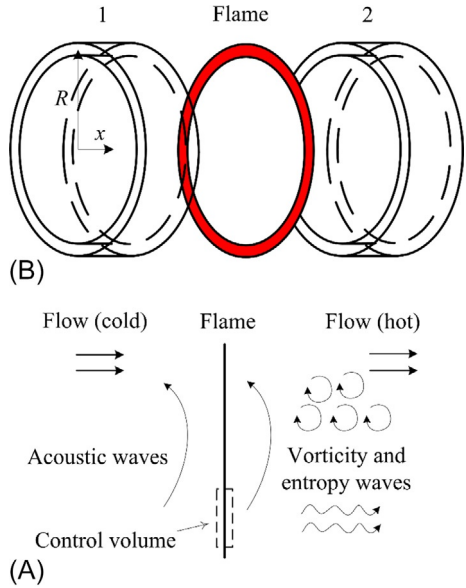

Fig. 7.7 Schematic of the annular chamber [20]. (A) Fluctuating waves in the chamber; (B) Geometry of the chamber.

considered, which is given to be uniform; (5) the radial gap is much smaller than axial and circumferential length so the radial dependence is ignored; (6) we focus on the azimuthal modes, hence the acoustically closed and choked boundary conditions are taken; and (7) the following analysis is limited in the linear range so that each variable can be written as a sum of its mean (denoted by superscript −) and fluctuating component (denoted by′), and the higher-order terms are ignored (e.g., $p = \overline{p} + p'$).

To validate this analytical model with the effect of the vorticity wave, the linear Euler equation method (LEEM) introduced in Section 7.3.2 is adopted. For the annular geometry, the radial dependence is ignored for the reason that the radial gap is much smaller than the axial and circumferential length. Therefore, the analytical description for the annular geometry can be recovered from the three-dimensional AMs introduced in Section 7.3.1. Analytical results without the vorticity wave are also given on the analogy of the network model and finite element method. A comparison of the results with and without vorticity waves shows that vorticity disturbance has a significant effect on the azimuthal instabilities in a chamber with mean flow. And the results also show that calculations of azimuthal instabilities using the network model and finite element

method may lead to significant prediction errors when the mean flow is considered. The work can be seen in the work of Li and Sun [20] in detail.

7.3.3.1 Description of disturbances

The flow parameters are given as axial velocity u, pressure p, density ρ, speed of sound c, and Mach number M. The acoustic disturbances can be written in the following forms using standard techniques:

$$p' = \left(P_m^+ e^{i\alpha_m^+ x} + P_m^- e^{i\alpha_m^- x}\right) e^{i(\omega t + m\theta)}, \tag{7.174}$$

$$u_a' = -\frac{1}{\overline{\rho}}\left(\frac{\alpha_m^+ P_m^+ e^{i\alpha_m^+ x}}{\omega + \alpha_m^+ \overline{u}} + \frac{\alpha_m^- P_m^- e^{i\alpha_m^- x}}{\omega + \alpha_m^- \overline{u}}\right) e^{i(\omega t + m\theta)}, \tag{7.175}$$

$$v_a' = -\frac{1}{\overline{\rho}}\left(\frac{mP_m^+ e^{i\alpha_m^+ x}}{R\left(\omega + \alpha_m^+ \overline{u}\right)} + \frac{mP_m^- e^{i\alpha_m^- x}}{R\left(\omega + \alpha_m^- \overline{u}\right)}\right) e^{i(\omega t + m\theta)}, \tag{7.176}$$

$$\rho_a' = \frac{1}{\overline{c}^2}\left(P_m^+ e^{i\alpha_m^+ x} + P_m^- e^{i\alpha_m^- x}\right) e^{i(\omega t + m\theta)}, \tag{7.177}$$

where p', u', v', ρ', and R denote pressure, axial velocity, circumferential velocity disturbances, and radius of the chamber, respectively. The subscript a denotes the acoustic quantities. P is the unknown parameter that denotes the magnitude of the acoustic disturbances. m is an integral, and it denotes the circumferential mode number. + and - denote the waves that propagate upstream and downstream, respectively. R is the mean radius of the annular chamber. x and θ denote axial and circumferential coordinates, respectively. α is the axial wave number that has the form:

$$\alpha_m^{+,-} = \frac{\overline{M}\left(\frac{\omega}{\overline{c}}\right) \pm \sqrt{\left(\frac{\omega}{\overline{c}}\right)^2 - (1-\overline{M}^2)\left(\frac{m}{R}\right)^2}}{1-\overline{M}^2}, \tag{7.178}$$

where $\omega = \omega_r + i\omega_i$ denotes complex frequency, the real part ω_r represents the radial frequency of oscillation, the imaginary part ω_i is the damping coefficient, and i is the imaginary unit. The value of ω_i determines the decay rate of an acoustic mode. The instability characteristics can be investigated through ω.

Density fluctuation can also be induced by an entropy wave, which has the form:

$$\rho_e' = -\frac{\overline{\rho}}{C_p} S_{em} e^{-i\frac{\omega}{\overline{u}}x} e^{i(m\theta + \omega t)}, \tag{7.179}$$

where C_p is specific heat at constant pressure, and S_{em} is the unknown parameter. Similarly, the velocity fluctuations induced by vorticity waves can be written as:

$$u'_v = V_{xm} e^{-\mathrm{i}\frac{\omega}{\overline{u}}x} e^{\mathrm{i}(m\theta+\omega t)}, \tag{7.180}$$

$$v'_v = V_{\theta m} e^{-\mathrm{i}\frac{\omega}{\overline{u}}x} e^{\mathrm{i}(m\theta+\omega t)}. \tag{7.181}$$

It should be pointed out that the divergence of the vorticity is zero, which leads to,

$$V_{\theta m} = \frac{\omega R}{\overline{u}m} V_{xm}. \tag{7.182}$$

Thus, the total density disturbance can be written as:

$$\rho' = \rho'_a + \rho'_e = \frac{1}{\overline{c}^2}\left(P_m^+ e^{\mathrm{i}\alpha_m^+ x} + P_m^- e^{\mathrm{i}\alpha_{mn}^- x} - \frac{\overline{\rho}\overline{c}^2}{C_p} S_{em} e^{-\mathrm{i}\frac{\omega}{\overline{u}}x}\right) e^{\mathrm{i}(\omega t+m\theta)}. \tag{7.183}$$

The total velocity disturbances are:

$$u' = u'_a + u'_v = -\frac{1}{\overline{\rho}}\left(\frac{\alpha_m^+ P_m^+ e^{\mathrm{i}\alpha_m^+ x}}{\omega+\alpha_m^+\overline{u}} + \frac{\alpha_m^- P_m^- e^{\mathrm{i}\alpha_m^- x}}{\omega+\alpha_m^-\overline{u}} - \overline{\rho} V_{xm} e^{-\mathrm{i}\frac{\omega}{\overline{u}}x}\right) e^{\mathrm{i}(\omega t+m\theta)}, \tag{7.184}$$

$$v' = v'_a + v'_v = -\frac{1}{\overline{\rho}}\left[\begin{array}{l}\dfrac{mP_m^+ e^{\mathrm{i}\alpha_m^+ x}}{R\left(\omega+\alpha_m^+\overline{u}\right)} + \dfrac{mP_m^- e^{\mathrm{i}\alpha_m^- x}}{R\left(\omega+\alpha_m^-\overline{u}\right)} \\ -\dfrac{\omega R\rho_0}{\overline{u}m} V_{xm} e^{-\mathrm{i}\frac{\omega}{\overline{u}}x}\end{array}\right] e^{\mathrm{i}(m\theta+\omega t)}. \tag{7.185}$$

It can be seen that, in the mean flow, the acoustic, vorticity, and entropy waves propagate independently. The pressure perturbation is dependent on acoustic disturbance only. But the density perturbation is the superposition of acoustic and entropy disturbances, and the velocity perturbation is induced by both acoustic and vorticity disturbances.

Eqs. (7.174) and (7.183)–(7.185) describe the unsteady flow fields of the up- and downstream regions of the flame. Actually, these two regions are coupled through several matching conditions. Applying conservation law of mass, momentum, and energy on the interface of two regions (as shown in Fig. 7.7) and employing a linearization procedure yields the following equations that describe the correlations of the disturbance quantities across the flame, where subscripts 1 and 2 denote the variables of up- and downstream regions of the flame.

Mass equation:

$$\overline{\rho}_1 u_1' + \overline{u}_1 \rho_1' = \overline{\rho}_2 u_2' + \overline{u}_2 \rho_2'. \tag{7.186}$$

Axial momentum equation:

$$\left(2\overline{u}_1\overline{\rho}_1 u_1' + \overline{u}_1^2 \rho_1'\right) - \left(2\overline{u}_2\overline{\rho}_2 u_2' + \overline{u}_2^2 \rho_2'\right) = p_2' - p_1'. \tag{7.187}$$

Circumferential momentum equation:

$$v_1' = v_2'. \tag{7.188}$$

Energy equation:

$$\begin{aligned} &\frac{\gamma\overline{u}_1}{\gamma-1}p_1' + \left(\frac{\gamma\overline{p}_1}{\gamma-1} + \frac{3}{2}\overline{\rho}_1\overline{u}_1^2\right)u_1' + \frac{\overline{u}_1^3}{2}\rho_1' \\ &= \frac{\gamma\overline{u}_2}{\gamma-1}p_2' + \left(\frac{\gamma\overline{p}_2}{\gamma-1} + \frac{3}{2}\overline{\rho}_2\overline{u}_2^2\right)u_2' + \frac{\overline{u}_2^3}{2}\rho_2' - Q', \end{aligned} \tag{7.189}$$

where γ is the ratio of specific heats. Q' denotes unsteady heat release per unit area.

Because we focus on the azimuthal modes, the inlet boundary condition is taken to be an acoustic closed end, which can be expressed as:

$$u_1'|_{x=0} = 0. \tag{7.190}$$

In the traditional method for analysis of combustion instabilities, impedance boundary conditions usually are given for the inlet and outlet. However, when it has a mean flow, there will be three types of waves, recognized as acoustic, entropy, and vorticity waves, propagating in the system. It has been discussed that the acoustic disturbance propagates up- and downstream, whereas the entropy and vorticity disturbances only travel downstream with the flow. Thus, in all three, inlet boundary conditions and one outlet boundary condition are needed to determine all the quantities of the four waves. Stow et al. have discussed the boundary conditions corresponding to choked outlet and choked inlet cases [15]. To observe the generation of the vorticity disturbance by the interaction of acoustic wave and heat source, the choked inlet boundary condition is not adopted here. We assume that the inlet entropy and vorticity disturbances are zero. Therefore, no entropy and vorticity waves propagate in region 1. These two complementary boundary conditions can be given as:

$$\rho_{e1}' = 0, \tag{7.191}$$

$$u_{v1}' = 0. \tag{7.192}$$

For the outlet, two forms of boundary conditions are considered, respectively, for the acoustically closed end:

$$u_2'|_{x=L} = 0. \tag{7.193}$$

and for the choked end [21]:

$$-\frac{p_2'}{\bar{p}_2} + \frac{\rho_2'}{\bar{\rho}_2} + 2\frac{u_2'}{\bar{u}_2}\bigg|_{x=L} = 0. \tag{7.194}$$

The azimuthal modes can be formed with either the closed or the choked outlet. For the closed boundary condition in Eq. (7.193), the sum of acoustic and vorticity axial velocity disturbances is constrained to be zero, which denotes that the acoustic and vorticity waves are coupled at the outlet, but the entropy wave will freely propagate out of the duct. So, with this boundary condition, we can investigate the coupling of vorticity and acoustic waves at the outlet without the effect of an entropy wave. The choked boundary is also investigated because it is coherent with the outlet of real annular combustors connected to a nozzle. For such a choked outlet boundary condition in Eq. (7.194), the three types of waves are all coupled at the outlet. When the flow velocity tends to zero, Eq. (7.193) can be recovered from Eq. (7.194).

With these assumptions, it can be found that, for the present case, there are no entropy and vorticity waves in region 1, and in region 2 they are generated by the interaction between acoustic waves and the heat source. The generation process of such disturbances is described by Eqs. (7.186)–(7.189).

For general cases, the unsteady heat release is given as:

$$Q' = K_u u_1'|_{x=L_1} + K_p p_1'|_{x=L_1}, \tag{7.195}$$

where L_1 is the length of the region 1. This equation denotes that the unsteady heat release is induced by axial velocity or pressure disturbances in region 1 at the place of the flame. In this chapter, the effect of unsteady heat release depending on velocity, pressure disturbance, and no unsteady heat release will be investigated, respectively.

Substituting Eqs. (7.174), (7.183)–(7.185) to (7.186)–(7.189), (7.190)–(7.194) and considering Eq. (7.195) yields:

$$\mathbf{X}\begin{pmatrix} P_{m1}^{+} \\ P_{m1}^{-} \\ P_{m2}^{+} \\ P_{m2}^{-} \\ s_{em2} \\ V_{xm2} \\ Q' \end{pmatrix} = 0, \tag{7.196}$$

where $\mathbf{X}$ is a 7×7 matrix, and it has the following form:

$$\begin{pmatrix}
\left(\frac{\overline{u}_1}{\overline{c}_1^2} - A_1\right)e_1 & \left(\frac{\overline{u}_1}{\overline{c}_1^2} - A_2\right)e_2 & -\left(\frac{\overline{u}_2}{\overline{c}_2^2} - A_3\right) & -\left(\frac{\overline{u}_2}{\overline{c}_2^2} - A_4\right) & -\overline{u}_2 & -\overline{\rho}_2 & 0 \\
-\left(1 + \overline{M}_1^2 - 2\overline{u}_1 A_1\right)e_1 & -\left(1 + \overline{M}_1^2 - 2\overline{u}_1 A_2\right)e_2 & \left(1 + \overline{M}_2^2 - 2\overline{u}_2 A_3\right) & \left(1 + \overline{M}_2^2 - 2\overline{u}_2 A_4\right) & \overline{u}_2^2 & 2\overline{u}_2\overline{\rho}_2 & 0 \\
\left(B_1\overline{u}_1 - \frac{B_3 A_1}{\overline{\rho}_1}\right)e_1 & \left(B_1\overline{u}_1 - \frac{B_3 A_2}{\overline{\rho}_1}\right)e_2 & -\left(B_2\overline{u}_2 - \frac{B_4 A_3}{\overline{\rho}_2}\right) & -\left(B_2\overline{u}_2 - \frac{B_4 A_4}{\overline{\rho}_2}\right) & -\frac{\overline{u}_2^3}{2} & -B_4 & 1 \\
A_5 e_1 & A_6 e_2 & -A_7 & -A_8 & 0 & \frac{\omega R\overline{\rho}_2}{m} & 0 \\
A_1 & A_2 & 0 & 0 & 0 & 0 & 0 \\
0 & 0 & A_3 e_3 & A_4 e_4 & 0 & -\overline{\rho}_2 e_5 & 0 \\
-\left(K_p - \frac{K_v}{\overline{\rho}_1}A_1\right)e_1 & -\left(K_p - \frac{K_v}{\overline{\rho}_1}A_2\right)e_2 & 0 & 0 & 0 & 0 & 1
\end{pmatrix}, \quad (7.197)$$

with

$$A_1 = \frac{\alpha_{m1}^+}{\omega + \alpha_{m1}^+\overline{u}_1}, \quad A_2 = \frac{\alpha_{m1}^-}{\omega + \alpha_{m1}^-\overline{u}_1}, \quad A_3 = \frac{\alpha_{m2}^+}{\omega + \alpha_{m2}^+\overline{u}_2}, \quad A_4 = \frac{\alpha_{m2}^-}{\omega + \alpha_{m2}^-\overline{u}_2}$$

$$A_5 = \frac{m\overline{u}_1}{R(\omega + \alpha_{m1}^+\overline{u}_1)}, \; A_6 = \frac{m\overline{u}_1}{R(\omega + \alpha_{m1}^-\overline{u}_1)}, \; A_7 = \frac{m\overline{u}_2}{R(\omega + \alpha_{m2}^+\overline{u}_2)}, \; A_8 = \frac{m\overline{u}_2}{R(\omega + \alpha_{m2}^-\overline{u}_2)}$$

$$B_1 = \frac{\gamma}{\gamma - 1} + \frac{\overline{M}_1^2}{2}, \quad B_2 = \frac{\gamma}{\gamma - 1} + \frac{\overline{M}_2^2}{2}, \quad B_3 = \frac{\gamma\overline{p}_1}{\gamma - 1} + \frac{3}{2}\overline{\rho}_1\overline{u}_1^2, \quad B_4 = \frac{\gamma\overline{p}_2}{\gamma - 1} + \frac{3}{2}\overline{\rho}_2\overline{u}_2^2$$

$$e_1 = e^{\mathrm{i}\alpha_{m1}^+ L_1}, \quad e_2 = e^{\mathrm{i}\alpha_{m1}^- L_1}, \quad e_3 = e^{\mathrm{i}\alpha_{m2}^+ L_2}, \quad e_4 = e^{\mathrm{i}\alpha_{m2}^- L_2}, \quad e_5 = e^{-\mathrm{i}\frac{\omega}{\overline{u}_2}L_2},$$

where L_2 is the length of the region 2. The matrix is for the boundary condition in Eq. (7.193). For choked boundary condition, it should substitute the sixth row to the corresponding terms. Eq. (7.196) has a zero solution unless the determinant of $\mathbf{X}$ vanishes. Therefore, only disturbances with which the determinant of $\mathbf{X}$ equal zero can exist. Because the mean flow parameters are known, it forms an equation for ω, which can be solved numerically. And the relative values of the unknown parameters of the flow disturbances in Eqs. (7.174), (7.183)–(7.185) can be determined through Eq. (7.196).

To investigate the effect of the vorticity wave, the results of AM without vorticity disturbance should also be given for comparison. If the vorticity wave is not considered, the flow disturbances are described by Eqs. (7.174)–(7.176) and (7.183). It should be noted that the entropy waves are included in the model all the same. The jump conditions are given by Eqs. (7.186), (7.187), and (7.189), which have been commonly used in the analysis of thermoacoustic instabilities. Because the vorticity disturbance is not included, the circumferential jump condition is not needed. Then the eigenfrequency can be obtained through the same process introduced earlier.

It has been discussed that vorticity waves exist in azimuthal instabilities, and an AM in which three types of disturbances are included has been given. With this analytical model, it is convenient to present the differences with or without the vorticity waves. However, whether the results from the analytical model are correct also needs to be validated. For this reason, LEEM as introduced in Section 7.3.2 will be used. In LEEM, the disturbances in regions 1 and 2 (as shown in Fig. 7.7) are described by a linear Euler equation, therefore all forms of flow disturbances are included. The heat source will be treated in two manners, which are compacted in a plate and distributed in a thin region, respectively. In the first case, the same jump conditions using the AM are also needed. In the second case, such conditions are no longer needed. The AM including vorticity disturbance can be validated by comparison of the results, and the jump conditions can also be validated by comparison of these methods.

Using the assumptions made in previous sections, the linearized equations for perturbations can be written in the following forms:

$$\frac{\partial \rho'}{\partial t} + \nabla \cdot (\bar{\rho}\boldsymbol{u}') + \nabla \cdot (\rho'\bar{\boldsymbol{u}}) = 0, \tag{7.198}$$

$$\left(\overline{\rho}\frac{\partial}{\partial t}+\overline{\rho}\overline{\boldsymbol{u}}\cdot\nabla\right)\boldsymbol{u}'+\overline{\rho}\boldsymbol{u}'\cdot\nabla\overline{\boldsymbol{u}}+\left(\frac{\partial\overline{\boldsymbol{u}}}{\partial t}+\overline{\boldsymbol{u}}\cdot\nabla\overline{\boldsymbol{u}}\right)\rho'+\nabla p'=0, \tag{7.199}$$

$$\begin{aligned}&\left(\frac{\partial}{\partial t}+\overline{\boldsymbol{u}}\cdot\nabla\right)p'-\left(\frac{\gamma}{\overline{\rho}}\frac{\partial\overline{\rho}}{\partial t}+\frac{\gamma}{\overline{\rho}}\overline{\boldsymbol{u}}\cdot\nabla\overline{\rho}\right)p'-\left(\overline{c}^2\frac{\partial}{\partial t}+\overline{c}^2\overline{\boldsymbol{u}}\cdot\nabla\right)\rho'\\&+\left(\frac{\overline{c}^2}{\overline{\rho}}\frac{\partial\overline{\rho}}{\partial t}+\frac{\overline{c}^2}{\overline{\rho}}\overline{\boldsymbol{u}}\cdot\nabla\overline{\rho}\right)\rho'-\overline{c}^2\boldsymbol{u}'\cdot\nabla\overline{\rho}+\boldsymbol{u}'\cdot\nabla\overline{p}=(\gamma-1)Q',\end{aligned} \tag{7.200}$$

where $u=(u,\ v)$ is the velocity vector. The perturbation variables can be written in forms of time harmonics:

$$\begin{aligned}\rho'&=\hat{\rho}e^{\mathrm{i}\omega t},\\p'&=\hat{p}e^{\mathrm{i}\omega t},\\\boldsymbol{u}'&=\hat{\boldsymbol{u}}e^{\mathrm{i}\omega t},\end{aligned} \tag{7.201}$$

Here, the overhat ∘ denotes a complex function of spatial coordinates. The equations are next expanded in cylindrical coordinates. Note that the mean flow of the circumferential direction is ignored, and then equations of such forms can be obtained that:

$$C_1\hat{\rho}+C_2\frac{\partial\hat{\rho}}{\partial x}+C_3\frac{\partial\hat{v}}{\partial\theta}+C_4\frac{\partial\hat{u}}{\partial x}+C_5\hat{v}+C_6\hat{u}=0, \tag{7.202}$$

$$D_1\hat{v}+D_2\frac{\partial\hat{v}}{\partial x}+D_3\frac{\partial\hat{p}}{\partial\theta}=0, \tag{7.203}$$

$$E_1\hat{\rho}+E_2\hat{u}+E_3\frac{\partial\hat{u}}{\partial x}+E_4\hat{v}+E_5\frac{\partial\hat{p}}{\partial x}=0, \tag{7.204}$$

$$F_1\hat{\rho}+F_2\frac{\partial\hat{\rho}}{\partial x}+F_3\hat{v}+F_4\hat{u}+F_5\hat{p}+F_6\frac{\partial\hat{p}}{\partial x}=(\gamma-1)\hat{Q}, \tag{7.205}$$

where the coefficients C, D, E, and F are functions of the mean flow parameters, which are given in Appendix C.

Spectral method is adopted here for solving the eigenvalue problem. In Eqs. (7.202) through (7.205), the unknowns are discretized by Fourier methods in the circumferential direction and Chebyshev methods in the axial direction:

$$\chi(x,\theta)=\sum_{i=0}^{N_x}\sum_{k=1}^{N_\theta}F_{ik}T_i(x)\mathrm{e}^{\mathrm{i}k\theta}, \tag{7.206}$$

where χ represents unknowns; F_{ik} denotes the unknown coefficients; N_x and N_θ are numbers of collocation points in axial and circumferential

directions, respectively; and $T_i(x)$ is the Chebyshev polynomial of degree i defined for x in the range [−1.1]. Thus, the derivatives of the variables at the collocation points can be obtained:

$$\left.\frac{\partial \chi}{\partial x}\right|_{i,k} = \chi_x^1(x_i, \theta_k) = \sum_{m=0}^{N_x} d_{i,m}^1 \chi(x_m, \theta_k), \tag{7.207}$$

$$\left.\frac{\partial \chi}{\partial \theta}\right|_{i,k} = \chi_\theta^1(x_i, \theta_k) = \sum_{p=1}^{N_\theta} e_{k,p}^1 \chi(x_i, \theta_p), \tag{7.208}$$

where $i = 0, \ldots, N_x$, and $k = 0, \ldots, N_\theta$. $e_{k,\,p}^1$, $d_{i,\,m}^1$ are the first Fourier and Chebyshev derivative matrix given by Peyret [19]. Eqs. (7.202) through (7.205) can be discretized using the technique introduced earlier on both regions 1 and 2 shown in Fig. 7.7. Next, the treatment of the heat source will be introduced.

The first kind of heat source treatment that the heat input is assumed to be concentrated on a plate was introduced in Section 7.3.2.3. Here, another kind of heat input treatment will be introduced, that is, when the flame is distributed in a thin region.

Such method for treating longitudinal modes with distributed heat source is detailed in Li et al. [22]. In this case, the whole duct is divided into three regions, as shown in Fig. 7.8. In zone 1 and zone 2, there is no heat source, and the flow is uniform. Therefore, Q' in Eq. (7.200) should also be set to zero for these two regions. In zone f, the relevant equations are also Eqs. (7.202) through (7.205). However, the flow is axially non-uniform for the existence of the heat release. It is assumed that the mean heat is uniformly distributed over an axial length d. Assume that the center of the heat source is

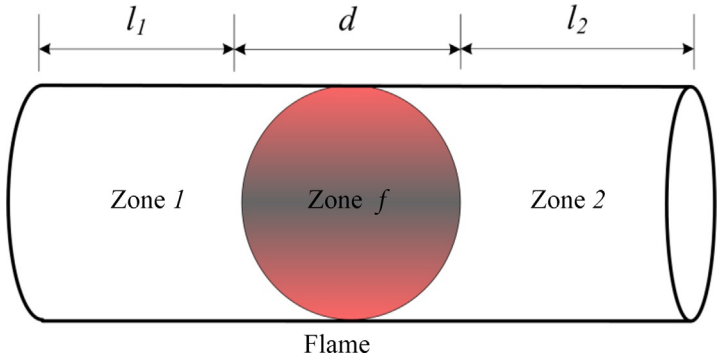

Fig. 7.8 The distributed heat source [20].

at $x = b$, where x is the axial coordinate. The mean heat input is given in the following form:

$$\overline{q}(x) = \begin{cases} c_p \overline{\rho}_1 \overline{u}_1 \left(\overline{T}_{02} - \overline{T}_{01}\right)/d & \text{for } |x-b| < \dfrac{1}{2}d \\ 0 & \text{for } |x-b| > \dfrac{1}{2}d \end{cases}. \tag{7.209}$$

Then it is easier to obtain the flow through the duct by integrating the one-dimensional conservation equations of mass, momentum, and energy. The distributed unsteady heat release can be written as:

$$Q'(x) = K_u(x) u'_1|_{x=L_1} + K_p(x) p'_1|_{x=L_1}. \tag{7.210}$$

Now the equations for these zones are discretized separately. In fact, the flow parameters are continuous across the interface of the two zones. Thus, we have:

$$\begin{aligned} p'_1 &= p'_f, \\ \rho'_1 &= \rho'_f, \\ u'_1 &= u'_f, \\ v'_1 &= v'_f, \end{aligned} \tag{7.211}$$

where the subscript f denotes zone f. The same relations are given for zone f and zone 2. It can be seen that, when zone f is thin enough, the case of distributed heat source is coherent with compacted heat source.

The basic equations and discretization method are particularly introduced in Section 7.3.2. The same boundary conditions as Eqs. (7.190)–(7.194) are needed for the LEEM. Actually, Eqs. (7.190), (7.193), and (7.194) can be used directly. However, no analytical form for entropy and vorticity disturbances can be found in linear Euler equations. Note that the difference between pressure and density disturbances is brought by entropy waves. Hence, a zero inlet entropy disturbance condition can be obtained by equation:

$$\left.\rho'_1 - \frac{p'_1}{\overline{c}_1^2}\right|_{x=0} = 0. \tag{7.212}$$

Similarly, a zero inlet vorticity disturbance condition can also be obtained by equation:

$$\left.\frac{1}{R}\frac{\partial u'_1}{\partial \theta} - \frac{\partial v'_1}{\partial x}\right|_{x=0} = 0. \tag{7.213}$$

In fact, substituting analytical expressions of the disturbances in Eqs. (7.174), (7.183)–(7.185) to Eqs. (7.212) and (7.213), we can obtain Eqs. (7.191) and (7.192). Hence, they are coherent.

For the compacted heat source, imposing the inlet and outlet boundary conditions, and jump conditions across the flame plane, the discrete forms of Eq. (7.202) through (7.205) can be written as:

$$\begin{pmatrix} \boldsymbol{\zeta_1} & \boldsymbol{\zeta_3} \\ \boldsymbol{\zeta_4} & \boldsymbol{\zeta_2} \end{pmatrix} \begin{pmatrix} \boldsymbol{\xi_1} \\ \boldsymbol{\xi_2} \end{pmatrix} = 0. \tag{7.214}$$

Here, $\boldsymbol{\zeta_1}$, $\boldsymbol{\zeta_2}$, $\boldsymbol{\zeta_3}$, and $\boldsymbol{\zeta_4}$ are submatrices of size $[4(N+1)]^2$ with only the complex frequency ω as the unknown, where $N = (N_x + 1)N_t - 1$. The column vectors $\boldsymbol{\xi_1}$ and $\boldsymbol{\xi_2}$ of length $4(N+1)$ contain the discrete unknowns in region 1 and 2, respectively. If Eq. (7.214) has non-zero solutions, the determinant of the matrix must be zero, and the complex frequency ω can be obtained by solving the equation:

$$\begin{vmatrix} \boldsymbol{\zeta_1} & \boldsymbol{\zeta_3} \\ \boldsymbol{\zeta_4} & \boldsymbol{\zeta_2} \end{vmatrix} = 0, \tag{7.215}$$

and with the frequency known, the spatial distributions in the flow can be acquired from Eq. (7.214).

For the distributed heat source, the system equations have the following form:

$$\begin{pmatrix} \boldsymbol{\zeta_1} & \boldsymbol{\zeta_3} & 0 \\ \boldsymbol{\zeta_4} & \boldsymbol{\zeta_f} & \boldsymbol{\zeta_5} \\ 0 & \boldsymbol{\zeta_6} & \boldsymbol{\zeta_2} \end{pmatrix} \begin{pmatrix} \boldsymbol{\xi_1} \\ \boldsymbol{\xi_f} \\ \boldsymbol{\xi_2} \end{pmatrix} = 0, \tag{7.216}$$

where $\boldsymbol{\zeta}$ and $\boldsymbol{\xi}$ are defined the same as Eq. (7.214). The eigenfrequency can also be solved through the same process.

As shown in Fig. 7.7, the geometry parameters are given as the entire length of the chamber $L = 0.2$ m, length of region 1 and region 2 $L1 = 0.1$ m, $L2 = 0.1$ m, respectively, and the mean radius of the annular chamber $R = 0.3$ m. For the mean flow of the region 1, the pressure is 4 Mpa, and the stagnation temperature is 700 K. Therefore, with the given inlet flow Mach number and the temperature ratio across the flame, the mean flow parameters of region 2 can be calculated through conservation relations. Some of these parameters are in reference to Stow and Dowling [23]. The mean heat input per unit area from the flame can be given as:

$$\overline{Q} = C_p\left(K_t \overline{T}_{01} - \overline{T}_{01}\right)\overline{\rho}_1 \overline{u}_1, \tag{7.217}$$

with

$$\overline{T}_{02} = K_t \overline{T}_{01},$$

where the subscript 0 denotes the stagnation temperature, and K_t denotes the stagnation temperature ratio across the flame. Three form of unsteady heat release are given as:

$$Q' = 0, \tag{7.218}$$

$$\frac{Q'}{\overline{Q}} = k_u \frac{u_1'}{\overline{u}_1} e^{-i\omega\tau}|_{x=L_1}, \tag{7.219}$$

$$\frac{Q'}{\overline{Q}} = k_p \frac{p_1'}{\overline{p}_1} e^{-i\omega\tau}|_{x=L_1}, \tag{7.220}$$

where τ denotes the time lag between the unsteady heat release and reference disturbance, and k_u and k_p are coefficients. Eq. (7.218 denotes no unsteady heat release. Eqs. (7.219) and (7.220) denote that the unsteady heat release is induced by velocity and pressure disturbances at the place of flame in region 1, respectively. For distributed heat source used in LEEM, the unsteady heat release can be written as:

$$\begin{aligned} Q'(x) &= 0, \\ \frac{Q'(x)}{\overline{q}(x)} &= k_u \frac{u_1'(L_1)}{\overline{u}_1} e^{-i\omega\tau}, \\ \frac{Q'(x)}{\overline{q}(x)} &= k_p \frac{p_1'(L_1)}{\overline{p}_1} e^{-i\omega\tau}, \end{aligned} \tag{7.221}$$

where $q(x)$ is given by Eq. (7.209).

Lieuwen [24] discussed the main causes of unsteady combustion. It shows that in a real lean premixed combustor, the unsteady heat release is greatly influenced by the velocity disturbance near the fuel bars rather than by the unsteady pressure. However, all three forms of the unsteady heat release are used here. On one hand, we want to investigate how the unsteady heat release affects the generation of vorticity waves. On the other hand, we also want to know whether it can reach a general conclusion by using these different forms of unsteady heat release.

7.3.3.2 Results and discussion

Results for the acoustically closed outlet boundary condition are given in the following section. Fig. 7.9 depicts the real and imaginary part of the frequency of azimuthal mode $m = 1$ as a function of temperature ratio across

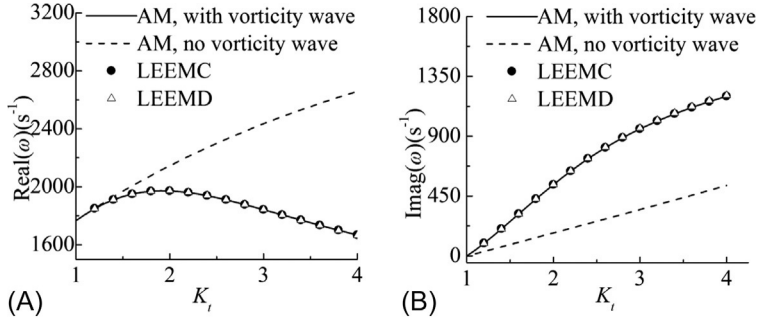

Fig. 7.9 The real and imaginary part of the frequency as a function of K_t, for no unsteady heat release, $m = 1$, no axial modes, and inlet flow Mach number 0.1 [20]. (A) Real part of the frequency; (B) Imaginary part of the frequency.

the flame K_t for no unsteady heat release (Eq. (7.213)) and inlet flow Mach number 0.1. Four types of results are given. They are the results from the AM with and without the effect of vorticity waves, LEEM with a compact heat source (denoted by LEEMC), and distributed heat source (LEEMD). For the distributed heat source, the length of the three regions is given as region 1 0.099 m, region f 0.02 m, and region 2 0.099 m. Good agreement is observed between results of AM with the vorticity disturbance and LEEM, which shows that the solutions of the unsteady flow field (Eqs. 7.174, 7.183–7.185) are correct. Moreover, the results of LEEMC and LEEMD are also the same. It indicates the jump conditions given by Eqs. (7.186)–(7.189) are reliable. Furthermore, for the real part of the frequency, when the temperature ratio across the flame K_t is small (<1.5), the results of the AM without vorticity waves are almost the same as the results with vorticity wave. However, with the increase of the value of K_t, a significant deviation appears between results with and without the vorticity wave. For the imaginary part of the frequency, the differences between the results with and without vorticity wave are large. Note that, because the unsteady heat release is zero, the imaginary part of the frequency is positive, which denotes that no instabilities occur. When the temperature and the mean velocity in regions 1 and 2 are not equal, the reflections of inlet and outlet are not symmetrical, which would bring damping to the system.

Fig. 7.10 depicts the real and imaginary part of the frequency of azimuthal mode $m = 1$ as a function of temperature ratio across the flame K_t for the unsteady heat release related to axial velocity disturbance (Eq. (7.48), $k_u = 1$ and $\tau = 0$) and inlet flow Mach number 0.1. Fig. 7.11 shows the results for the unsteady heat release related to pressure disturbance

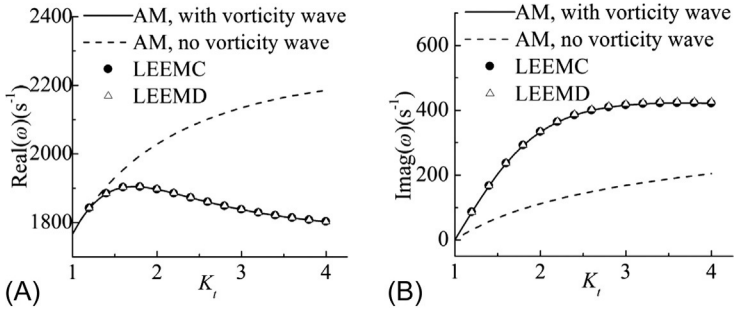

Fig. 7.10 The real and imaginary part of the frequency as a function of K_t, for unsteady heat release related to axial velocity disturbance $k_u = 1$, $\tau = 0$, $m = 1$, no axial modes, and inlet flow Mach number 0.1 [20]. (A) Real part of the frequency; (B) Imaginary part of the frequency.

(Eq. (7.49), $k_p = 2$, $\tau = 0.0003$ s) and flow Mach number 0.05. If the angular frequency is given to be 2000 s^{-1}, the value of the time delay is about one-tenth of the period. Good agreements are also found between the results of AM with vorticity wave and LEEM in Figs. 7.10 and 7.11. When the value of K_t is small, the real part of the frequencies obtained by AM with vorticity wave almost equals the results without the vorticity wave, which is the same as Fig. 7.9. When K_t becomes large, the difference is significant. For the imaginary part of the frequency, the results with and without vorticity waves are not the same at all. In Fig. 7.11, it is found that the imaginary part of the frequency obtained by AM without the vorticity wave is below zero, which denotes that this mode is unstable. But the results with the effect of the vorticity wave are positive, which shows the mode is stable.

The outlet boundary condition is given to be acoustically closed end, where the coupling between axial velocity and vorticity disturbances occurs. The coupling of the acoustic and vorticity disturbances significantly changes the reflection of the outlet boundary. Therefore, in Figs. 7.9–7.11, we can observe that, for the real part of the frequency, the results with and without the vorticity waves are different. It can also be observed from Figs. 7.9–7.11 that the imaginary parts of the frequencies obtained by AM with the vorticity wave are significantly greater than the results without the vorticity waves. In Fig. 7.11, the calculated results without the vorticity wave show the system is unstable, but the results with the vorticity wave denote that the system is very stable. In fact, the generation of a vorticity disturbance from the interaction of an acoustic disturbance and heat release transfers energy from the acoustic mode to vertical mode, which causes damping to the acoustic perturbation. Such vorticity waves propagate out of the boundary with the

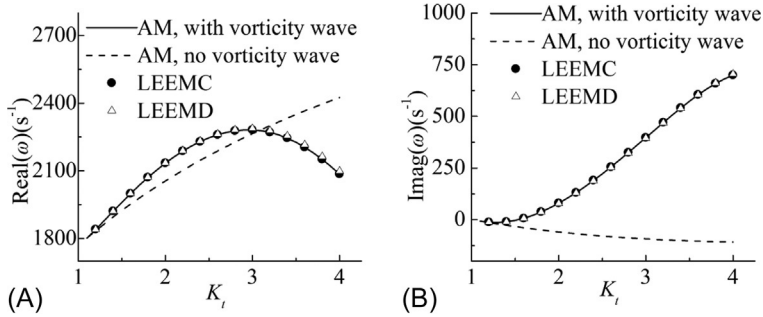

Fig. 7.11 The real and imaginary part of the frequency as a function of K_t, for unsteady heat release related to pressure disturbance, $k_p = 2$, $\tau = 0.0003$ s, $m = 1$, no axial modes, and inlet flow Mach number 0.05[20]. (A) Real part of the frequency; (B) Imaginary part of the frequency.

flow. Then, the interaction between vorticity disturbances and the outlet boundary generates acoustic wave propagating upstream. All the results show that the system is more stable when the vorticity waves are considered. It means that the vorticity disturbances cause damping to the system. From Figs. 7.9–7.11, it is also found that vorticity waves are generated with all forms of unsteady heat release, even when the unsteady heat release is zero.

Fig. 7.12 depicts the frequencies as a function of inlet flow Mach number for $m = 1$, no axial modes, the unsteady heat release is related to the axial velocity disturbances ($k_u = 1$, $\tau = 0$), and inlet temperature ratio across flame $K_t = 3$. Good agreements are observed between the results of AM with the vorticity wave and LEEM. The results of LEEMC and LEEMD are the same. The differences between results with and without the vorticity

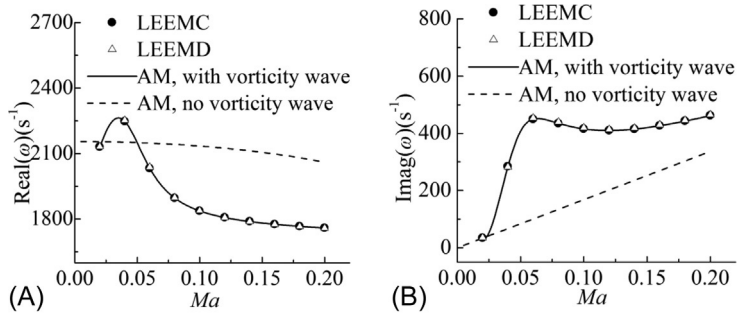

Fig. 7.12 The real and imaginary part of the frequency as a function of inlet flow Mach number, for unsteady heat release related to axial velocity disturbance, $k_u = 1$, $\tau = 0$, $m = 1$, no axial modes, and inlet temperature ratio across flame $K_t = 3$ [20]. (A) Real part of the frequency; (B) Imaginary part of the frequency.

wave are significant. For the real part of the frequency, the results without the vorticity wave decrease with an increase of flow Mach number. This phenomenon accords with the results that the frequency of axial mode decrease as the flow Mach number is increased [9]. With the effect of the vorticity disturbance, when the flow Mach number increases, the frequencies also increase if the Mach number is not large. However, when the flow Mach number is greater than some value (e.g., 0.05), the frequencies decrease. If the values are given as $K_t = 3$, it can be estimated that $\omega = 2200$ Hz, and the sound speed of the region 2 is about 900 m/s. The wavelength of vorticity wave in region 2 is determined by $2\pi u_2/\omega$. If the wavelength is 0.1 m, which is the length of the region 2, the value of the mean flow velocity is about 35 m/s, and the flow Mach number is about 0.04. The Mach number of the flow in region 1 is the same order with this. When the flow Mach number is greater than this value, there will not be an entire wavelength of vorticity wave in region 2. But if the flow Mach number is less than the value, there will be one more wavelength in region 2. This is why the reflection points exist in the curves of frequency-flow Mach number. When the wavelength is equal to 0.1 m, it can be deduced that the vorticity disturbance at the outlet boundary is just in phase with the acoustic wave. At this condition, the frequency will not be affected by the vorticity disturbances.

Next, the eigenfrequency with the choked outlet boundary condition will be discussed. For the choked outlet boundary, the acoustic, vorticity, and entropy waves are coupled. This is different from the closed outlet boundary condition, for which only acoustic and vorticity disturbance are constrained, but the entropy wave is free. Fig. 7.13 depicts the real and imaginary part of the frequency of azimuthal mode $m = 1$ as a function of

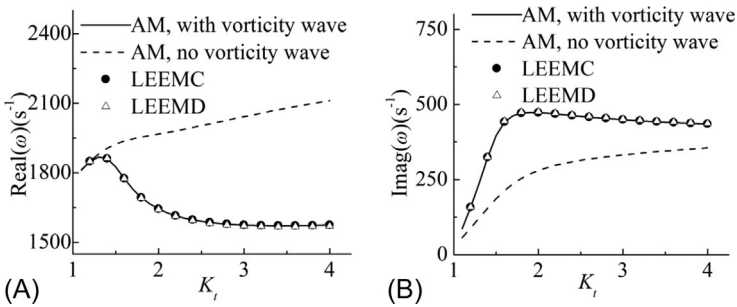

Fig. 7.13 The real and imaginary part of the frequency as a function of K_t, for unsteady heat release related to axial velocity disturbance, $k_u = 0.2$, $\tau = 0$, $m = 1$, no axial modes, and inlet flow Mach number 0.1 [20]. (A) Real part of the frequency; (B) Imaginary part of the frequency.

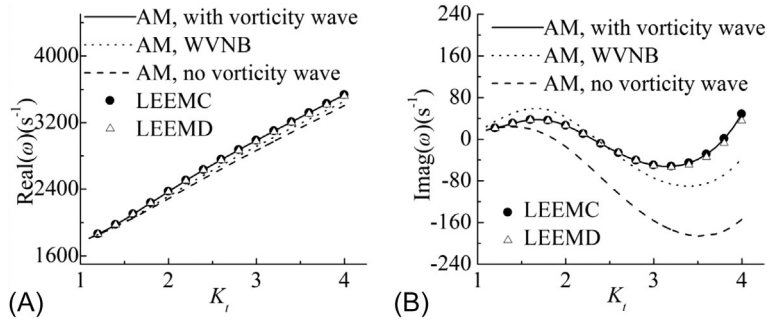

Fig. 7.14 The real and imaginary part of the frequency as a function of K_t, for unsteady heat release related to axial velocity disturbance, $k_u = 0.2$, $\tau = 0.0015$ s, $m = 1$, no axial modes, and inlet flow Mach number 0.05; WVNB denotes the results with vorticity wave but no boundary coupling with vorticity wave [20]. (A) Real part of the frequency; (B) Imaginary part of the frequency.

temperature ratio across the flame K_t for unsteady heat release related with axial velocity disturbances ($k_u = 0.2$, $\tau = 0$) and inlet flow Mach number 0.1. It also gives results of four methods. The results with and without vorticity waves have large discrepancies. The agreement between results of AM with vorticity wave and LEEM is good. And the results of LEEMC and LEEMD are the same, as well. Fig. 7.14 shows the eigenfrequency of azimuthal mode $m = 1$ for $k_u = 0.1$, $\tau = 0.0015$ s, and inlet flow Mach number 0.05. For angular frequency 3000 s^{-1}, the period is about 0.002 s. The time lag is 3/4 of the period. From the results without the vorticity wave, it can be seen that the imaginary part of the frequency is negative, which denotes the system is unstable. But with the vorticity wave, the imaginary part of frequency is positive for some range of K_t. And the value with the vorticity wave is always greater than the value without the vorticity wave. Moreover, the real part of a frequency obtained with and without vorticity disturbance are almost the same. This is because, under this condition, the wavelength of such a disturbance is just equal to length of the region 2 (see Fig. 7.7).

Fig. 7.14 gives the results with the vorticity wave, but no boundary coupling of the vorticity wave is given. Under this condition, the vorticity disturbances propagate out of the system without reflection. It means that all the energy transferred from the acoustics to the vertical mode is damped. The imaginary part of the frequency is greater than the results without the vorticity wave. When K_t is small, the imaginary part is also greater than the results with the coupling of the vorticity wave at the boundary. However, when K_t gets larger, the value is less than that with the coupling effect at the boundary. It denotes that, under this condition, the coupling between

acoustic, vorticity, and entropy waves reflects less perturbation energy than that without coupling effect of the vorticity waves. The mode structures of the pressure, density, and velocity disturbances and the specific explanation of the generation of vorticity wave can be seen in a study by Lieuwen [24].

In this section, the problem of the azimuthal instabilities in an annular chamber is investigated. With the assumptions of mean flow and compacted heat release, the effects of vorticity waves are studied in an analytical model. The LEEM is applied to validate the analytical model with the vorticity wave. In the Euler equation method, the heat source is assumed to be compacted in a plate or distributed in a thin region. The results of AM without the vorticity wave are also given on the analogy of a network model and finite element method. After the calculations, good agreements are observed between results of the AM with the effect of the vorticity wave and the linear Euler equations method. And results of the LEEM with compacted and distributed heat sources are also the same. However, for pure azimuthal modes, significant differences are found between the results with and without vorticity waves in AM. For the mixed mode of azimuthal and axial modes, the results with and without vorticity waves are almost the same, which shows that the effects of vorticity waves are weak for mixed modes. Moreover, for longitudinal modes, the results without vorticity disturbances and LEEM are the same. From these investigations, the following conclusions can be obtained: (a) The comparison of AM and LEEM shows that the description of the flow disturbances in AM is correct; (b) The comparison of the heat source treatments shows that the jump conditions used for a compacted heat source are reliable; (c) For azimuthal and axial mixed modes, the vorticity disturbance indeed exists; however, its effect on the instabilities is very weak and can be even ignored; (d) For longitudinal modes with mean flow and uniform heat source, no vorticity waves exist.; and (e) For pure azimuthal mode, the vorticity waves are generated by the interaction between acoustic waves and the heat source. Also, the circumferential velocity disturbance continuity across the flame sheet is the mechanism of vorticity disturbance generation in the present case. In conclusion, two kinds of effects of vorticity waves are observed: (i) the coupling of axial acoustic and vorticity disturbances at the acoustically closed end affects the frequencies of the system and (ii) the generation of vorticity disturbance causes damping to the system. For the pure azimuthal modes, the effects of the vorticity disturbances are significant. When the flow Mach number is small, such effects become weak. However, in the combustor of a gas turbine, the effect of mean flow is inevitable; therefore. it can be concluded that the calculations of azimuthal

instabilities using network model and finite element method may lead to a severe prediction error if the mean flow is considered. This also indicates the essence and necessity of the three-dimensional AM.

7.4 Control of thermoacoustic instability in a Rijke tube

The control methods of combustion instability can be grouped into passive control methods and active control methods. Because of the intrinsic disadvantages of an active control method, in practical applications, a passive control method is widely adopted, for example, the baffles in rocket engines, the Helmholtz resonators in gas turbines, and the perforated liners in afterburners of aeroengines, and so on. Although the mathematical description of Helmholtz resonators is easy by analytical approach, they are not widely used in rocket engines and aeroengines for the shortcoming of bulk and narrow frequency bandwidth. The cooling system in the afterburners of aeroengines can be models as perforated liners with bias flow. It is severely wrong to model the distributed damping system as a lumped parameter system. Thus, only a three-dimensional model is able to do that. The traditional way to consider the effect of the wall boundary is to provide the boundary condition of the wall, then the impedance of the wall is obtained. For example, the boundary condition for a hard wall is:

$$\left.\frac{\partial p}{\partial r}\right|_{r=R} = 0, \tag{7.222}$$

The eigenvalue of the radial eigenfunction can be obtained by solving the following equation:

$$J'_m(k_{mn}R) = 0, \tag{7.223}$$

where $J_m(k_{mn}r)$ is the m order Bessel function. Obviously, the eigenvalue k_{mn} is only related to the radius R. However, for the soft wall boundary condition, the impedance is always related to the frequency, $Z = Z(\omega)$. It is very difficult to find the impedance corresponding to some specific frequency. Moreover, the eigenvalue k_{mn} is related to the impedance of the wall. As a consequence, the eigenvalue k_{mn} is indirectly related to the frequency. If we solve the problem by the traditional way, it is needed to carry out two complex processes of iteration because Fig. 7.15 shows which is unreliable and unstable in numerical calculation, and the solutions are not accurate. Therefore, the traditional way of solving the thermoacoustic problems associated with soft wall boundary is not feasible. Sun and Wang [26–28]

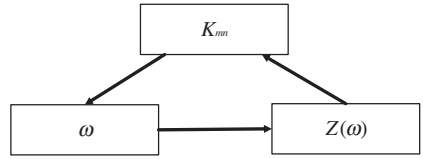

Fig. 7.15 The double iteration [25].

posed a new method named the "Transfer Element Method (TEM)" that is used to consider the interaction between the acoustic source and the soft acoustic treatment, which can be adopted here to avoid obstacles.

7.4.1 Perforated liner with bias flow

In this part, the control method using perforated liner with bias flow is presented. First, the main idea of the TEM will be briefly introduced.

As sketched in Fig. 7.16, a section of a circular tube is installed with a combination of perforated liner and a back cavity. In the view of acoustics, it is called nonlocally reacting liner. The main flow parameters are respectively denoted with the pressurep_0, the density ρ_0, the speed of sound C_0, and the Mach number M_a. For simplicity, we assume $M_a < 1$. As shown in Fig. 7.16, the pressure disturbance in the tube can be regarded as the sum of the incident acoustic pressure and the scattered acoustic pressure of the liner,

$$p = p_i + p_s, \tag{7.224}$$

where p_i is the acoustic pressure without the liner. At the hole on the liner, the displacement of the fluid particles is not zero. Thus, the motion of the particle can be seen as a mass source, which will induce the scattered acoustic

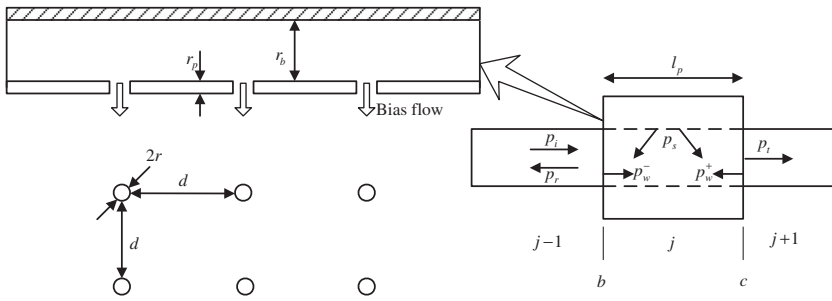

Fig. 7.16 Perforated liner with back cavity [25].

pressure p_s. If the acoustic pressure in the cavity and in the tube are respectively denoted as p^+ and p^-, then in the annular cavity with bias flow, according to the Rayleigh conductivity, we have:

$$c = \frac{i\omega_0 \rho_0 Q}{p^+ - p^-}, \tag{7.225}$$

where $p^+ = p_s^+$, $p^- = p_s^- + p_i^-$, and Q is the volume flux in the hole. Therefore, we obtain the oscillation equation:

$$p_s^- - p_s^+ + \frac{i\omega_0 \rho_0 Q}{c} = -p_i^-. \tag{7.226}$$

With the help of sine transform, Eq. (7.226) can be written as:

$$\begin{aligned} &\frac{2}{l_p}\int_0^{l_p}\left(p_s^- - p_s^+\right)\sin\frac{j'\pi x}{l_p}dx + \frac{2}{l_p}\int_0^{l_p}\frac{i\omega_0\rho_0 Q}{c}\sin\frac{j'\pi x}{l_p}dx \\ &= -\frac{2}{l_p}\int_0^{l_p} p_i \sin\frac{j'\pi x}{l_p}dx, \end{aligned} \tag{7.227}$$

where $j' = 1, 2, 3, 4, \cdots$, $\frac{Q}{c} = \frac{V_n}{\eta}$, $V_n = \sum_{j'} V_{j'} \sin\frac{j'\pi x'}{l_p}$ represents the averaged velocity fluctuation of the mass source in the hole, and l_p is the length of the liner. Thus, Eq. (7.227) can be written as:

$$\sum_k \left(z_{j'k}^- - z_{j'k}^+ + \delta_{j'k}\frac{i\omega_0\rho_0}{\eta}\right) V_{j'} = -I_{j'}, \tag{7.228}$$

where $k = 1, 2, 3, 4, \ldots$, and η is given by Eldredge & Dowling [29],

$$\frac{1}{\eta} = \frac{\pi r_o^2}{\sigma}\frac{1}{K_a} + \frac{r_p}{\sigma}, \tag{7.229}$$

where r_o is the radius of the hole, r_p is the thickness of the perforated liner, $\sigma = \pi {r_o}^2/d^2$, $K_a = 2r_o(\gamma + i\delta)$, and γ and δ are both given by Howe [30].

To solve this problem, the relationship between the scattered acoustic pressure and the velocity fluctuation of the mass source in the hole need to be found. By applying the Green function method [26], the acoustic field induced by the mass source is obtained:

$$\widetilde{p}\left(\vec{x}, t\right) = -\int_{-T}^{T}\int_{s(\tau)} \rho_0 \widetilde{V}_n' \frac{D_0 G}{D\tau} ds\left(\vec{\gamma}\right) d\tau, \tag{7.230}$$

where $\frac{D_0}{D\tau}=\frac{\partial}{\partial\tau}+U\frac{\partial}{\partial x}$ is the total derivative, and n denotes the outer normal direction. What needs to be pointed out is the outer normal direction in the tube, whereas the cavity is opposite. G is the Green's function, which has a different form in the tube and in the cavity respectively as:

$$G=\frac{-i}{4\pi}\sum_{m=-\infty}^{+\infty}\sum_{n=1}^{+\infty}\left[\frac{\psi_m(k_{mn}r)e^{im\theta}\psi_m(k_{mn}r')e^{-im\theta'}}{\Gamma_{nm}}\times\int_{-\infty}^{\infty}\frac{1}{\kappa_{mn}}e^{i\omega(t-\tau)+i\alpha^{\pm}_{m,n}(x-x')}d\omega\right], \tag{7.231}$$

$$G=-\frac{1}{2\pi}\sum_{m=-\infty}^{+\infty}\sum_{n=1}^{+\infty}\sum_{q=0}^{+\infty}\left[\frac{\phi_m(k_{mn}r)e^{im\theta}\cos\frac{q\pi x}{l_p}\phi_m(k_{mn}r')e^{-im\theta'}\cos\frac{q\pi x'}{l_p}}{\Gamma_{mnq}}\times\int_{-\infty}^{\infty}\frac{e^{i\omega(t-\tau)}}{k_0^2-k_{mnq}^2}d\omega\right], \tag{7.232}$$

where $\psi_m(k_{mn}r)$ is the radial eigenfunction of the tube, i.e., the first kind of Bessel function. $\phi_m(k_{mn}r)$ is the radial eigenfunction of the annular tube, which is the linear combination of the first kind of Bessel function and the second kind of Bessel function. $k_0=\frac{\omega}{C_0}$, $\alpha^{\pm}_{mn}$ is the axial wave numbers as stated before,

$$\alpha^{\pm}_{mn}=\frac{M_a^2k_0\pm\sqrt{k_0^2-\left(1-M_a^2\right)k_{mn}^2}}{1-M_a^2}. \tag{7.233}$$

Γ_{mn}, Γ_{mnq} and κ_{mn} are given as:

$$\Gamma_{mn}=\int_A\left|\psi_m(k_{mn}r)e^{im\theta}\right|^2drd\theta, \tag{7.234}$$

$$\Gamma_{mnq}=\begin{cases}\Gamma_{mn}\cdot l & q=0\\ \Gamma_{mn}\cdot\dfrac{l}{2} & q\neq0\end{cases}, \tag{7.235}$$

$$\kappa_{mn}=\begin{cases}\sqrt{k_0^2-\left(1-M_a^2\right)k_{mn}^2} & k_0^2>\left(1-M_a^2\right)k_{mn}^2\\ -i\sqrt{\left(1-M_a^2\right)k_{mn}^2-k_0^2} & k_0^2<\left(1-M_a^2\right)k_{mn}^2\end{cases}. \tag{7.236}$$

Substitute the Green function and $\lim_{T\to\infty}\int_{-T}^{T}e^{i(\omega_0-\omega)\tau}d\tau=2\pi\delta(\omega_0-\omega)$ into Eq. (7.230), we get:

$$\widetilde{p}_s^- = \frac{\rho_0 e^{i\omega_0 t}}{2} \sum_{m=-\infty}^{\infty} \sum_{n=1}^{\infty} \frac{\psi_m(k_{mn} r) e^{im\theta}}{\Gamma_{mn}} \int_{s(\tau)} V_n' \psi_m(k_{mn} r') e^{-im\theta'} \frac{\left[\omega + U\alpha_{mn}^{\pm}\right]}{\kappa_{mn}} e^{i\alpha_{mn}^{\pm}(x-x')} ds\left(\vec{\gamma}\right), \tag{7.237}$$

$$\widetilde{p}_s^+ = i\rho_0 \omega_0 e^{i\omega_0 t} \sum_{m=-\infty}^{+\infty} \sum_{n=1}^{+\infty} \sum_{q=0}^{+\infty} \frac{\phi_m(k_{mn} r) e^{im\theta} \cos\frac{q\pi x}{l_p}}{\Gamma_{mnq}\left(k_0^2 - k_{mnq}^2\right)} \int_{s(\tau)} V_n \phi_m(k_{mn} r') e^{-im\theta'} \cos\frac{q\pi x'}{l_p} dS\left(\vec{\gamma}\right). \tag{7.238}$$

According to the continuity of the displacement of the particle, the velocity fluctuation at the hole can be expanded as sine forms along the axial direction,

$$V_n' = \frac{\partial \eta}{\partial \tau} + U\frac{\partial \eta}{\partial x'} = V_n + \frac{U}{i\omega}\frac{\partial V_n}{\partial x'} = \left(1 + \frac{U}{i\omega}\frac{\partial}{\partial x'}\right) \sum_{k=1}^{\infty} V_k^{\theta\prime} \sin\frac{k\pi x'}{l_p}. \tag{7.239}$$

Substitute $\int_0^{2\pi} V_k^{\theta\prime} e^{-im\theta'} d\theta' = 2\pi V_k^m$ into the acoustic pressure equation, then take the[0] sine transformation, and then the radiation impedance equation can be expressed as:

$$z_{j'k}^- = \frac{\rho_0 e^{i\omega_0 t}}{l} \sum_{m=-\infty}^{\infty} \sum_{n=1}^{\infty} \frac{\psi_m(k_{mn} r_h)\psi_m(k_{mn} r_h)}{\Gamma_{mn}\kappa_{nm}} \int_0^l \int_0^l \left[\omega + U\alpha_{mn}^{\pm}\right] e^{i\alpha_{mn}^{\pm}(x-x')} \left(1 + \frac{U}{i\omega}\frac{\partial}{\partial x'}\right) \sin\frac{k\pi x'}{l} dx' \sin\frac{j'\pi x}{l} dx, \tag{7.240}$$

$$z_{j'k}^+ = \frac{4i\pi\rho_0\omega_0 r_h e^{i\omega_0 t}}{l} \sum_m \sum_n \sum_q \frac{\phi_m(k_{mn} r_h)\phi_m(k_{mn} r_h)}{\Gamma_{mnq}\left(k_0^2 - k_{mnq}^2\right)} \int_0^l \cos\frac{q\pi x}{l} \sin\frac{k\pi x}{l} dx \int_0^l \cos\frac{q\pi x'}{l} \sin\frac{j'\pi x'}{l} dx'. \tag{7.241}$$

Substitute Eqs. (7.240) and (7.241) into Eq. (7.228), then the velocity fluctuation quantity at the hole is solved. The scattered acoustic pressure can now be expressed with the coefficients of the incident acoustic pressure. As shown in Fig. 7.16, the section with perforated liner is denoted by j, the left side and

the right side of the liner section are respectively denoted by b and c, p_i and p_r are respectively the incident and reflected acoustic pressure at the b interface, and P_w^+,P_w^- and p_s are respectively the propagating acoustic pressure and the scattered acoustic pressure. P_w^+ and P_w^- can be written as:

$$P_w^m = \sum_n P_{mn}^{m\,j} \psi_m(k_{mn} r) e^{i\alpha_{mn}^m x + im\theta}. \tag{7.242}$$

Eq. (7.228) can be written as:

$$V_{j'} = -I_{j'} Z_{j'k,\mu,P}^{-1}, \tag{7.243}$$

where $Z_{j'k,\mu,P} = \sum_k \left(z_{j'k}^- - z_{j'k}^+ + \delta_{j'k} \frac{i\omega_0 \rho_0}{\eta} \right)$. And the scattered acoustic pressure is expressed as:

$$\begin{aligned} p_s = {} & \pi \rho_0 r_0 \sum_{n=1}^{\infty} \frac{\psi_m(k_{mn} r) \psi_m(k_{mn} r_0) e^{im\theta + i\alpha_{m,n}^{\pm} x}}{\Gamma_{mn}} \frac{\left[\omega + U\alpha_{m,n}^{\pm}\right]}{\kappa_{mn}} \\ & \left\{ \sum_{\mu=1}^{\infty} \psi_m(k_{m\mu} r_0) \left[P_{m\mu}^{-\,j} Q_{n-}^{P_{m\mu}^{-\,j}} + P_{m\mu}^{+\,j} Q_{n+}^{P_{m\mu}^{+\,j}} \right] \right\}, \end{aligned} \tag{7.244}$$

where P_{mn}^{-j} and P_{mn}^{+j} are the unknown amplitudes, moreover,

$$Q_{n\mp}^{P_{m\mu}^{\mp\,j}} = \sum_{k=1}^{\infty} z_{j'k,\mu,P}^{-1} I_{j'}^{P_{m\mu}^{\mp\,j}} S_k^{n\mp}, \tag{7.245}$$

$$S_k^{n\pm} = \int_0^1 e^{-i\alpha_{mn}^{\pm} x'} \left(1 + \frac{U}{i\omega} \frac{\partial}{\partial x'} \right) \sin \frac{k\pi x'}{l} dx'. \tag{7.246}$$

Finally, the total acoustic pressure in the tube is obtained,

$$\begin{aligned} p = P_w^+ + P_w^- + p_s = {} & \sum_n P_{mn}^{-\,j} \psi_m(k_{mn} r) e^{i\alpha_{mn}^- x + im\theta} \\ & + \sum_n P_{mn}^{+\,j} \psi_m(k_{mn} r) e^{i\alpha_{mn}^+ x + im\theta} \\ & + \pi \rho_0 r_0 \sum_{n=1}^{\infty} \frac{\psi_m(k_{mn} r) \psi_m(k_{mn} r_0) e^{im\theta + i\alpha_{mn}^{\pm} x}}{\Gamma_{m,n}} \frac{\left[\omega + U\alpha_{m,n}^{\pm}\right]}{\kappa_{n,m}} \\ & \left\{ \sum_{\mu=1}^{\infty} \psi_m(k_{m\mu} r_0) \left[P_{m\mu}^{-\,j} Q_{n-}^{P_{m\mu}^{-\,j}} + P_{m\mu}^{+\,j} Q_{n+}^{P_{m\mu}^{+\,j}} \right] \right\} \\ = {} & \sum_{n=1}^{\infty} \psi_{mn}(r) \sum_{\mu=1}^{\infty} \left(P_{m\mu}^{+\,j} p_{\mu n}^+ + P_{m\mu}^{-\,j} p_{\mu n}^- \right) e^{im\theta}, \end{aligned} \tag{7.247}$$

where $\psi_{mn}(r)$ is written as the form of $\psi_m(k_{m,n}r)$, $p^+_{\mu n}$ and $p^-_{\mu n}$ can be written as the following forms,

$$p^{\pm}_{\mu n} = \pi\rho_0 r_0 \frac{\psi_m(k_{m,n}r_0)e^{i\alpha^{\pm}_{m,n}x}}{\Gamma_{m,n}} \times \frac{\left[\omega + U\alpha^{\pm}_{m,n}\right]}{\kappa_{n,m}} \psi_m\left(k_{m\mu}r_0\right) Q^{p^{\pm j}_{m\mu}}_{n\pm} + \delta_{n\mu}e^{i\alpha^{\pm}_{mn}x}. \tag{7.248}$$

Both the velocity fluctuation and density fluctuation in the tube can be expressed similarly as the pressure fluctuation. Therefore, the derivation aforementioned is aimed at achieving the specific forms of the TEM used on the three-dimensional analytical model.

As the fluctuation quantities are obtained, as shown in Fig. 7.16, the equations of mass, momentum, and energy are formed. For example, at the interface b, we have:

$$\sum_{n=1}^{\infty}[A^{+\,j-1}_{mn}\psi^{+\,j-1}_{mn}(r)P^{+\,j-1}_{mn} + A^{-\,j-1}_{mn}\psi^{-\,j-1}_{mn}(r)P^{-\,j-1}_{mn} + A^{+\,j-1}_{vmn}\psi^{+\,j-1}_{vmn}(r)\rho^{+\,j-1}_{vmn} + \psi^{+\,j}_{mn}(r)\sum_{\mu=1}^{\infty}A^{+\,j}_{mn\mu}P^{+\,j}_{m\mu} + \psi^{-\,j}_{mn}(r)\sum_{\mu=1}^{\infty}A^{-\,j}_{mn\mu}P^{-\,j}_{m\mu} + A^{+\,j}_{vmn}\psi^{+\,j}_{vmn}(r)\rho^{+\,j}_{vmn}] = 0, \tag{7.249}$$

$$\sum_{n=1}^{\infty}[B^{+\,j-1}_{mn}\psi^{+\,j-1}_{mn}(r)P^{+\,j-1}_{mn} + B^{-\,j-1}_{mn}\psi^{-\,j-1}_{mn}(r)P^{-\,j-1}_{mn} + B^{+\,j-1}_{vmn}\psi^{+\,j-1}_{vmn}(r)\rho^{+\,j-1}_{vmn} + \psi^{+\,j}_{mn}(r)\sum_{\mu=1}^{\infty}B^{+\,j}_{mn\mu}P^{+\,j}_{m\mu} + \psi^{-\,j}_{mn}(r)\sum_{\mu=1}^{\infty}B^{-\,j}_{mn\mu}P^{-\,j}_{m\mu} + B^{+\,j}_{vmn}\psi^{+\,j}_{vmn}(r)\rho^{+\,j}_{vmn}] = 0, \tag{7.250}$$

$$\sum_{n=1}^{\infty}[C^{+\,j-1}_{mn}\psi^{+\,j-1}_{mn}(r)P^{+\,j-1}_{mn} + C^{-\,j-1}_{mn}\psi^{-\,j-1}_{mn}(r)P^{-\,j-1}_{mn} + C^{+\,j-1}_{vmn}\psi^{+\,j-1}_{vmn}(r)\rho^{+\,j-1}_{vmn} + \psi^{+\,j}_{mn}(r)\sum_{\mu=1}^{\infty}C^{+\,j}_{mn\mu}P^{+\,j}_{m\mu} + \psi^{-\,j}_{mn}(r)\sum_{\mu=1}^{\infty}C^{-\,j}_{mn\mu}P^{-\,j}_{m\mu} + C^{+\,j}_{vmn}\psi^{+\,j}_{vmn}(r)\rho^{+\,j}_{vmn}] = 0, \tag{7.251}$$

where A_{mn}, B_{mn}, C_{mn} are the coefficients related to the equation of mass, momentum, and energy, respectively. Obviously, they are different from those from the hard-wall situation. For the hard-wall boundary condition, each radial mode at one side of the interface is matched with the same radial mode at the other side of the interface. However, when the soft treatment such as a liner is included in the tube, each incident radial mode is matched with infinite radial modes at the other side.

At the interface c with the same pattern, similar expressions are obtained. At last, a series of equations are obtained including the end boundary conditions and heat release functions. Although the radial eigenfunction $\psi_{mn}(r)$ is still orthogonal, after the orthogonal transformation the modes still stay tangled. Thus, the equations need to be solved with all the modes considered, which is different from that of a hard-wall condition. If the calculation is only aimed at low-order modes, we set $\mu = N_\mu$ approximately; in fact, for the fundamental incident acoustic wave, it is precise enough to assume $N_\mu = 3$. For the situation shown in Fig. 7.16, for the three parts of $j-1, j,$ and $j+1$, assuming that $N_\mu = 2$, when the two interfaces of b, c are considered, we have:

$$\begin{pmatrix} D_{11} & D_{12} & 0 \\ 0 & D_{22} & D_{23} \end{pmatrix} \begin{pmatrix} P_1 \\ P_2 \\ P_3 \end{pmatrix} = 0, \tag{7.252}$$

where the submatrix D and P have the forms as:

$$D_{11} = \begin{pmatrix} A_{m1}^{+\,j-1} & A_{m1}^{-\,j-1} & A_{vm1}^{+\,j-1} & 0 & 0 & 0 \\ B_{m1}^{+\,j-1} & B_{m1}^{-\,j-1} & B_{vm1}^{+\,j-1} & 0 & 0 & 0 \\ C_{m1}^{+\,j-1} & C_{m1}^{-\,j-1} & C_{vm1}^{+\,j-1} & 0 & 0 & 0 \\ 0 & 0 & 0 & A_{m2}^{+\,j-1} & A_{m2}^{-\,j-1} & A_{vm2}^{+\,j-1} \\ 0 & 0 & 0 & B_{m2}^{+\,j-1} & B_{m2}^{-\,j-1} & B_{vm2}^{+\,j-1} \\ 0 & 0 & 0 & C_{m2}^{+\,j-1} & C_{m2}^{-\,j-1} & C_{vm2}^{+\,j-1} \end{pmatrix}, \tag{7.253}$$

$$D_{12} = \begin{pmatrix} A_{Lm11}^{+\,j} & A_{Lm11}^{-\,j} & A_{Lvm12}^{+\,j} & A_{Lm12}^{+\,j} & A_{Lm12}^{-\,j} & 0 \\ B_{Lm11}^{+\,j} & B_{Lm11}^{-\,j} & B_{Lvm1}^{+\,j} & B_{Lm12}^{+\,j} & B_{Lm12}^{-\,j} & 0 \\ C_{Lm11}^{+\,j} & C_{Lm11}^{-\,j} & C_{Lvm1}^{+\,j} & C_{Lm12}^{+\,j} & C_{Lm12}^{-\,j} & 0 \\ A_{Lm21}^{+\,j} & A_{Lm21}^{-\,j} & 0 & A_{Lm22}^{+\,j} & A_{Lm22}^{-\,j} & A_{Lvm22}^{+\,j} \\ B_{Lm21}^{+\,j} & B_{Lm21}^{-\,j} & 0 & B_{Lm22}^{+\,j} & B_{Lm22}^{-\,j} & B_{Lvm22}^{+\,j} \\ C_{Lm21}^{+\,j} & C_{Lm21}^{-\,j} & 0 & C_{Lm22}^{+\,j} & C_{Lm22}^{-\,j} & C_{Lvm22}^{+\,j} \end{pmatrix}, \tag{7.254}$$

$$D_{22} = \begin{pmatrix} A_{Rm11}^{+\,j} & A_{Rm11}^{-\,j} & A_{Rvm12}^{+\,j} & A_{Rm12}^{+\,j} & A_{Rm12}^{-\,j} & 0 \\ B_{Rm11}^{+\,j} & B_{Rm11}^{-\,j} & B_{Rvm1}^{+\,j} & B_{Rm12}^{+\,j} & B_{Rm12}^{-\,j} & 0 \\ C_{Rm11}^{+\,j} & C_{Rm11}^{-\,j} & C_{Rvm1}^{+\,j} & C_{Rm12}^{+\,j} & C_{Rm12}^{-\,j} & 0 \\ A_{Rm21}^{+\,j} & A_{Rm21}^{-\,j} & 0 & A_{Rm22}^{+\,j} & A_{Rm22}^{-\,j} & A_{Rvm22}^{+\,j} \\ B_{Rm21}^{+\,j} & B_{Rm21}^{-\,j} & 0 & B_{Rm22}^{+\,j} & B_{Rm22}^{-\,j} & B_{Rvm22}^{+\,j} \\ C_{Rm21}^{+\,j} & C_{Rm21}^{-\,j} & 0 & C_{Rm22}^{+\,j} & C_{Rm22}^{-\,j} & C_{Rvm22}^{+\,j} \end{pmatrix}, \tag{7.255}$$

$$D_{23}=\begin{pmatrix} A_{m1}^{+\,j+1} & A_{m1}^{-\,j+1} & A_{vm1}^{+\,j+1} & 0 & 0 & 0 \\ B_{m1}^{+\,j+1} & B_{m1}^{-\,j+1} & B_{vm1}^{+\,j+1} & 0 & 0 & 0 \\ C_{m1}^{+\,j+1} & C_{m1}^{-\,j+1} & C_{vm1}^{+\,j+1} & 0 & 0 & 0 \\ 0 & 0 & 0 & A_{m2}^{+\,j+1} & A_{m2}^{-\,j+1} & A_{vm2}^{+\,j+1} \\ 0 & 0 & 0 & B_{m2}^{+\,j+1} & B_{m2}^{-\,j+1} & B_{vm2}^{+\,j+1} \\ 0 & 0 & 0 & C_{m2}^{+\,j+1} & C_{m2}^{-\,j+1} & C_{vm2}^{+\,j+1} \end{pmatrix}, \quad (7.256)$$

$$P_1=\begin{pmatrix} P_{m1}^{+\,j-1} \\ P_{m1}^{-\,j-1} \\ \rho_{vm1}^{+\,j-1} \\ P_{m2}^{+\,j-1} \\ P_{m2}^{-\,j-1} \\ \rho_{vm2}^{+\,j-1} \end{pmatrix}, P_2=\begin{pmatrix} P_{m1}^{+\,j} \\ P_{m1}^{-\,j} \\ \rho_{vm1}^{+\,j} \\ P_{m2}^{+\,j} \\ P_{m2}^{-\,j} \\ \rho_{vm2}^{+\,j} \end{pmatrix}, P_3=\begin{pmatrix} P_{m1}^{+\,j+1} \\ P_{m1}^{-\,j+1} \\ \rho_{vm1}^{+\,j+1} \\ P_{m2}^{+\,j+1} \\ P_{m2}^{-\,j+1} \\ \rho_{vm2}^{+\,j+1} \end{pmatrix}, \quad (7.257)$$

where D_{11} corresponds to the interface b of the $j-1$ section, D_{12} corresponds to the interface b of the j section, D_{22} corresponds to the interface c of the j section, and D_{23} corresponds to the interface c of the section $j+1$. Therefore, the liner section is integrally included in the three-dimensional analytical model.

To validate the effectiveness of this method, once again, the model presented by Heckl [11] is used here; what is different is we will add a section of liner and back cavity to the original model to investigate the effect of the liner with bias flow. The parameters are not changed. The length of the tube is $l_j = 1\,\mathrm{m}$, the radius of the tube is $r_j = 0.0223\,\mathrm{m}$, the temperature of the heated wire is $T_w = 700\,\mathrm{K}$, and the heated gauze is placed in the tube 0.3 m from the left end. The reflection coefficients of the end are $R_o = R_L = -0.986 + 0.12i$, and the heat release function is:

$$Q'(t) = \beta u(t-\tau), \quad (7.258)$$

where β is the amplitude with value of 187 kg m s^{-2}, and τ is the delay time. Under these conditions, for the hard-wall situation, the complex frequency varies through only the delay time τ; the resonance frequency calculated with the analytical model is shown in Fig. 7.17.

The imaginary of the complex frequency represents the stability of the system, as shown in Fig. 7.18. There is a phase delay between the real part of the resonance frequency and the imaginary. When the delay time lays in the range of $0 < \tau < T/2$, the instability occurs.

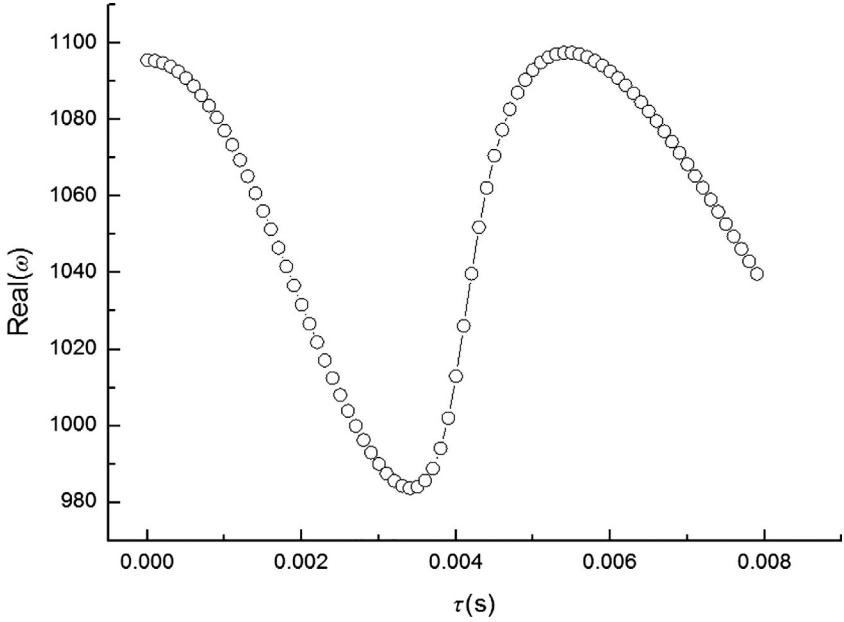

Fig. 7.17 The variation of the fundamental frequency through the delay time.

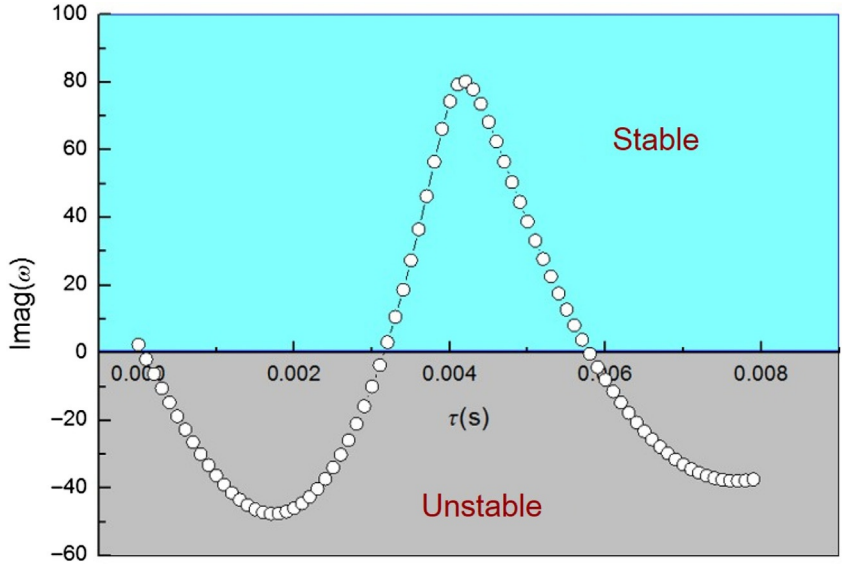

Fig. 7.18 The imaginary part of the complex resonance frequency.

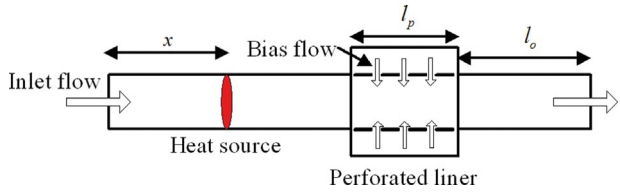

Fig. 7.19 Control of thermoacoustic instability occurred in a Rijke tube with perforated liner.

The length of each part of the tube is shown in the sketch diagram in Fig. 7.19. Specifically, the length of the liner or the back cavity is l_p, the radius of the perforated hole is r_o, the distance between neighboring holes is d, the cavity depth is r_b, and the position of the liner can be determined by the length of l_0. The perforation ratio depends on two parameters, r_0 and d, $\sigma = \pi r_o^2/d^2$.

In the following section, the parameters of the liner, the back cavity, and the bias flow are investigated for the control effect on the instability with the three-dimensional analytical model.

Fig. 7.20 shows the variation of the real part of the resonance frequency with the nondimensional length of the liner. Three lines represent different Mach numbers of 0.000, 0.001, and 0.005. The radius of the hole is

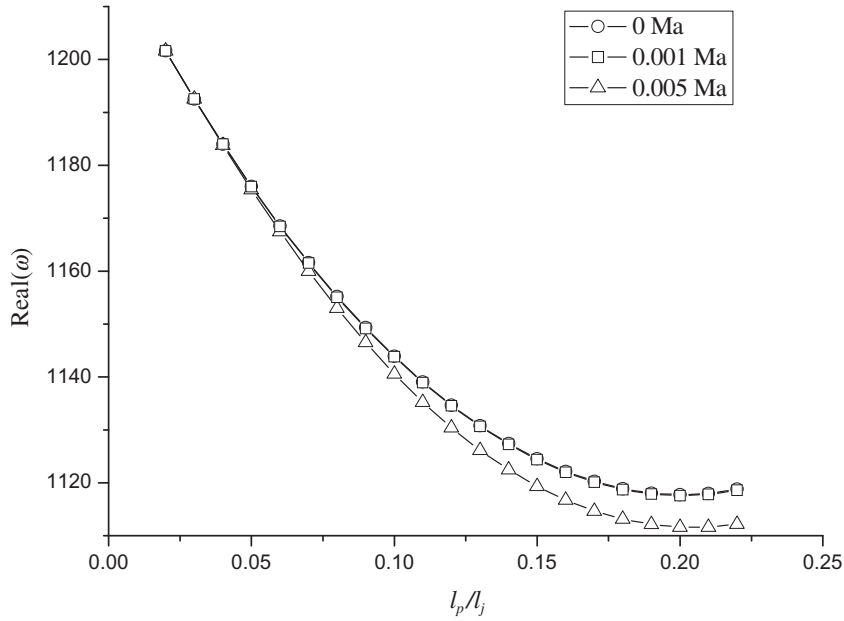

Fig. 7.20 Variation of the real part of the complex frequency with the nondimensional length of the liner.

$r_o = 0.001$m, the perforation ratio is $\sigma = 0.01$, the depth of the back cavity is $r_b = 0.01$m, and $l_p + l_0 = 0.4$m. It is found that the length of the liner has little effect on the resonance frequency with the maximum change less than 10%. However, it greatly affects the stability of the system from Fig. 7.21, which reveals that, at the highest Mach number circumstance, when the nondimensional length reaches 15% of the tube, the system becomes stable, whereas the on the other two conditions, it is still unstable. It is concluded that the bias flow enhances the dissipation of acoustic energy, and it is really effective to increase the length of the liner.

The results of the investigation of the perforation ratio is displayed in Figs. 7.22 and 7.23; at high bias Mach number, when $\sigma < 0.012$, the imaginary part of the resonance frequency is positive, which means the system is stable.

The influence of the depth of the back cavity is also investigated with the results shown in Figs. 7.24 and 7.25. The resonance frequency is comparatively sensitive because the volume of the back cavity plays an important role in changing the reactance of the impedance of the wall.

From the calculation results mentioned before, the bias flow in the hole indeed has a positive effect on suppressing the instability. The variation of

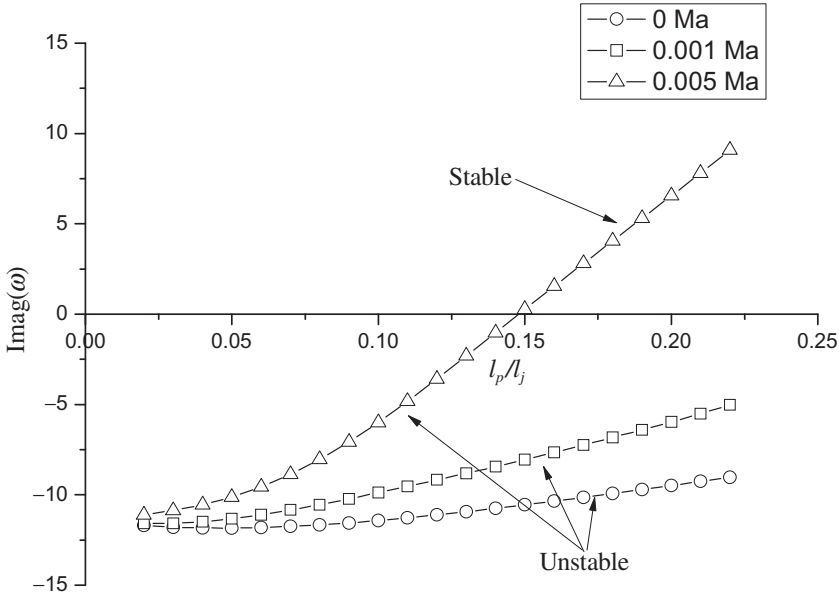

Fig. 7.21 Variation of the imaginary part of the complex frequency with the nondimensional length of the liner.

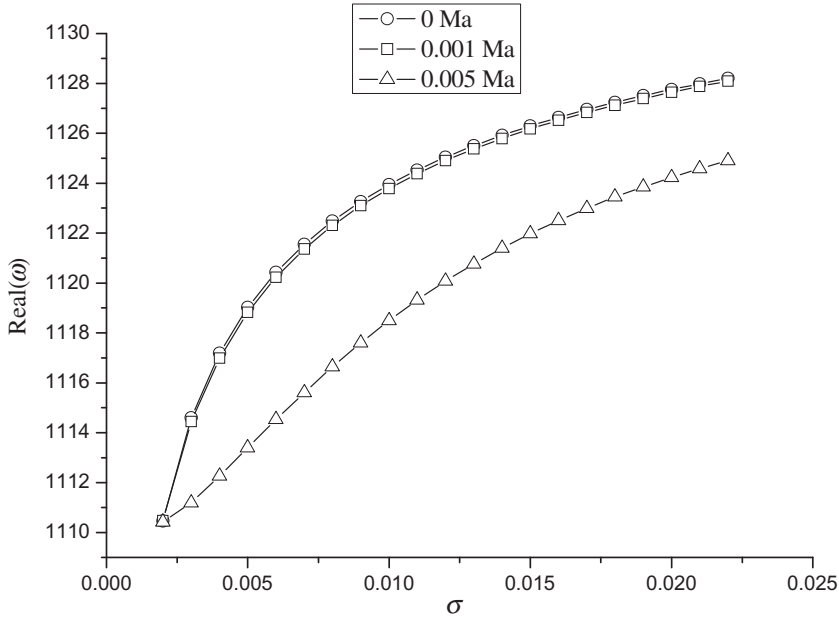

Fig. 7.22 Variation of the real part of the complex frequency with the perforation ratio.

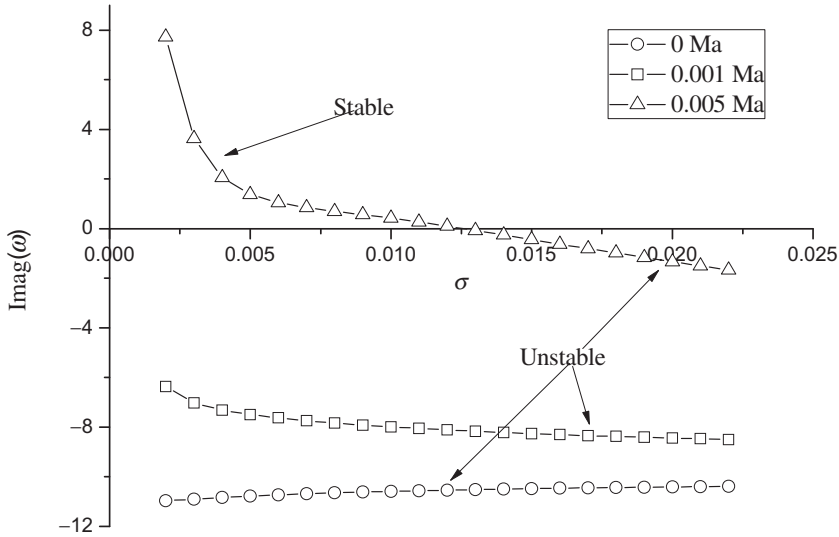

Fig. 7.23 Variation of the imaginary part of the complex frequency with the perforation ratio.

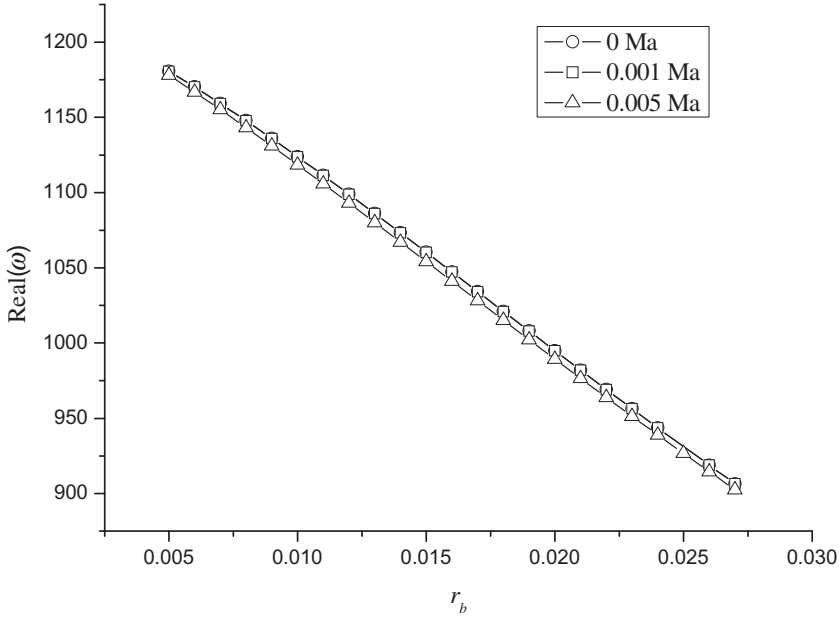

Fig. 7.24 Variation of the real part of the complex frequency with the depth of the back cavity.

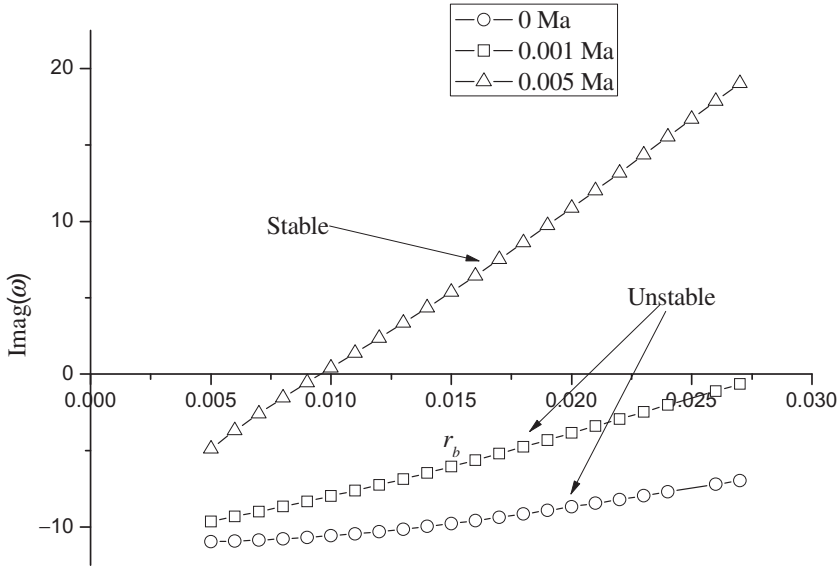

Fig. 7.25 Variation of the imaginary part of the complex frequency with the depth of the back cavity.

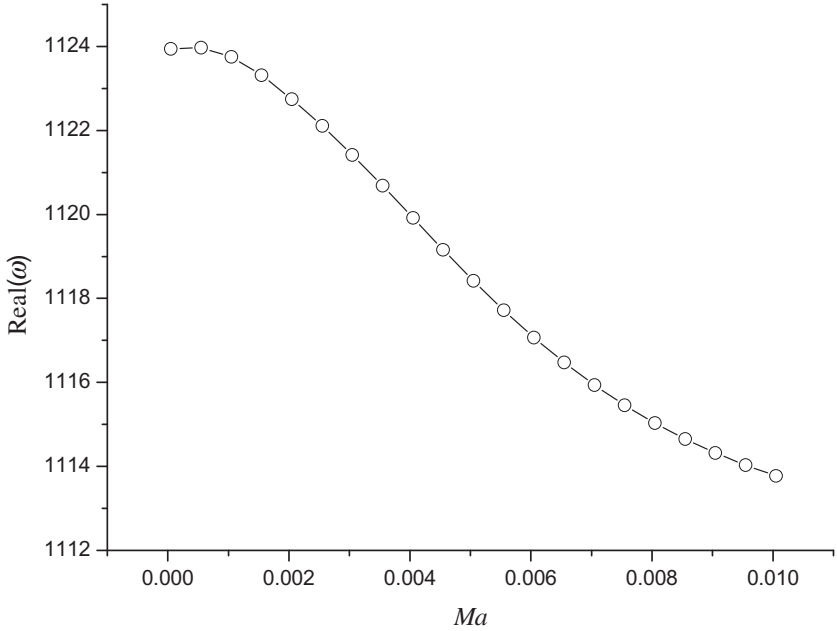

Fig. 7.26 Variation of the real part of the complex frequency with the Mach number of the bias flow.

the complex resonance frequency with the Mach number of the bias flow is displayed in Figs. 7.26 and 7.27, with $\sigma = 0.01$, $l_p/l_j = 0.15$, and $r_b = 0.01$m. The real part of the frequency changes little, yet the system falls into stable region from unstable region when the Mach number reaches 0.0045. Thus, the bias flow really helps to suppress instability and enhance the energy dissipation.

According to the calculated results, it is valid to suppress thermoacoustic instability by the liner with bias flow. This kind of liner actually works as an acoustic damping structure in the system, which dissipated the acoustic energy, as a result, making the dissipated acoustic energy larger than that enhanced, thus, the instability will never occur. In the meantime, the bias flow will produce vortexes at the hole, interacting with the acoustic pressure, and making the acoustic energy converted to the energy of vortex that is to be dissipated. In a word, the existence of the bias flow indeed enhanced the control effectiveness. In the operation of propulsion systems, the working condition is changing continuously; at some specific state, it works on the boundary of the stable region. The passive control methods are unable to change according to the working condition as soon as the control devices

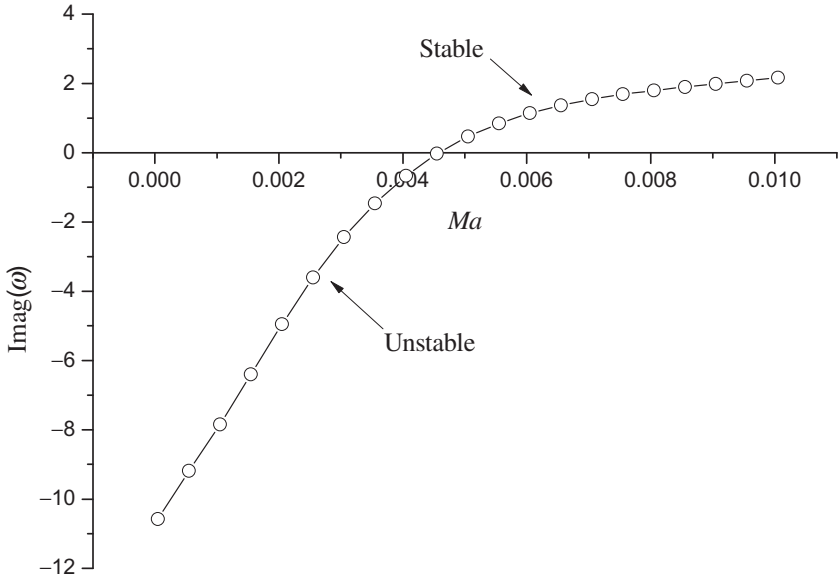

Fig. 7.27 Variation of the imaginary part of the complex frequency with the Mach number of the bias flow.

are established. However, from the model presented before, the bias flow can change the impedance of the wall, thus it can enhance the damping effect by increasing the bias flow rate, consequently enlarging the stable working region. Therefore, in a practical application, we can change the bias flow rate to avert the instability, which is called the hybrid control method. The result is shown in Fig. 7.28, from which the contour of zero, which is the dividing line of the instability region and stability region, is obtained as Fig. 7.29 shows. According to this control line, the stable working region is obtained and, according to which, we know how to change the bias flow to control the instability. Li et al. [25] conducted experiments to validate this idea of hybrid control method.

7.4.2 Drum-like silencer

A perforated liner with bias flow functions by adding a damping source into the thermoacoustic system. However, based on the fact that the unsteady heat release contributes to the instability through the interaction with acoustic pressure, the acoustic energy converted from the heat release depends on the phase difference between pressure and heat release. Thus, we proposed a method that is helpful in controlling thermoacoustic instability by a

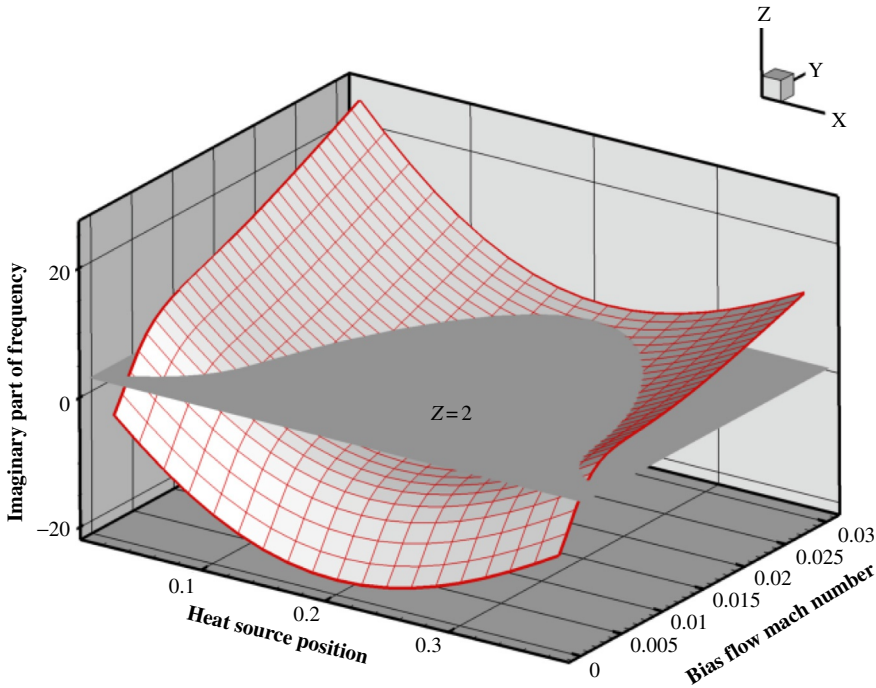

Fig. 7.28 Variation of the imaginary part of the complex frequency through the heat source position and the bias flow Mach number.

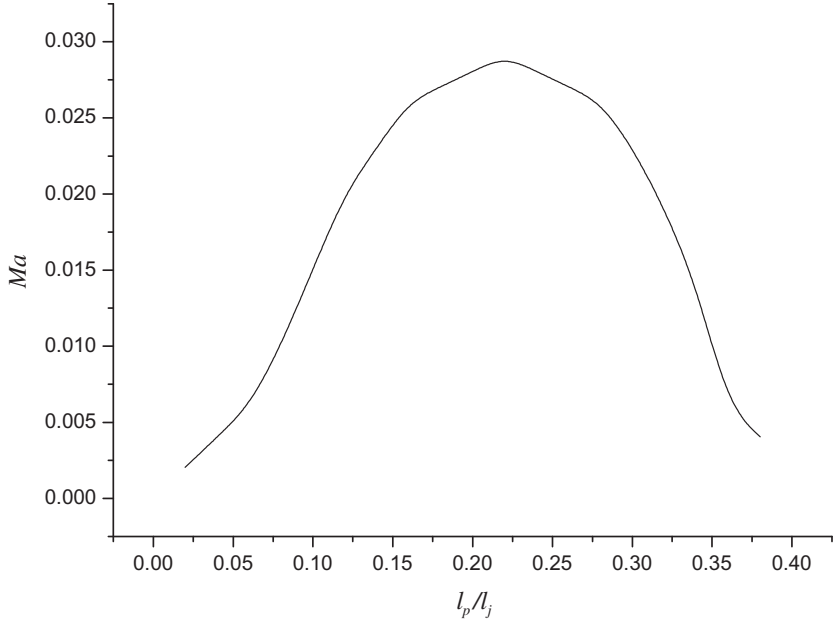

Fig. 7.29 Control line with heat source position and bias flow Mach number.

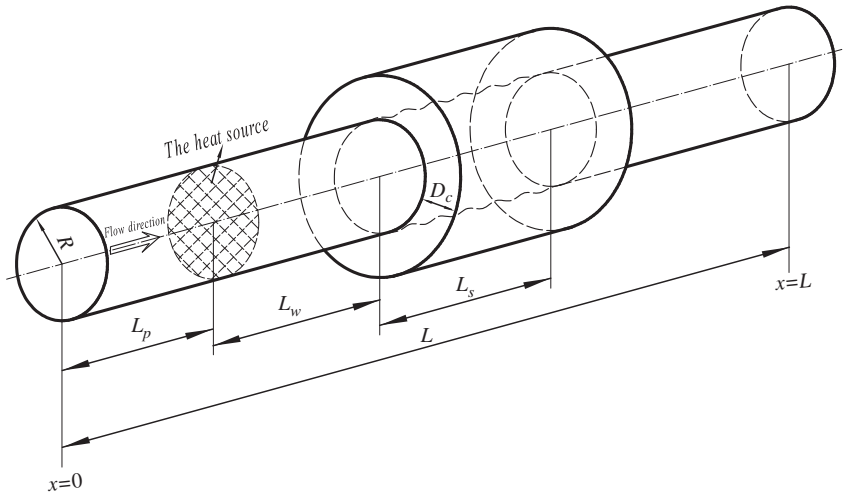

Fig. 7.30 Sketch of the control configuration [31].

drum-like silencer. Similar to the liner, TEM is used to consider the interaction between the soft boundary and the acoustics in the tube. The control configuration is illustrated by Fig. 7.30.

The modeling process is similar to that of the perforated liner in Section 7.4.1. The only difference is the impedance equation of the perforated liner is replaced by the oscillation equation of the membrane.

The symbols representing the relative positions of the components are specified in Fig. 7.30. The Rijke tube, of length $L = 1$ m and radius $R = 0.0223$ m, is lined in part by an annular membrane of length L_s, and the position of the silencer is defined by L_w. The membrane is enclosed by an annular rigid-wall cavity of depth D_c and length L_s. The heated gauze is displaced inside the pipe, with a distance of L_p from the upper end. The tension of the membrane per unit length is denoted by T_x, and the mass of the membrane per unit area is denoted by m_x.

Detailed modeling and validation can be referred to Zhang et al. [31]. Actually, for this kind of Rijke tube with radius of 0.0223 m, the higher modes reflected by the drum-like silencer cannot propagate in a resonance condition. Therefore, the following results are limited to the planar mode.

It is shown from Figs. 7.31 and 7.32 that incorporation of a drum-like silencer decreases the natural frequency of the system. And, as a result, the fundamental mode becomes stable. Note, however, the time delay is assumed to be constant, which is physically reasonable for the heated wire

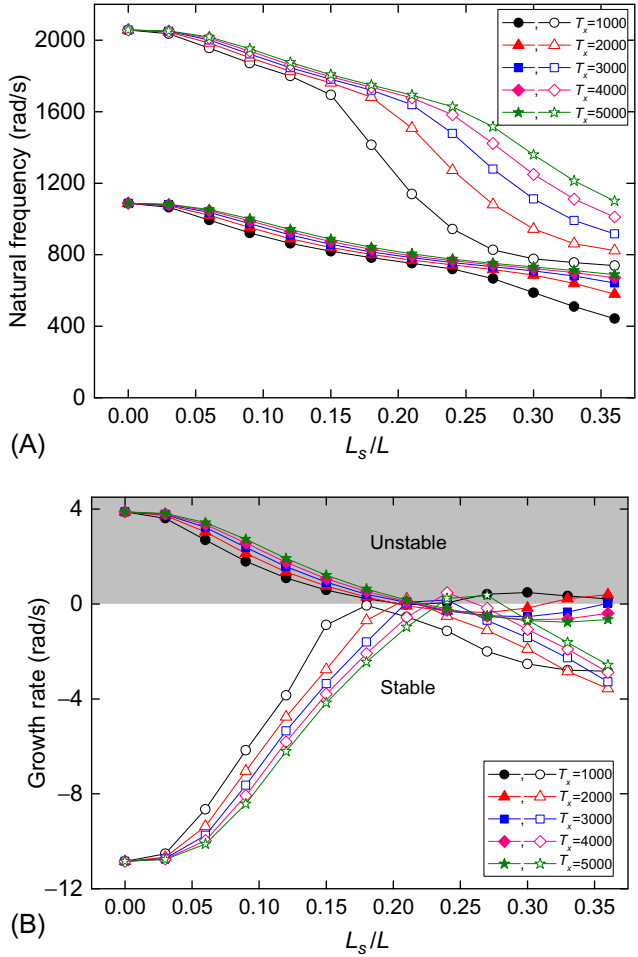

Fig. 7.31 Complex frequency against length of drum-like silencer with $D_c/R = 1$.: (A) Natural frequency (rad/s); (B) growth rate (rad/s) [31].

case as depicted by Heckl [11]. When the frequency is decreased, the phase between the unsteady heat release and the velocity is decreased. In the tube, because of the approximately open-end condition, the velocity leads the pressure by 90 degrees. Thus, the phase difference between the pressure and the heat release is increased as the frequency decreases. Consequently, the acoustic energy converted from the heat release is reduced according to Rayleigh criterion [2]. Thus, the acoustic energy quantity transferred from the heat can be dissipated at the ends of the tube. Consequently, the thermoacoustic instability is controlled.

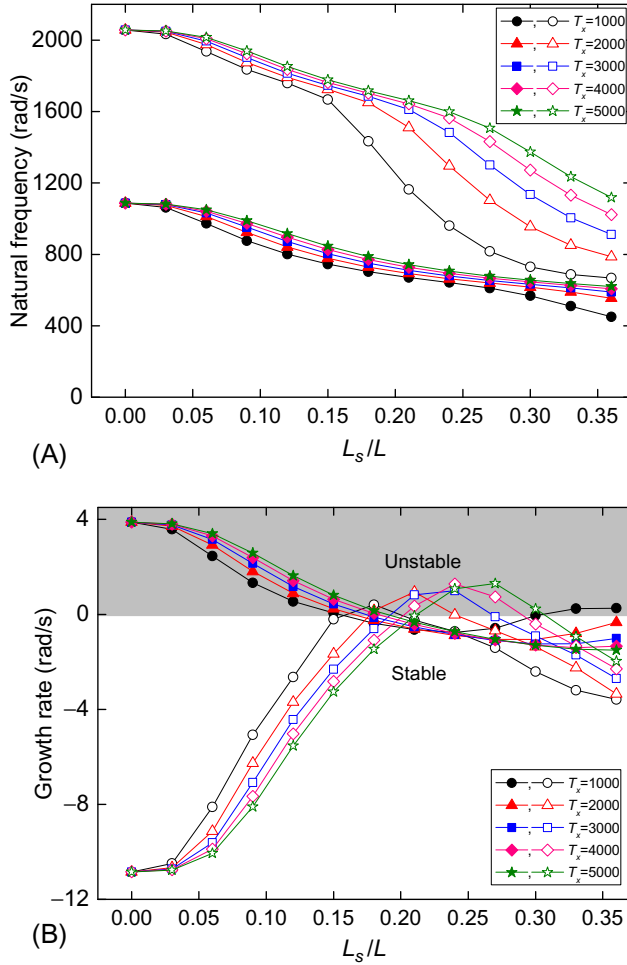

Fig. 7.32 Complex frequency against length of drum-like silencer with $D_c/R = 1.3$: (A) Natural frequency (rad/s); (B) growth rate (rad/s) [31]

Appendix A Coefficients of the matching conditions

$$A_{mn}^{+\,j} = \left(\frac{U^j}{C_0^2} - \frac{\alpha_{mn}^{+\,j}}{\omega + \alpha_{mn}^{+\,j} U^j}\right) e^{i\alpha_{mn}^{+\,j} L^j}$$

$$A_{mn}^{-\,j} = \left(\frac{U^j}{C_0^2} - \frac{\alpha_{mn}^{-\,j}}{\omega + \alpha_{mn}^{-\,j} U^j}\right) e^{i\alpha_{mn}^{-\,j} L^j}$$

$$A_{vmn}^{+\,j} = U^j e^{-i\frac{\omega}{U^j} L^j}$$

$$A_{mn}^{+\,j+1} = -\left(\frac{U^{j+1}}{C_0^2} - \frac{\alpha_{mn}^{+\,j+1}}{\omega + \alpha_{mn}^{+\,j+1} U^{j+1}}\right)$$

$$A_{mn}^{-\,j+1} = -\left(\frac{U^{j+1}}{C_0^2} - \frac{\alpha_{mn}^{-\,j+1}}{\omega + \alpha_{mn}^{-\,j+1} U^{j+1}}\right)$$

$$A_{vmn}^{+\,j} = -U^{j+1}$$

$$B_{mn}^{+\,j} = \left(1 + \left(M_a^j\right)^2 - \frac{2U^j \alpha_{mn}^{+\,j}}{\omega + \alpha_{mn}^{+\,j} U^j}\right) e^{i\alpha_{mn}^{+\,j} L^j}$$

$$B_{mn}^{+\,j} = \left(1 + \left(M_a^j\right)^2 - \frac{2U^j \alpha_{mn}^{-\,j}}{\omega + \alpha_{mn}^{-\,j} U^j}\right) e^{i\alpha_{mn}^{-\,j} L^j}$$

$$B_{vmn}^{+\,j} = \left(U^j\right)^2 e^{-i\frac{\omega}{U^j} L^j}$$

$$B_{mn}^{+\,j+1} = -1 - \left(\left(M_a^{j+1}\right)^2 - \frac{2U^{j+1} \alpha_{mn}^{+\,j+1}}{\omega + \alpha_{mn}^{+\,j+1} U^{j+1}}\right)$$

$$B_{mn}^{-\,j+1} = -1 - \left(\left(M_a^{j+1}\right)^2 - \frac{2U^{j+1} \alpha_{mn}^{-\,j+1}}{\omega + \alpha_{mn}^{-\,j+1} U^{j+1}}\right)$$

$$B_{vmn}^{+\,j} = -\left(U^{j+1}\right)^2$$

$$C_{mn}^{+\,j} = \left[U^j \left(\frac{\gamma}{\gamma - 1} + \frac{\left(M_a^j\right)^2}{2}\right) - \frac{1}{\rho_0^j}\left(\frac{\gamma P_0^j}{\gamma - 1} + \frac{3}{2}\rho_0^j \left(U^j\right)^2\right) \frac{\alpha_{mn}^{+\,j}}{\omega + \alpha_{mn}^{+\,j} U^j}\right] e^{i\alpha_{mn}^{+\,j} L^j}$$

$$C_{mn}^{-\,j} = \left[U^j \left(\frac{\gamma}{\gamma - 1} + \frac{\left(M_a^j\right)^2}{2}\right) - \frac{1}{\rho_0^j}\left(\frac{\gamma P_0^j}{\gamma - 1} + \frac{3}{2}\rho_0^j \left(U^j\right)^2\right) \frac{\alpha_{mn}^{-\,j}}{\omega + \alpha_{mn}^{-\,j} U^j}\right] e^{i\alpha_{mn}^{-\,j} L^j}$$

$$C_{vmn}^{+\,j} = \frac{\left(U^j\right)^3}{2} e^{-i\frac{\omega}{U^j} L^j}$$

$$C_{mn}^{+\,j+1} = -U^{j+1}\left(\frac{\gamma}{\gamma - 1} + \frac{\left(M_a^{j+1}\right)^2}{2}\right) + \frac{1}{\rho_0^{j+1}}\left(\frac{\gamma P_0^{j+1}}{\gamma - 1} + \frac{3}{2}\rho_0^{j+1}\left(U^{j+1}\right)^2\right) \frac{\alpha_{mn}^{+\,j+1}}{\omega + \alpha_{mn}^{+\,j+1} U^{j+1}}$$

$$C_{mn}^{-\,j+1} = -U^{j+1}\left(\frac{\gamma}{\gamma - 1} + + \frac{\left(M_a^{j+1}\right)^2}{2}\right) + \frac{S^{j+1}}{\rho_0^{j+1}}\left(\frac{\gamma P_0^{j+1}}{\gamma - 1} + \frac{3}{2}\rho_0^{j+1}\left(U^{j+1}\right)^2\right) \frac{\alpha_{mn}^{-\,j+1}}{\omega + \alpha_{mn}^{-\,j+1} U^{j+1}}$$

$$C_{vmn}^{+\,j+1} = -\frac{\left(U^{j+1}\right)^3}{2}$$

$$D_{mn}^{+\,j} = \frac{\rho_0^j}{z_0} + \frac{\alpha_{mn}^{+\,j}}{\omega + \alpha_{mn}^{+\,j} U^j}$$

$$D_{mn}^{-\,j} = \frac{\rho_0^j}{z_0} + \frac{\alpha_{mn}^{-\,j}}{\omega + \alpha_{mn}^{-\,j} U^j}$$

$$D_{vmn}^{+\,j} = 0$$

$$D_{mn}^{+\,j+1} = 0$$

$$D_{mn}^{-\,j+1} = 0$$

$$D_{vmn}^{+\,j+1} = 0$$

$$E_{mn}^{+\,j} = 0$$

$$E_{mn}^{-\,j} = 0$$

$$E_{vmn}^{+\,j} = 0$$

$$E_{mn}^{+\,j+1} = \left(\frac{\rho_0^{j+1}}{z_{end}} + \frac{\alpha_{mn}^{+\,j+1}}{\omega + \alpha_{mn}^{+\,j+1} U^{j+1}} \right) e^{i\alpha_{mn}^{+\,j+1} L^{j+1}}$$

$$E_{mn}^{-\,j+1} = \left(\frac{\rho_0^{j+1}}{z_0} + \frac{\alpha_{mn}^{-\,j+1}}{\omega + \alpha_{mn}^{-\,j+1} U^{j+1}} \right) e^{i\alpha_{mn}^{-\,j+1} L^{j+1}}$$

$$E_{vmn}^{+\,j+1} = 0$$

$$F_{mn}^{+\,j} = \left(R_p - \frac{R_v}{\rho_0^j} \frac{\alpha_{mn}^{+\,j}}{\omega + \alpha_{mn}^{+\,j} U^j} \right) e^{i\alpha_{mn}^{+\,j} L^j}$$

$$F_{mn}^{-\,j} = \left(R_p - \frac{R_v}{\rho_0^j} \frac{\alpha_{mn}^{-\,j}}{\omega + \alpha_{mn}^{-\,j} U^j} \right) e^{i\alpha_{mn}^{-\,j} L^j}$$

$$F_{vmn}^{+\,j} = 0$$

$$F_{mn}^{+\,j+1} = 0$$

$$F_{mn}^{-\,j+1} = 0$$

$$F_{vmn}^{+\,j+1} = 0$$

Appendix B Coefficients of the matching conditions for variable cross-sections cases

$$Ab_{101}^{+\,j} = A_{01}^{+\,j} \int_0^{r_j} r dr$$

$$Ab_{101}^{-\,j} = A_{01}^{-\,j}\int_0^{r_j} r dr$$

$$Ab_{\nu 101}^{+\,j} = A_{\nu 01}^{+\,j}\int_0^{r_j} r dr$$

$$Ab_{1mn}^{+\,j} = A_{mn}^{+\,j}\int_0^{r_j} r\psi_{mn}^{j}(r) dr$$

$$Ab_{1mn}^{-\,j} = A_{mn}^{-\,j}\int_0^{r_j} r\psi_{mn}^{j}(r) dr$$

$$Ab_{\nu 1mn}^{+\,j} = A_{\nu mn}^{+\,j}\int_0^{r_j} r\psi_{mn}^{j}(r) dr$$

$$Ab_{101}^{+\,j+1} = -\frac{U^{j+1}}{C_0^2}\int_0^{r_j} r dr + \frac{\alpha_{mn}^{+\,j+1}}{\omega + \alpha_{mn}^{+\,j+1}U^{j+1}}\int_0^{r_{j+1}} r dr$$

$$Ab_{101}^{-\,j+1} = -\frac{U^{j+1}}{C_0^2}\int_0^{r_j} r dr + \frac{\alpha_{mn}^{-\,j+1}}{\omega + \alpha_{mn}^{-\,j+1}U^{j+1}}\int_0^{r_{j+1}} r dr$$

$$Ab_{\nu 101}^{+\,j+1} = A_{\nu 01}^{+\,j+1}\int_0^{r_j} r dr$$

$$Ab_{1mn}^{+\,j+1} = -\frac{U^{j+1}}{C_0^2}\int_0^{r_j} r\psi_{mn}^{j+1}(r) dr + \frac{\alpha_{mn}^{+\,j+1}}{\omega + \alpha_{mn}^{+\,j+1}U^{j+1}}\int_0^{r_{j+1}} r\psi_{mn}^{j+1}(r) dr$$

$$Ab_{mn}^{-\,j+1} = -\frac{U^{j+1}}{C_0^2}\int_0^{r_j} r\psi_{mn}^{j+1}(r) dr + \frac{\alpha_{mn}^{-\,j+1}}{\omega + \alpha_{mn}^{-\,j+1}U^{j+1}}\int_0^{r_{j+1}} r\psi_{mn}^{j+1}(r) dr$$

$$Ab_{\nu 1mn}^{+\,j+1} = A_{\nu mn}^{+\,j+1}\int_0^{r_j} r\psi_{mn}^{j+1}(r) dr$$

$$\int r J_m(K_{mn}r) J_m(K_{m\nu}r) dr = \frac{r(K_{mn}J_{m+1}(K_{mn}r)J_m(K_{m\nu}r) - K_{m\nu}J_m(K_{mn}r)J_{m+1}(K_{m\nu}r))}{K_{mn}^2 - K_{m\nu}^2},\ n \neq \nu$$

$$\int r J_m^2(K_{mn}r) dr = \frac{1}{2}r^2\left\{\left(1 - \frac{m^2}{K_{mn}^2 r^2}\right)J_m^2(K_{mn}r) + J_m'^2(K_{mn}r)\right\}$$

For $m = 0$:

$$\int_0^{r_j} r dr = \frac{1}{2}r_j^2$$

$$\int_0^{r_j} r\psi_{mn}^{j}(r)\,dr = 0;\ \ n > 1$$

$$\int_0^{r_j} r\psi_{mn}^{j+1}(r)\,dr = \frac{r_j J_1\left(K_{mn}^{j+1} r_j\right)}{K_{mn}^{j+1}}$$

$$Ab_{201}^{+\,j} = A_{01}^{+\,j} \int_0^{r_j} r\psi_{mv}^{j}(r)\,dr$$

$$Ab_{201}^{-\,j} = A_{01}^{-\,j} \int_0^{r_j} r\psi_{mv}^{j}(r)\,dr$$

$$Ab_{v201}^{+\,j} = A_{v01}^{+\,j} \int_0^{r_j} r\psi_{mv}^{j}(r)\,dr$$

$$Ab_{2mn}^{+\,j} = A_{mn}^{+\,j} \int_0^{r_j} r\psi_{mn}^{j}(r)\psi_{mv}^{j}(r)\,dr$$

$$Ab_{2mn}^{-\,j} = A_{mn}^{-\,j} \int_0^{r_j} r\psi_{mn}^{j}(r)\psi_{mv}^{j}(r)\,dr$$

$$Ab_{v2mn}^{+\,j} = A_{vmn}^{+\,j} \int_0^{r_j} r\psi_{mn}^{j}(r)\psi_{mv}^{j}(r)\,dr$$

$$Ab_{201}^{+\,j+1} = -\frac{U^{j+1}}{a_0^2} \int_0^{r_j} r\psi_{mv}^{j}(r)\,dr + \frac{\alpha_{mn}^{+\,j+1}}{\omega + \alpha_{mn}^{+\,j+1} U^{j+1}} \int_0^{r_{j+1}} r\psi_{mv}^{j}(r)\,dr$$

$$Ab_{201}^{-\,j+1} = -\frac{U^{j+1}}{a_0^2} \int_0^{r_j} r\psi_{mv}^{j}(r)\,dr + \frac{\alpha_{mn}^{-\,j+1}}{\omega + \alpha_{mn}^{-\,j+1} U^{j+1}} \int_0^{r_{j+1}} r\psi_{mv}^{j}(r)\,dr$$

$$Ab_{v201}^{+\,j+1} = A_{v01}^{+\,j+1} \int_0^{r_j} r\psi_{mv}^{j}(r)\,dr$$

$$Ab_{2mn}^{+\,j+1} = -\frac{U^{j+1}}{C_0^2} \int_0^{r_j} r\psi_{mn}^{j+1}(r)\psi_{mv}^{j}(r)\,dr + \frac{\alpha_{mn}^{+\,j+1}}{\omega + \alpha_{mn}^{+\,j+1} U^{j+1}} \int_0^{r_{j+1}} r\psi_{mn}^{j+1}(r)\psi_{mv}^{j}(r)\,dr$$

$$Ab_{2mn}^{-\,j+1} = -\frac{U^{j+1}}{a_0^2} \int_0^{r_j} r\psi_{mn}^{j+1}(r)\psi_{mv}^{j}(r)\,dr + \frac{\alpha_{mn}^{-\,j+1}}{\omega + \alpha_{mn}^{-\,j+1} U^{j+1}} \int_0^{r_{j+1}} r\psi_{mn}^{j+1}(r)\psi_{mv}^{j}(r)\,dr$$

$$Ab_{v2mn}^{+\,j+1} = A_{vmn}^{+\,j+1} \int_0^{r_j} r\psi_{mn}^{j+1}(r)\psi_{mv}^{j}(r)\,dr$$

where, $m = 0$:

$$\int_0^{r_j} r\psi_{mv}^{j}(r)\,dr = 0$$

$$\int_0^{r_j} r\psi_{mn}^{j}(r)\psi_{mv}^{j}(r)\,dr = \begin{cases} 0; & n \neq v \\ \dfrac{1}{2} r_j^2 J_0^2\left(K_{mn} r_j\right); & n = v \end{cases}$$

$$\int_0^{r_j} r\psi_{mn}^{j+1}(r)\psi_{mv}^{j}(r)\,dr = \frac{r_j K_{mn}^{j+1} J_1\left(K_{mn}^{j+1} r_j\right) J_0\left(K_{mv}^{j} r\right)}{\left(K_{mn}^{j+1}\right)^2 - \left(K_{mv}^{j}\right)^2}$$

$$Bb_{101}^{+\,j} = B_{01}^{+\,j} \int_0^{r_j} r\,dr$$

$$Bb_{101}^{-\,j} = B_{01}^{-\,j} \int_0^{r_j} r\,dr$$

$$Bb_{v101}^{+\,j} = B_{v01}^{+\,j} \int_0^{r_j} r\,dr$$

$$Bb_{1mn}^{+\,j} = B_{mn}^{+\,j} \int_0^{r_j} r\psi_{mn}^{j}(r)\,dr$$

$$Bb_{1mn}^{-\,j} = B_{mn}^{-\,j} \int_0^{r_j} r\psi_{mn}^{j}(r)\,dr$$

$$Bb_{v1mn}^{+\,j} = B_{vmn}^{+\,j} \int_0^{r_j} r\psi_{mn}^{j}(r)\,dr$$

$$Bb_{101}^{+\,j+1} = \left(-1 - \left(M_a^{j+1}\right)^2\right) \int_0^{r_j} r\,dr + \frac{2U^{j+1}\alpha_{mn}^{+\,j+1}}{\omega + \alpha_{mn}^{+\,j+1} U^{j+1}} \int_0^{r_{j+1}} r\,dr$$

$$Bb_{101}^{-\,j+1} = \left(-1 - \left(M_a^{j+1}\right)^2\right) \int_0^{r_j} r\,dr + \frac{2U^{j+1}\alpha_{mn}^{-\,j+1}}{\omega + \alpha_{mn}^{-\,j+1} U^{j+1}} \int_0^{r_{j+1}} r\,dr$$

$$Bb_{v101}^{+\,j} = -U^{j+1^2} \int_0^{r_j} r\,dr$$

$$Bb_{1mn}^{+\,j+1} = \left(-1 - \left(M_a^{j+1}\right)^2\right) \int_0^{r_j} r\psi_{mn}^{j+1}(r)\,dr + \frac{2U^{j+1}\alpha_{mn}^{+\,j+1}}{\omega + \alpha_{mn}^{+\,j+1} U^{j+1}} \int_0^{r_{j+1}} r\psi_{mn}^{j+1}(r)\,dr$$

$$Bb_{1mn}^{-\,j+1} = \left(-1 - \left(M_a^{j+1}\right)^2\right) \int_0^{r_j} r\psi_{mn}^{j+1}(r)\,dr + \frac{2U^{j+1}\alpha_{mn}^{-\,j+1}}{\omega + \alpha_{mn}^{-\,j+1} U^{j+1}} \int_0^{r_{j+1}} r\psi_{mn}^{j+1}(r)\,dr$$

$$Bb^{+\,j}_{\nu 1mn} = -U^{j+1^2}\int_0^{r_j} r\psi^{j+1}_{mn}(r)\,dr$$

$$Bb^{+\,j}_{201} = B^{+\,j}_{01}\int_0^{r_j} r\psi^{j}_{m\nu}(r)\,dr$$

$$Bb^{-\,j}_{201} = B^{-\,j}_{01}\int_0^{r_j} r\psi^{j}_{m\nu}(r)\,dr$$

$$Bb^{+\,j}_{\nu 201} = B^{+\,j}_{\nu 01}\int_0^{r_j} r\psi^{j}_{m\nu}(r)\,dr$$

$$Bb^{+\,j}_{2mn} = B^{+\,j}_{mn}\int_0^{r_j} r\psi^{j}_{mn}(r)\psi^{j}_{m\nu}(r)\,dr$$

$$Bb^{-\,j}_{2mn} = B^{-\,j}_{mn}\int_0^{r_j} r\psi^{j}_{mn}(r)\psi^{j}_{m\nu}(r)\,dr$$

$$Bb^{+\,j}_{\nu 2mn} = B^{+\,j}_{\nu mn}\int_0^{r_j} r\psi^{j}_{mn}(r)\psi^{j}_{m\nu}(r)\,dr$$

$$Bb^{+\,j+1}_{201} = \left(-1-\left(M^{j+1}_{a}\right)^2\right)\int_0^{r_j} r\psi^{j}_{m\nu}(r)\,dr + \frac{2U^{j+1}\alpha^{+\,j+1}_{mn}}{\omega+\alpha^{+\,j+1}_{mn}U^{j+1}}\int_0^{r_{j+1}} r\psi^{j}_{m\nu}(r)\,dr$$

$$Bb^{-\,j+1}_{201} = \left(-1-\left(M^{j+1}_{a}\right)^2\right)\int_0^{r_j} r\psi^{j}_{m\nu}(r)\,dr + \frac{2U^{j+1}\alpha^{-\,j+1}_{mn}}{\omega+\alpha^{-\,j+1}_{mn}U^{j+1}}\int_0^{r_{j+1}} r\psi^{j}_{m\nu}(r)\,dr$$

$$Bb^{+\,j+1}_{\nu 201} = -U^{j+1^2}\int_0^{r_j} r\psi^{j}_{m\nu}(r)\,dr$$

$$Bb^{+\,j+1}_{2mn} = \left(-1-M^{j+1^2}\right)\int_0^{r_j} r\psi^{j+1}_{mn}(r)\psi^{j}_{m\nu}(r)\,dr + \frac{2U^{j+1}\alpha^{+\,j+1}_{mn}}{\omega+\alpha^{+\,j+1}_{mn}U^{j+1}}\int_0^{r_{j+1}} r\psi^{j+1}_{mn}(r)\psi^{j}_{m\nu}(r)\,dr$$

$$Bb^{-\,j+1}_{2mn} = \left(-1-\left(M^{j+1}_{a}\right)^2\right)\int_0^{r_j} r\psi^{j+1}_{mn}(r)\psi^{j}_{m\nu}(r)\,dr + \frac{2U^{j+1}\alpha^{-\,j+1}_{mn}}{\omega+\alpha^{-\,j+1}_{mn}U^{j+1}}\int_0^{r_{j+1}} r\psi^{j+1}_{mn}(r)\psi^{j}_{m\nu}(r)\,dr$$

$$Bb_{v2mn}^{+\,j+1} = -U^{j+1^2}\int_0^{r_j} r\psi_{mn}^{j}(r)\psi_{mv}^{j}(r)dr$$

$$Cb_{101}^{+\,j} = C_{01}^{+\,j}\int_0^{r_j} rdr$$

$$Cb_{101}^{-\,j} = C_{01}^{-\,j}\int_0^{r_j} rdr$$

$$Cb_{v101}^{+\,j} = C_{v01}^{+\,j}\int_0^{r_j} rdr$$

$$Cb_{1mn}^{+\,j} = C_{mn}^{+\,j}\int_0^{r_j} r\psi_{mn}^{j}(r)dr$$

$$Cb_{1mn}^{-\,j} = C_{mn}^{-\,j}\int_0^{r_j} r\psi_{mn}^{j}(r)dr$$

$$Cb_{v1mn}^{+\,j} = C_{vmn}^{+\,j}\int_0^{r_j} r\psi_{mn}^{j}(r)dr$$

$$Cb_{101}^{+\,j+1} = -U^{j+1}\left(\frac{\gamma}{\gamma-1}+\frac{\left(M_a^{j+1}\right)^2}{2}\right)\int_0^{r_j} rdr + \frac{1}{\rho_0^{j+1}}\left(\frac{\gamma P_0^{j+1}}{\gamma-1}+\frac{3}{2}\rho_0^{j+1}U^{j+1^2}\right)\frac{\alpha_{mn}^{+\,j+1}}{\omega+\alpha_{mn}^{+\,j+1}U^{j+1}}\int_0^{r_{j+1}} rdr$$

$$Cb_{101}^{-\,j+1} = -U^{j+1}\left(\frac{\gamma}{\gamma-1}+\frac{\left(M_a^{j+1}\right)^2}{2}\right)\int_0^{r_j} rdr + \frac{1}{\rho_0^{j+1}}\left(\frac{\gamma P_0^{j+1}}{\gamma-1}+\frac{3}{2}\rho_0^{j+1}U^{j+1^2}\right)\frac{\alpha_{mn}^{-\,j+1}}{\omega+\alpha_{mn}^{-\,j+1}U^{j+1}}\int_0^{r_{j+1}} rdr$$

$$Cb_{v01}^{+\,j} = -\frac{U^{j+1^3}}{2}\int_0^{r_j} rdr$$

$$Cb_{1mn}^{+\,j+1} = -U^{j+1}\left(\frac{\gamma}{\gamma-1}+\frac{\left(M_a^{j+1}\right)^2}{2}\right)\int_0^{r_j} r\psi_{mn}^{j+1}(r)dr + \frac{1}{\rho_0^{j+1}}\left(\frac{\gamma P_0^{j+1}}{\gamma-1}+\frac{3}{2}\rho_0^{j+1}U^{j+1^2}\right)\frac{\alpha_{mn}^{+\,j+1}}{\omega+\alpha_{mn}^{+\,j+1}U^{j+1}}\int_0^{r_{j+1}} r\psi_{mn}^{j+1}(r)dr$$

$$Cb_{1mn}^{-\,j+1} = -U^{j+1}\left(\frac{\gamma}{\gamma-1}+\frac{\left(M_a^{j+1}\right)^2}{2}\right)\int_0^{r_j} r\psi_{mn}^{j+1}(r)dr + \frac{1}{\rho_0^{j+1}}\left(\frac{\gamma P_0^{j+1}}{\gamma-1}+\frac{3}{2}\rho_0^{j+1}U^{j+1^2}\right)\frac{\alpha_{mn}^{-\,j+1}}{\omega+\alpha_{mn}^{-\,j+1}U^{j+1}}\int_0^{r_{j+1}} r\psi_{mn}^{j+1}(r)dr$$

$$Cb_{201}^{+\,j} = C_{01}^{+\,j}\int_0^{r_j} r\psi_{mv}^{j}(r)dr$$

$$Cb_{201}^{-\,j} = C_{01}^{-\,j}\int_0^{r_j} r\psi_{mv}^{j}(r)dr$$

$$Cb_{v201}^{+\,j} = C_{v01}^{+\,j}\int_0^{r_j} r\psi_{mv}^{j}(r)dr$$

$$Cb_{2mn}^{+\,j} = C_{mn}^{+\,j}\int_0^{r_j} r\psi_{mn}^{j}(r)\psi_{mv}^{j}(r)dr$$

$$Cb_{2mn}^{-\,j} = C_{mn}^{-\,j}\int_0^{r_j} r\psi_{mn}^{j}(r)\psi_{mv}^{j}(r)dr$$

$$Cb_{v2mn}^{+\,j} = -\frac{U^{j+1^3}}{2}\int_0^{r_j} r\psi_{mn}^{j}(r)dr$$

$$Cb_{v2mn}^{+\,j} = C_{vmn}^{+\,j}\int_0^{r_j} r\psi_{mn}^{j}(r)\psi_{mv}^{j}(r)dr$$

$$Cb_{201}^{+\,j+1} = -U^{j+1}\left(\frac{\gamma}{\gamma-1}+\frac{\left(M_a^{j+1}\right)^2}{2}\right)\int_0^{r_j} r\psi_{mv}^{j}(r)dr + \frac{1}{\rho_0^{j+1}}\left(\frac{\gamma P_0^{j+1}}{\gamma-1}+\frac{3}{2}\rho_0^{j+1}U^{j+1^2}\right)\frac{\alpha_{mn}^{+\,j+1}}{\omega+\alpha_{mn}^{+\,j+1}U^{j+1}}\int_0^{r_{j+1}} r\psi_{mv}^{j}(r)dr$$

$$Cb_{201}^{-\,j+1} = -U^{j+1}\left(\frac{\gamma}{\gamma-1}+\frac{\left(M_a^{j+1}\right)^2}{2}\right)\int_0^{r_j} r\psi_{mv}^{j}(r)dr + \frac{1}{\rho_0^{j+1}}\left(\frac{\gamma P_0^{j+1}}{\gamma-1}+\frac{3}{2}\rho_0^{j+1}U^{j+1^2}\right)\frac{\alpha_{mn}^{-\,j+1}}{\omega+\alpha_{mn}^{-\,j+1}U^{j+1}}\int_0^{r_{j+1}} r\psi_{mv}^{j}(r)dr$$

$$Cb_{v201}^{+\,j} = -\frac{U^{j+1^3}}{2}\int_0^{r_j} r\psi_{mv}^{j}(r)dr$$

$$Cb_{2mn}^{+\,j+1} = -U^{j+1}\left(\frac{\gamma}{\gamma-1}+\frac{\left(M_a^{j+1}\right)^2}{2}\right)\int_0^{r_j} r\psi_{mv}^{j}(r)\psi_{mn}^{j}(r)dr$$
$$+\frac{1}{\rho_0^{j+1}}\left(\frac{\gamma P_0^{j+1}}{\gamma-1}+\frac{3}{2}\rho_0^{j+1}U^{j+1^2}\right)\frac{\alpha_{mn}^{+\,j+1}}{\omega+\alpha_{mn}^{+\,j+1}U^{j+1}}\int_0^{r_{j+1}} r\psi_{mn}^{j}(r)\psi_{mv}^{j}(r)dr$$

$$Cb_{2mn}^{-\,j+1} = -U^{j+1}\left(\frac{\gamma}{\gamma-1}+\frac{\left(M_a^{j+1}\right)^2}{2}\right)\int_0^{r_j} r\psi_{mn}^{j+1}(r)\psi_{mv}^{j}(r)dr$$
$$+\frac{1}{\rho_0^{j+1}}\left(\frac{\gamma P_0^{j+1}}{\gamma-1}+\frac{3}{2}\rho_0^{j+1}U^{j+1^2}\right)\frac{\alpha_{mn}^{-\,j+1}}{\omega+\alpha_{mn}^{-\,j+1}U^{j+1}}\int_0^{r_{j+1}} r\psi_{mn}^{j+1}(r)\psi_{mv}^{j}(r)dr$$

$$Cb_{v2mn}^{+\,j} = -\frac{U^{j+1^3}}{2}\int_0^{r_j} r\psi_{mn}^{j+1}(r)\psi_{mv}^{j}(r)dr$$

Appendix C Coefficients in Eq. (7.149)

$$A_1 = \frac{(r+1)}{C_w}\left(i\omega+\frac{\partial\overline{v}_x}{\partial x}\right)$$

$$A_2 = \frac{(r+1)\overline{v}_x}{C_w}$$

$$A_3 = \frac{\overline{\rho}(r+1)}{C_w}$$

$$A_4 = \frac{\overline{\rho}}{C_w}$$

$$A_5 = \frac{\overline{\rho}(r+1)}{C_w}$$

$$A_6 = \frac{\overline{\rho}}{C_w}+\frac{\partial\overline{\rho}}{\partial r}\frac{(r+1)}{C_w}$$

$$A_7 = \frac{1}{C_w}\frac{\partial\overline{\rho}}{\partial\theta}$$

$$A_8 = \frac{1}{C_w}\frac{\partial \overline{\rho}}{\partial x}(r+1)$$

$$B_1 = \frac{i\omega\overline{\rho}}{C_w}$$

$$B_2 = \frac{\overline{\rho}\overline{v}_x}{C_w}$$

$$B_3 = \frac{1}{C_w}$$

$$C_1 = \frac{i\omega\overline{\rho}(r+1)}{C_w}$$

$$C_2 = \frac{\overline{\rho}\overline{v}_x(r+1)}{C_w}$$

$$C_3 = \frac{1}{C_w}$$

$$D_1 = \frac{\overline{v}_x}{C_w}\frac{\partial \overline{v}_x}{\partial x}(r+1)$$

$$D_2 = \left(i\omega\overline{\rho} + \overline{\rho}\frac{\partial \overline{v}_x}{\partial x}\right)\frac{(r+1)}{C_w}$$

$$D_3 = \frac{\overline{\rho}\overline{v}_x(r+1)}{C_w}$$

$$D_4 = \frac{\overline{\rho}}{C_w}\frac{\partial \overline{v}_x}{\partial r}(r+1)$$

$$D_5 = \frac{\overline{\rho}}{C_w}\frac{\partial \overline{v}_x}{\partial \theta}$$

$$D_6 = \frac{r+1}{C_w}$$

$$E_1 = \left(-i\omega + \frac{\overline{v}_x}{\overline{\rho}}\frac{\partial \overline{\rho}}{\partial x}\right)\frac{(r+1)}{C_w}$$

$$E_2 = -\frac{\overline{v}_x}{C_w}(r+1)$$

$$E_3 = \left(\frac{1}{\overline{c}^2}\frac{\partial \overline{p}}{\partial r} - \frac{\partial \overline{\rho}}{\partial r}\right)\frac{(r+1)}{C_w}$$

$$E_4 = \left(\frac{1}{\overline{c}^2}\frac{\partial \overline{p}}{\partial \theta} - \frac{\partial \overline{\rho}}{\partial \theta}\right)\frac{1}{C_w}$$

$$E_5 = \left(\frac{1}{\overline{c}^2}\frac{\partial \overline{p}}{\partial x} - \frac{\partial \overline{\rho}}{\partial x}\right)\frac{(r+1)}{C_w}$$

$$E_6 = \left(i\omega\frac{1}{\overline{c}^2} - \frac{\gamma \overline{v}_x}{\overline{c}^2\overline{\rho}}\frac{\partial \overline{\rho}}{\partial x}\right)\frac{(r+1)}{C_w}$$

$$E_7 = \frac{(r+1)}{\overline{c}^2}\frac{\overline{v}_x}{C_w}$$

C_w is a dimensionless number included to adjust the determinant of the matrix for calculation need.

Appendix D Coefficients in Eq. (7.169)

$$K_{a1} = \overline{v}_{x1}$$
$$K_{a2} = \overline{\rho}_1$$
$$K_{a3} = -\overline{v}_{x2}$$
$$K_{a4} = -\overline{\rho}_2$$

$$K_{b1} = \overline{v}_{x1}^2$$
$$K_{b2} = 2\overline{\rho}_1\overline{v}_{x1}$$
$$K_{b3} = 1$$
$$K_{b4} = -\overline{v}_{x2}^2$$
$$K_{b5} = -2\overline{\rho}_2\overline{v}_{x2}$$
$$K_{b6} = -1$$

$$K_{c1} = \overline{\rho}_1 \overline{v}_{x1}$$

$$K_{c2} = -\overline{\rho}_2 \overline{v}_{x2}$$

$$K_{d1} = \overline{\rho}_1 \overline{v}_{x1}$$

$$K_{d2} = -\overline{\rho}_2 \overline{v}_{x2}$$

$$K_{e1} = \left(c_p \overline{T}_{01} \overline{v}_{x1} - c_p T_1 \overline{v}_{x1}\right)$$

$$K_{e2} = \left(\lambda_v + c_p \overline{T}_{01} \overline{\rho}_1 + \overline{\rho}_1 \overline{v}_{x1}^2\right)$$

$$K_{e3} = \lambda_p + \frac{c_p \overline{v}_{x1}}{Rg}$$

$$K_{e4} = -\left(c_p \overline{T}_{02} \overline{v}_{x2} - c_p T_2 v_{x2}\right)$$

$$K_{e5} = -\left(c_p \overline{T}_{02} \overline{\rho}_2 + \overline{\rho}_2 \overline{v}_{x2}^2\right)$$

$$K_{e6} = -\frac{c_p v_{x2}}{Rg}$$

References

[1] J. Tyndall, Sound, D. Appleton, 1897.
[2] L. Rayleigh, Theory of Sound (Two Volumes), Dover Publications, New York, 1945 1877, re-issued 1945.
[3] B.T. Zinn, T.C. Lieuwen, Combustion instabilities: basic concepts, in: Combustion Instabilities in Gas Turbine Engines: Operational Experience, Fundamental Mechanisms, and Modeling, 210 2005, pp. 3–26.
[4] T.C. Lieuwen, V. Yang, Combustion Instabilities in Gas Turbine Engines: Operational Experience, Fundamental Mechanisms, and Modeling, American Institute of Aeronautics and Astronautics, 2005.
[5] T. Poinsot, Prediction and control of combustion instabilities in real engines, Proc. Combust. Inst. 36 (1) (2017) 1–28.
[6] K.R. McManus, T. Poinsot, S.M. Candel, A review of active control of combustion instabilities, Prog. Energy Combust. Sci. 19 (1) (1993) 1–29.
[7] B. Zinn, Y. Neumeier, B. Zinn, Y. Neumeier, An overview of active control of combustion instabilities, in: 35th Aerospace Sciences Meeting and Exhibit, 1997, p. 461.
[8] A.P. Dowling, A.S. Morgans, Feedback control of combustion oscillations, Annu. Rev. Fluid Mech. 37 (2005) 151–182.
[9] A.P. Dowling, The calculation of thermoacoustic oscillations, J. Sound Vib. 180 (4) (1995) 557–581.
[10] A.P. Dowling, J.E. Ffowcs Williams, Sound and Sources of Sound, Horwood, 1983.
[11] M.A. Heckl, Active control of the noise from a Rijke tube, J. Sound Vib. 124 (1) (1988) 117–133.
[12] G.J. Bloxsidge, A.P. Dowling, P.J. Langhorne, Reheat buzz: an acoustically coupled combustion instability. Part 2. Theory, J. Fluid Mech. 193 (1988) 445–473.
[13] T. Schuller, D. Durox, P. Palies, S. Candel, Acoustic decoupling of longitudinal modes in generic combustion systems, Combust. Flame 159 (5) (2012) 1921–1931.

[14] A.P. Dowling, S.R. Stow, Acoustic analysis of gas turbine combustors, J. Propuls. Power 19 (5) (2003) 751–764.
[15] S.R. Stow, A.P. Dowling, T.P. Hynes, Reflection of circumferential modes in a choked nozzle, J. Fluid Mech. 467 (2002) 215–239.
[16] D. You, X. Sun, V. Yang, A three-dimensional linear acoustic analysis of gas turbine combustion instability, in: 41st Aerospace Sciences Meeting and Exhibit, 2003, p. 118.
[17] D. You, X. Sun, V. Yang, Three-dimensional linear stability analysis of gas turbine combustion dynamics, in: Combustion Instabilities in Gas Turbine Engines: Operational Experience, Fundamental Mechanisms, and Modeling, Progress in Astronautics and Aeronautics, 2005.
[18] R.J. Alfredson, The propagation of sound in a circular duct of continuously varying cross-sectional area, J. Sound Vib. 23 (4) (1972) 433–442.
[19] R. Peyret, Spectral Methods for Incompressible Viscous Flow, Vol. 148, Springer Science & Business Media, 2013.
[20] L. Li, X. Sun, Effect of vorticity waves on azimuthal instabilities in annular chambers, Combust. Flame 162 (3) (2015) 628–641.
[21] F.E. Marble, S.M. Candel, Acoustic disturbance from gas non-uniformities convected through a nozzle, J. Sound Vib. 55 (2) (1977) 225–243.
[22] L. Li, L. Yang, X. Sun, Effect of distributed heat source on low frequency thermoacoustic instabilities, J. Sound Vib. 332 (12) (2013) 3098–3111.
[23] S.R. Stow, A.P. Dowling, Modelling of circumferential modal coupling due to Helmholtz resonators, in: ASME Turbo Expo 2003, Collocated with the 2003 International Joint Power Generation Conference, American Society of Mechanical Engineers, 2003, January, pp. 129–137.
[24] T. Lieuwen, Modeling premixed combustion-acoustic wave interactions: a review, J. Propuls. Power 19 (5) (2003) 765–781.
[25] L. Li, Z. Guo, C. Zhang, X. Sun, A passive method to control combustion instabilities with perforated liner, Chin. J. Aeronaut. 23 (6) (2010) 623–630.
[26] X. Sun, X. Wang, L. Du, X. Jing, A new model for the prediction of turbofan noise with the effect of locally and non-locally reacting liners, J. Sound Vib. 316 (1–5) (2008) 50–68.
[27] X. Wang, X. Sun, A new segmentation approach for sound propagation in non-uniform lined ducts with mean flow, J. Sound Vib. 330 (10) (2011) 2369–2387.
[28] X. Wang, X. Sun, Transfer element method with application to acoustic design of aero-engine nacelle, Chin. J. Aeronaut. 28 (2) (2015) 327–345.
[29] J.D. Eldredge, A.P. Dowling, The absorption of axial acoustic waves by a perforated liner with bias flow, J. Fluid Mech. 485 (2003) 307–335.
[30] M.S. Howe, On the theory of unsteady high Reynolds number flow through a circular aperture, Proc. R. Soc. Lond. A 366 (1725) (1979) 205–223 M.E. Goldstein, Aeroacoustics, McGraw-Hill International Book Co., New York, 1976.
[31] G. Zhang, X. Wang, L. Li, X. Jing, X. Sun, Control of thermoacoustic instability with a drum-like silencer, J. Sound Vib. 406 (2017) 253–276.